https://doi.org/10.5194/egusphere-2026-4116
Preprint. Discussion started: 29 July 2026


# Version 8 of IMK/IAA MIPAS reactive nitrogen reservoir gases

Gabriele P. Stiller[1], Thomas von Clarmann[1,†], Stefan Bender[2], Bernd Funke[2], Maya García-Comas[2], Norbert Glatthor[1], Udo Grabowski[1], Sylvia Kellmann[1], Michael Kiefer[1], Alexandra Laeng[1], Andrea Linden[1,†], and Manuel López-Puertas[2]

[1]Karlsruhe Institute of Technology, Institute of Meteorology and Climate Research, Karlsruhe, Germany
[2]Instituto de Astrofísica de Andalucía, CSIC, Granada, Spain
[†]T. von Clarmann deceased, January 13, 2024; A. Linden deceased, November 18, 2024

**Correspondence:** Gabriele Stiller (gabriele.stiller@kit.edu)

**Abstract.** Version 8 infrared limb emission spectra provided by the Michelson Interferometer for Passive Atmospheric Sounding (MIPAS) on Envisat were used to infer global distributions of $HNO_3$, $ClONO_2$, $HNO_4$, and $N_2O_5$ in the altitude range from about 6 to 80 km. Here we describe in detail the analysis of the spectral data by means of constrained non-linear least-squares fitting, and provide information about the averaging kernels, the vertical and horizontal resolutions, and the error budgets of the derived trace gas profiles. For $HNO_3$ and $N_2O_5$, the error budgets are dominated by systematic errors, mainly spectroscopic uncertainties, in the relevant altitude range, while for $HNO_4$ and $ClONO_2$ they are dominated by spectral noise. This implies that systematic biases of up to 20% and $<$10% cannot be excluded for $HNO_3$ and $N_2O_5$, respectively, while the information about spatial and temporal variability is quite certain. Random uncertainties of $HNO_4$ and $ClONO_2$ can be favourably reduced by averaging, while systematic uncertainties in the order of 3% ($ClONO_2$) and 20% ($HNO_4$) will remain. The vertical resolution is in the order of 2 to 6 km in the lower and middle stratosphere, depending on the species and the atmospheric situation. Besides the four nitrogen reservoir species, we also present $NO_y$ as a derived data product. It is constructed from $[HNO_3]$ + $[ClONO_2]$ + $[HNO_4]$ + 2 × $[N_2O_5]$ + $[NO]$ + $[NO_2]$ and characterised in terms of its random and systematic error budget. Along with the regular data product of the four nitrogen reservoir species, an additional representation of the data on a coarser vertical grid is offered. These data can be used without consideration of the averaging kernels. The new trace gas distributions are compared to the previous data version, and they are discussed along the most relevant signatures of processes to be observed. We find that the new data products provide improved consistency between the full- and reduced-resolution mission periods of MIPAS, as well as between the observation modes covering different altitude ranges, and they exhibit all the analysed features caused by known atmospheric processes.

## 1 Introduction

The main source of nitrogen in the stratosphere is nitrous oxide ($N_2O$) which has its own main sources at the surface (McElroy and McConnell, 1971; Crutzen, 1971; Minschwaner and Siskind, 1993; Volk et al., 1997; McLinden et al., 2003; Morgan et al.,

https://doi.org/10.5194/egusphere-2026-4116
Preprint. Discussion started: 29 July 2026


2004). In the stratosphere $N_2O$ is photolyzed and oxidized with an atmospheric lifetime of about 114 years (Montzka and Fraser, 2003), forming $NO_2$ and finally a series of further reactive nitrogen compounds, namely NO, $HNO_3$, $ClONO_2$, $N_2O_5$, $HNO_4$ (also known as $HO_2NO_2$), and $BrONO_2$. All these reactive nitrogen species are commonly summarized as $NO_y$. $NO_y$ concentrations in the stratosphere are expected to increase with time due to increasing tropospheric $N_2O$ with an approximately linear rate of 0.26% per year for the past few decades (Forster et al., 2007, Section 2.3.3), mainly due to enhanced microbial production from agricultural expansion. Because $NO_y$ is formed at the expense of $N_2O$, an anticorrelation is expected between $NO_y$ and $N_2O$ spatial distributions (Fahey et al., 1990). More recently, the lifetime of $N_2O$ in the atmosphere has been assessed from observational data to be $116 \pm 9$ years (Prather et al., 2015), while in the same study four independent chemistry-transport models were found to consistently overestimate its lifetime because of too low abundances in the critical loss region of $N_2O$. $N_2O$ has been reported to be the single most important ozone depleting substance emitted and is expected to remain so during the 21st century (Ravishankara et al., 2009). The World Meteorological Organization suggested that observed $N_2O$ increases and ozone decreases explained a trend in the $NO_2$ total column of $5 \pm 1\%$ per decade (Ennis, 2003). However, Stolarski et al. (2015) studied the interaction of global warming due to $CO_2$ increase and $NO_y$ changes with the two- dimensional Goddard Space Flight Center coupled chemistry–radiation–dynamics model (GSFC2D). They found that under an accelerating Brewer-Dobson circulation, as a consequence of global warming, total global $NO_y$ can even decrease in future despite constant $N_2O$ entry from the surface. These findings were confirmed by Funke et al. (2019) by making use of future projections from the WACCM chemistry-climate model; they found that the future trend of $NO_y$ can be both positive or negative, depending on the status of the Brewer-Dobson circulation in a changing climate.

$NO_y$ species play a crucial role in stratospheric ozone destruction. While $NO_x$ (N, NO, $NO_2$, $NO_3$) species are directly involved in the catalytic cycles of ozone destruction, stratospheric nitrogen is also available as $HNO_3$, $N_2O_5$, $ClONO_2$, $HNO_4$, and $BrONO_2$, which are so-called nitrogen reservoir gases. During polar night, at very low temperatures, polar stratospheric cloud particles (PSCs) containing nitrogen in the form of solid NAT (nitric acid trihydrate) and NAD (nitric acid dihydrate), are formed. Because of the lower temperatures in the Antarctic polar vortex and its stronger confinement compared to the Arctic, Antarctic polar stratospheric air is largely denitrified by the formation of these nitrogen-containing ice particles and subsequent sedimentation. As a consequence, there is not much $NO_2$ left to form $ClONO_2$, and the main pathway of chlorine deactivation is the formation of HCl. The situation is different in the Arctic, where $ClONO_2$ formation is the predominant pathway of chlorine deactivation at the end of the polar winter (von Clarmann et al., 1993).

Persistent gas phase chemistry and heterogeneous chemistry on the ice particle surfaces convert nitrogen species into each other, which plays a major role in polar ozone depletion (Granier and Brasseur, 1992). However, not only the catalytic cycles based on the nitrogen-containing species, but also chlorine-based catalytic cycles are important. They are linked to each other by the formation of $ClONO_2$ (e.g. Chipperfield et al., 1997; von Clarmann and Johansson, 2018), and are therefore both affected.

Further contributions to stratospheric $NO_y$ are due to air subsiding from the thermosphere and mesosphere, where reactive nitrogen is produced by dissociation of molecular nitrogen by solar photons and energetic particles, and subsequent reaction with oxygen to form NO. These energetic particles are principally auroral and precipitating electrons from the outer trapping

https://doi.org/10.5194/egusphere-2026-4116
Preprint. Discussion started: 29 July 2026


region of the magnetosphere. In polar night regions this $NO_x$-enriched air is transported downward by the downwelling branch of the mesospheric overturning pole-to-pole circulation. Here, reactive nitrogen survives the transport through the mesosphere because of the absence of sunlight under polar winter conditions.

$NO_y$ species have their maxima typically in the lower stratosphere of high latitudes (Mengistu Tsidu et al., 2005). In the upper troposphere of lower latitudes, other nitrogen-containing species like PAN (= peroxyacetyl nitrate), HONO, HCN, or $NH_3$ and ammonium nitrate and -sulphate aerosols are found in relevant concentrations. However, compared to the main reactive nitrogen species in the stratosphere, the mixing ratios of these species are low and they rarely survive the transport deep into the stratosphere; thus, they do not contribute by relevant amounts to the budget of reactive nitrogen species there.

Since the 1970s a multitude of ground-based as well as balloon- and satellite-borne techniques have been used to remotely measure stratospheric abundances of nitrogen species. Pioneering work includes measurement of NO by Ridley and Hastie (1981), $NO_2$ by Noxon (1979), $HNO_3$ by Murcray et al. (1968, 1973), $ClONO_2$ by Murcray et al. (1979) and Zander et al. (1986), $N_2O_5$ by Toon et al. (1986) and by Rinsland et al. (1989), and $HNO_4$ by Rinsland et al. (1987).

The Michelson Interferometer for Passive Sounding (MIPAS, Fischer et al., 2008) on Envisat has been the only satellite instrument so far that could measure all relevant $NO_y$ species (NO, $NO_2$, $HNO_3$, $N_2O_5$, $ClONO_2$, $HNO_4$, and $BrONO_2$) in the stratosphere, upper troposphere and mesosphere during day and night. Hegglin and Tegtmeier (2017) reported about an intercomparison of $HNO_3$, $HNO_4$, $N_2O_5$, $ClONO_2$, NO, $NO_2$, $NO_x$, and $NO_y$ of data records from several satellite instruments. The comparisons were updated with more recent data versions of all instruments by Hegglin et al. (2021).

MIPAS $NO_y$ data were used within the analysis of several special events during its mission, and contributed to basic understanding of atmospheric processes. The first observed Antarctic vortex split in Austral spring 2002 was studied on basis of $ClONO_2$ (Höpfner et al., 2004), $N_2O_5$ (Mengistu Tsidu et al., 2004) and $NO_y$ distributions (Mengistu Tsidu et al., 2005).

In October/November 2003 a strong solar proton event (SPE), the so-called Halloween SPE, affected the Earth's atmosphere, and the strongest effects were observed over the poles. López-Puertas et al. (2005a), López-Puertas et al. (2005b), Jackman et al. (2008), Verronen et al. (2008), Baumgaertner et al. (2010), Funke et al. (2011) and Friederich et al. (2013) analysed the impact on $NO_x$, $HNO_3$, $N_2O_5$ and $ClONO_2$. Triggered by this event, the impact of energetic particle precipitation in general, i.e. also from electrons and galactic cosmic rays, were studied on basis of early versions of MIPAS data (Funke et al., 2005a; Stiller et al., 2005; Funke et al., 2014a, b, and references therein). Further SPEs during the mission lifetime of MIPAS were also studied on basis of its data (Jackman et al., 2011; Damiani et al., 2012; von Clarmann et al., 2013). The downward transport of enhanced $NO_y$ produced by high-energetic particles in polar winters with strong stratospheric warmings and elevated stratopause events was studied by Funke et al. (2005a), Damiani et al. (2014), Sinnhuber et al. (2014), Funke et al. (2017), and Sinnhuber et al. (2018). Friederich et al. (2014) correlated the $A_p$ index and $NO_2$ in the upper stratosphere and mesosphere at high latitudes and found direct impact of electron precipitation on $NO_x$. From the polar winters covered by MIPAS, Funke et al. (2016) derived a semi-empirical model that related the produced and subsided $NO_y$ in polar winters to the geomagnetic $A_p$ index measuring the geomagnetic activity. The impact on ozone via $NO_x$ was studied by Fytterer et al. (2015), and a direct correlation to indices of solar and geomagnetic activity was derived.

https://doi.org/10.5194/egusphere-2026-4116
Preprint. Discussion started: 29 July 2026


Adams et al. (2017) used $NO_2$ and $N_2O_5$ data from MIPAS to study the impact of aerosols from strong volcanic eruptions on nitrogen compounds in the atmosphere and found that they decreased in consonance with a photochemical model. Processes of stratospheric ozone depletion chemistry related to $HNO_4$, $N_2O_5$ and $NO_x$ were studied in detail, and MIPAS data served for model validation studies (Tilmes et al., 2003; Stiller et al., 2007; Konopka et al., 2007; Brühl et al., 2007). Formation of polar stratospheric clouds and related denitrification was studied by Grooß et al. (2014), and Khosrawi et al. (2018), as well as Höpfner et al. (2006b, a, 2018) for the Antarctic. The first global distribution of $BrONO_2$ was also provided from MIPAS (Höpfner et al., 2009).

In this paper we present recent updates of the retrieval of nitrogen reservoir species $HNO_3$, $N_2O_5$, $ClONO_2$, and $HNO_4$, from the nominal (NOM), middle atmosphere (MA), upper atmosphere (UA), noctilucent clouds (NLC) and UTLS modes of MIPAS observations. The version 8 data of $BrONO_2$, including a complete climatology covering the mission lifetime, have already been presented and discussed by Höpfner et al. (2021), while the version 8 NO and $NO_2$ data products are presented by Funke et al. (2023) and Funke et al. (2026), respectively. Along with the version 8 retrievals, we present an extensive error analysis for the four $NO_y$ species that is compliant with most recent recommendations by the APARC activity 'Towards Unified Error Reporting' (TUNER, von Clarmann et al., 2020, 2022). After summarizing the MIPAS instrument characteristics that are relevant for the retrieval of the title species (Section 2), we discuss for each species the retrieval set-up (Section 3), their horizontal and vertical resolutions, and their error budgets (Section 4). Since we provide the aggregated $NO_y$ (including NO, $NO_2$, $HNO_3$, $N_2O_5$, $ClONO_2$, and $HNO_4$) as an additional data product, we discuss the construction of $NO_y$ and its properties in Section 5. A critical discussion of the improvements compared to the previous data versions is provided in Section 6. Section 7 presents the new data sets and discuss their latitudinal distributions, and their seasonal and inter-annual variations. A special data version for all four species, the so-called maximum-likelihood or coarse-grid retrieval version, is presented in Section 8. In Section 9 we conclude with a summary.

## 2 MIPAS

### 2.1 Mission, instrument, and spectral data

MIPAS was an infrared Fourier transform spectrometer observing the infrared emission of the Earth's limb. MIPAS was hosted by the Envisat research satellite, which was launched on 1 March 2002 into a polar sun-synchronous orbit with 10 a.m. and 10 p.m. equatorial crossing time. Envisat performed about 14 orbits per day. Data acquisition of MIPAS started in July 2002. MIPAS took about 1000 radiance profiles per day until an instrument failure in March 2004. Operation was resumed in January 2005. The maximum optical path difference of the interferometer had to be reduced. This went along with an improved spatial sampling pattern with about 1300 profiles per day until communication with Envisat was lost in April 2012. The spectral resolution was 0.025 $cm^{-1}$ (unapodized) before and 0.0625 $cm^{-1}$ after the instrument failure. We refer to the first mission phase as full resolution (FR) and to the second mission phase as reduced resolution (RR). The vertical sampling was 3 km before the failure, while it reached 1.5 km at some altitudes after the failure. The spectral coverage was 4.1 to 14.7 $\mu$m (685–2410 $cm^{-1}$). During the second mission phase, several observation modes with different horizontal spacings,

https://doi.org/10.5194/egusphere-2026-4116
Preprint. Discussion started: 29 July 2026


altitude coverages, and vertical tangent altitude spacings were run. An overview on the observation modes can be found on https://eodg.atm.ox.ac.uk/MIPAS/rrmodes.html. Here we refer to the RR NOM, RR UTLS-1, RR MA, RR UA, and RR NLC mode (see Table 1). For the FR NOM and RR NOM observation modes, the horizontal along-orbit sampling was 500 km and 410 km, respectively. Further technical details on the instrument and the mission are documented by Fischer et al. (2008) and references therein.

For this work, we used level-1 spectra version 8.03 distributed by ESA. A thorough assessment of the uncertainties of these level-1 data has been provided by Kleinert et al. (2018). Kiefer et al. (2021) discussed the consequences of the most recent calibration for the level-2 data. Major changes refer to the nonlinearity correction. The data version numbers of our $HNO_3$, $ClONO_2$, $N_2O_5$ and $HNO_4$ data are compiled in Table 1 for the relevant MIPAS observation modes, Nominal (FR or RR NOM), Upper Troposphere and Lower Stratosphere (RR UTLS-1), Middle Atmosphere (RR MA), Upper Atmosphere (RR UA) and Noctilucent Cloud (RR NLC) measurement modes. To complete the $NO_y$ budget, we also use NO and $NO_2$ data from Funke et al. (2023) and Funke et al. (2026).

## 2.2 Performance of previous data versions

### 2.2.1 $HNO_3$

MIPAS $NO_y$ species of previous data versions have been frequently compared to other satellite measurements and balloon-borne data. If not mentioned explicitly, these were all from the FR or RR NOM observation modes.

Comparisons of an early data version of $HNO_3$ to MLS (Wang et al., 2007) indicated a positive bias of MIPAS that was, however, almost constant over various atmospheric situations; structures in global distributions and time series appeared to be similar. Wolff et al. (2008) compared ACE-FTS $HNO_3$ data v2.2 to MIPAS $HNO_3$ version V3O_HNO3_8 data and found mean differences of about 0.2 ppbv between 10 and 31 km (with MIPAS being larger), while above 31 km MIPAS was biased negative against ACE-FTS with differences between 5 and 17%. Hegglin and Tegtmeier (2017) reported about monthly mean comparisons of MIPAS V3O_HNO3_9 and MIPAS V4O_HNO3_220 with Odin/SMR, Aura-MLS, ACE-FTS, and HIRDLS. While the MIPAS data agreed within 5% with the multi-instrument mean in mid-latitudes, they showed a negative bias of up to -40% in the tropics around 50 hPa, and a pronounced positive bias of more than 50% between 20 and 50 hPa in the Southern polar winter. At least the latter bias, under Antarctic winter conditions, could be explained as a sampling bias: since MIPAS cannot measure in the presence of clouds, it probed the PSC-free and most probably less processed and thus $HNO_3$-richer air masses only. In an update of this work, Hegglin et al. (2021) compared the seasonal cycle at 10 hPa for three latitude bands of MIPAS V5H_HNO3_22 and V5R_HNO3_224 to more recent data versions of the same other instruments. The agreement to the multi-instrument mean is best among all instruments, both in absolute values and in amplitudes. The findings by Wang et al. (2007) were confirmed by Khosrawi et al. (2018) for the MIPAS IMK-IAA data version V5H_HNO3_20/V5R_HNO3_224/225. Khosrawi et al. (2018) used both MLS and MIPAS $HNO_3$ data to validate the PSC formation scheme in the chemistry-climate model ECHAM5/MESSy Atmospheric Chemistry (EMAC). Sheese et al. (2016) and Sheese et al. (2017) compared the same data version to ACE-FTS $HNO_3$ v3.5 data and found agreement within 10% between 10 and 40 km altitude.

https://doi.org/10.5194/egusphere-2026-4116
Preprint. Discussion started: 29 July 2026


### 2.2.2 $ClONO_2$

MIPAS $ClONO_2$ comparisons were reported by Höpfner et al. (2007), Wolff et al. (2008), Virolainen et al. (2015), and Sheese et al. (2016). Hegglin et al. (2021) compared monthly zonal means of data version V3O_CLONO2_12 and V4O_CLONO2_220 with ACE-FTS v2.2 data and found agreement within ± 10% relative to the multi-instrument mean around the stratospheric maximum. In the lower stratosphere, however, where the $ClONO_2$ profiles decrease again, relative differences were far larger. Höpfner et al. (2007) compared MIPAS data of version V3O_CLONO2_10/11, covering the first phase of MIPAS, 2002 - 2004, only, to a large number of ground-based, balloon-borne, airborne and satellite instruments. Because of the photochemically induced diurnal variation of $ClONO_2$ above about 26 km, the observed $ClONO_2$ amounts were corrected for the time difference of the otherwise coincident observations by a chemical transport model. The only other satellite data set available for comparisons was ACE-FTS v2.2. Differences to balloon-borne measurements remained, except for FIRS, below 0.1 ppbv, while differences to ACE-FTS were smaller than 0.03 ppbv below 26 km; the photochemical correction above 26 km turned a negative daytime bias of MIPAS into a positive bias in the order of 0.1 ppbv (and vice versa for nighttime observations), i.e. the photochemical correction over-corrected the differences. Partial columns compared to ground-based FTIR measurements agreed within less than 1%. Wolff et al. (2008) repeated the comparison of ACE-FTS $ClONO_2$ v2.2 to MIPAS V3O_CLONO2_10/11 and confirmed the findings by Höpfner et al. (2007). Virolainen et al. (2015) compared $ClONO_2$ partial columns between 13 and 45 km measured by ground-based FTIR instruments in St. Petersburg with MIPAS of the version V5R_CLONO2_220. They found no systematic biases, an average 0.8% discrepancy, and high correlation (R = 0.8) for the seasonality of the measurements. Sheese et al. (2016) compared MIPAS V5R_CLONO2_222 to ACE-FTS version 3.5, accounting for the diurnal cycle by a photochemical correction. Differences were between 0 and 10% (with MIPAS being higher) between about 17 and 35 km. Below 17 km, relative differences became larger with rapidly decreasing $ClONO_2$ vmrs.

### 2.2.3 $N_2O_5$

The only other satellite instrument that provides $N_2O_5$ is ACE-FTS. Previous versions of MIPAS $N_2O_5$ were compared to ACE-FTS by Wolff et al. (2008) and Sheese et al. (2016). Wolff et al. (2008) compared ACE-FTS v2.2 data to MIPAS V3O_N2O5_9 that were measured within ± 9h, 800 km, and PV values of $\pm$ 3 x $10^{-6}$ K $m^2$ $kg^{-1}$ $s^{-1}$ at 475 K. At the altitude of the $N_2O_5$ vmr maximum at 25 to 30 km, ACE-FTS vmrs were appr. 0.5 ppbv (75%) smaller than MIPAS daytime and appr. 0.4 ppbv (70%) smaller than nighttime observations. After correction of potential biases caused by differing local observation times and the diurnal cycle of $N_2O_5$ by CTM calculations, the differences at the vmr maximum were reduced by a factor of 2 to 4. In relative units, ACE-FTS $N_2O_5$ was about 40% smaller than MIPAS near the vmr maximum. Adjustment of the vertical resolution of ACE-FTS to that of MIPAS further reduced the differences in the lower part of the profiles. Convolved ACE-FTS vmrs differed by 5 to 10% from the MIPAS CTM-corrected daytime vmrs and by 30 to 40% from the MIPAS CTM-corrected nighttime vmrs. Sheese et al. (2016) compared ACE-FTS v3.5 $N_2O_5$ profiles to MIPAS V5R_N2O5_222/223. They applied a diurnal correction for the differing observation times from a box model and adjusted the vertical resolution of ACE-FTS to MIPAS by a Gaussian kernel function. They found large discrepancies for evening observations of ACE-FTS and MIPAS with differences between

https://doi.org/10.5194/egusphere-2026-4116
Preprint. Discussion started: 29 July 2026


**Table 1.** Observation modes and version numbering

| Observation mode | FR NOM | RR NOM | RR UTLS-1 | RR MA | RR UA | RR NLC |
|---|---|---|---|---|---|---|
| Spectral version | V8H_ | V8R_ | V8R_ | V8R_ | V8R_ | V8R_ |
| Altitude range[1] | 6–68 km | 7–72 km[2] | 8.5–49 km | 18-102 km | 42–172 km | 39-102 km |
| $HNO_3$ | HNO3_61 | HNO3_261 | HNO3_161 | HNO3_561 | HNO3_661 | HNO3_761 |
| $ClONO_2$ | ClONO2_61 | ClONO2_261 | ClONO2_161 | ClONO2_561 | | |
| $N_2O_5$ | N2O5_61 | N2O5_261 | N2O5_161 | N2O5_561 | | |
| $HNO_4$ | HNO4_62 | HNO4_262 | HNO4_162 | HNO4_562 | | |
| NO | NO_61 | NO_261 | NO_161 | NO_561 | NOT_662 | NO_761 |
| $NO_2$ | NO2_62/63 | NO2_261 | NO2_161 | NO2_561 | NO2_661 | NO2_761 |
| $BrONO_2$ | BrONO2_M[3] | BrONO2_M[3] | | | | |

[1] The altitude range is given from the lowest to the highest tangent altitude.
[2] The altitude range is shifted along with the tropopause height versus latitude.
[3] $BrONO_2$ results are not available as individual profiles but as 3-day 10° zonal averages.

-130 to +200%. In contrast, comparisons between morning ACE-FTS and both morning and evening MIPAS measurements were within ±10% between 22 and 40 km altitude, while large positive deviations far beyond +50% (ACE-FTS being larger than MIPAS) were observed below 22 km, and up to +35% between 40 and 50 km. Hegglin and Tegtmeier (2017) compared zonal means of ACE-FTS v2.2 and MIPAS V4O_N2O5_220 observations, however without consideration of the diurnal cycle. As expected, ACE-FTS $N_2O_5$ abundances at sunrise were highest and those at sunset the lowest, while MIPAS measurement were in between, except for the 60 to 65° latitude band in both hemispheres. This finding is in contradiction to the expected diurnal cycle and was explained by sampling issues.

#### 2.2.4 $HNO_4$

Similar to $N_2O_5$, $HNO_4$ is another product that is available from MIPAS and ACE-FTS satellite instruments only. Stiller et al. (2007) compared early MIPAS data versions V3O_HNO4_9 and V3O_HNO4_10 of the 2002 to 2004 MIPAS mission phase to balloon-borne observations in a climatological manner, while Hegglin and Tegtmeier (2017) compared zonal mean distributions of MIPAS V5R_HNO4_220 and ACE-FTS v2.2. Data versions V3O_HNO4_9 and V3O_HNO4_10 differ only with respect to the spectroscopic data used. Although version 10, using absorption cross sections and providing larger abundances by a factor of about 1.5, has been considered as the more reliable one, version 9 has been compared to MkIV and MIPAS-B balloon observations because of the use of the same spectroscopic data. The diurnal cycle of $HNO_4$ complicates the comparison in this case, too. MkIV sunset profiles at 35°N of September 2003 were found to be higher by 11 pptv in the vmr peak, compared to a September 2003 monthly mean of MIPAS 10 p.m. measurements within a 5° latitude band around 35° N, while at the upper end of the profile, MIPAS-measured abundances were about 30 pptv higher. Other comparisons, also those to MIPAS-B, were less conclusive since the observation times were years apart, and the profiles showed a large inter-annual variation, particularly in polar regions. The differences found in the zonal mean comparisons performed by Hegglin and Tegtmeier (2017) could be interpreted below 10 hPa only, where the diurnal cycle of $HNO_4$ is week. In this case, MIPAS V5R_HNO4_220 and ACE-FTS v2.2 data versions were compared. Differences up to ± 50% were found, with MIPAS larger than ACE-FTS almost everywhere.

https://doi.org/10.5194/egusphere-2026-4116
Preprint. Discussion started: 29 July 2026


## 3 Retrieval

The general approach to MIPAS level-2 processing is constrained nonlinear least-squares fitting as reported by von Clarmann et al. (2003), von Clarmann et al. (2009b) and Chauhan et al. (2009). Each retrieval analyzes measured radiances from one limb scan. A sequential approach is employed in the sense that one (or a small number) of species is analyzed after the other. In the retrieval of one certain gas, abundance information on the gas mixing ratios from preceding retrieval steps are used for spectrally interfering species. For interfering gases for which no results from preceding V8 retrievals are available, data from older MIPAS versions (typically V5) are used. Occasionally, gases causing strong mutual interference are retrieved jointly in the same retrieval step. For mixing ratio estimates for interfering gases on which no other data are available, mixing ratio profiles from Kiefer et al. (2002) and updates thereof are used (Figure 1).

The forward model used to simulate radiance spectra and evaluate Jacobians is the Karlsruhe Optimized and Precise Radiative Transfer Algorithm (KOPRA, Stiller, 2000; Stiller et al., 2002). Ill-conditionedness and instabilities of the retrieval are fought by regularization involving a smoothing constraint. The implementation relies on a squared first-order finite difference matrix (Tikhonov, 1963; Twomey, 1963; Phillips, 1962). A formalism to control the altitude dependence of the regularization strength as described by Kiefer et al. (2021, their Eq. (3)) replaces the approach by Steck and von Clarmann (2001) used for older data versions. For reasons discussed in von Clarmann et al. (2003), in all retrievals, a background continuum and a radiance offset are fitted along with the target gas concentrations. In the following, we discuss the gas-specific retrieval settings according to the target gas position in the retrieval chain.

### 3.1 The retrieval of $HNO_3$

Earlier versions of MIPAS $HNO_3$ retrievals have been reported by Stiller et al. (2005) and von Clarmann et al. (2009b) for FR and RR NOM measurements, respectively. The validation of these data versions (Hegglin and Tegtmeier, 2017; Hegglin et al., 2021; Sheese et al., 2017, 2016) did not provide hints at serious problems with these data; thus, the V8 retrieval setup is essentially the same as that of V5.

In the retrieval chain, the retrievals of temperature along with elevation pointing and 3-D information of the temperature field, $O_3$ and $H_2O$ precede the retrieval of $HNO_3$ (Fig. 1). The $HNO_3$ retrieval uses lines in the MIPAS A band in the region of the $\nu_5$ and $2\nu_9$ bands near 880 $cm^{-1}$. For measurements with tangent altitudes higher than 44.5 km also lines in the MIPAS B band around 1320 $cm^{-1}$ are used. The spectral region used for the retrieval, the so-called microwindows, are summarized in Table 2.

The spectroscopic dataset used for $HNO_3$ is based on HITRAN2008 (Rothman et al., 2009). In addition, and different to version 5 data, updates by A. Perrin for the 1320 $cm^{-1}$ spectral region that were included in the dedicated MIPAS spectroscopic database v4.45 (Flaud et al., 2015) have been used. In the 860 $cm^{-1}$ region, this spectroscopic dataset is identical to HITRAN2016 (Gordon et al., 2017). The updates by A. Perrin in the 1320 $cm^{-1}$ region, however, have not found their way into HITRAN.

https://doi.org/10.5194/egusphere-2026-4116
Preprint. Discussion started: 29 July 2026


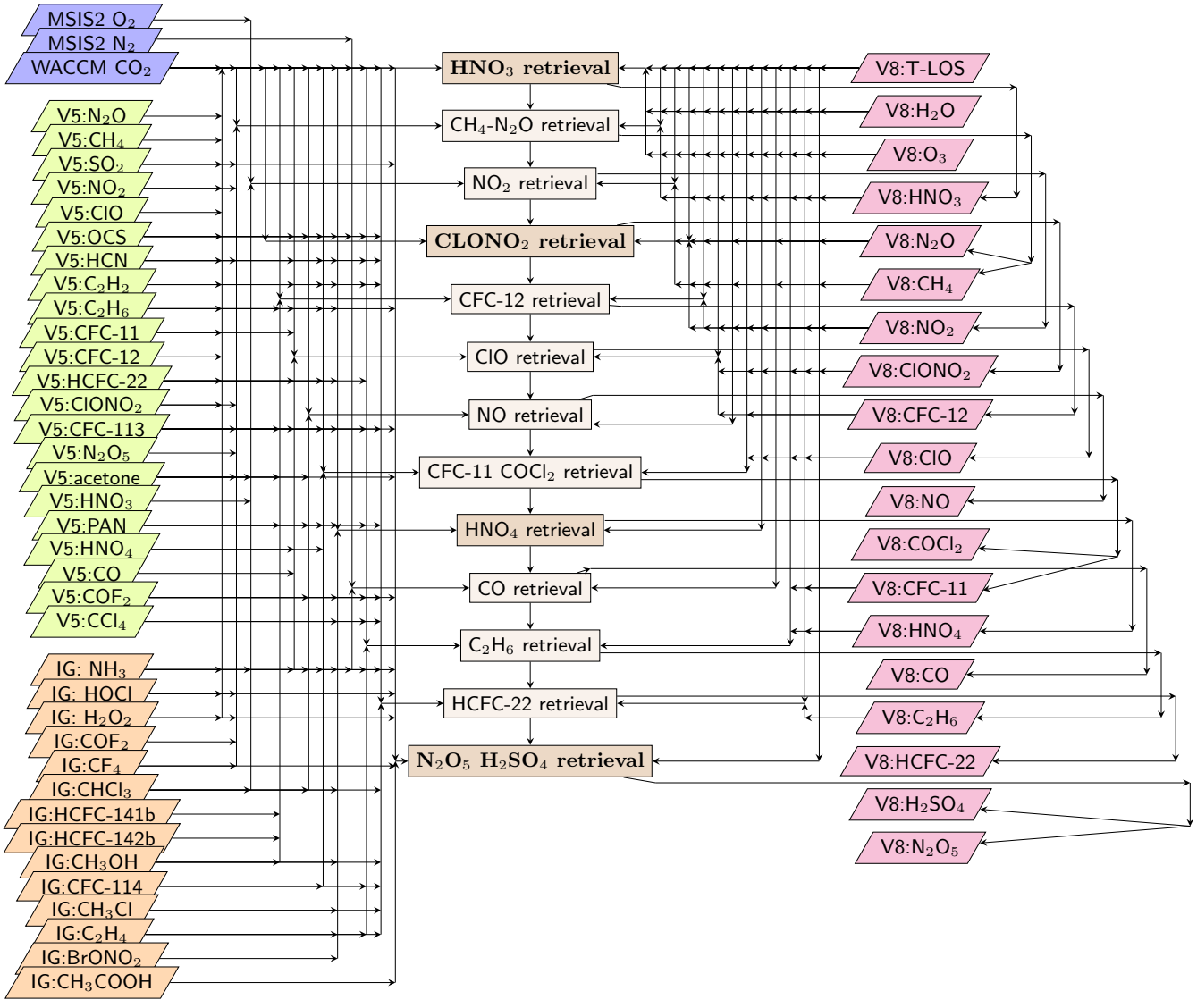


**Figure 1.** Processing sequence and related data flow. $N_2$ and $O_2$ mixing ratios are taken from the MSIS2 model (Emmert et al., 2020), while $CO_2$ mixing ratios are generated using WACCM model output (Marsh, 2011; Marsh et al., 2013; García et al., 2017) as described by (Kiefer et al., 2021). The origin of the other trace gases used for spectral modelling is colour coded. Green: V5 data, pink: V8 data, and light brown: climatology database Kiefer et al. (2002). Retrieving NO and CO concentrations prior to those of HCFC-22 is a merely pragmatic choice, since these are not needed as input of the HCFC-22 retrieval.

https://doi.org/10.5194/egusphere-2026-4116
Preprint. Discussion started: 29 July 2026


**Table 2.** Microwindows used in the MIPAS $HNO_3$ retrieval

| Wavenumber in $cm^{-1}$ | |
|---|---|
| FR | RR |
| 862.5000–864.0000 | 862.5000–864.0000 |
| 865.8000–868.0000 | 865.8125–868.0000 |
| 868.2500–871.0000 | 868.2500–871.0000 |
| 871.8500–874.0000 | 871.8125–874.0000 |
| 878.8500–881.3000 | 878.8125–881.3125 |
| 881.6250–883.6250 | 881.6250–883.6250 |
| 1310.0000–1311.1500 | 1310.0000–1311.1875 |
| 1311.6250–1312.2000 | 1311.6250–1312.1875 |
| 1312.8000–1313.3000 | 1312.8125–1313.3125 |
| 1313.9500–1314.5000 | 1313.9375–1314.5000 |
| 1315.0000–1316.6000 | 1315.0000–1316.5625 |
| 1317.2500–1318.5000 | 1317.2500–1318.5000 |
| 1319.1250–1319.8750 | 1319.1250–1319.8750 |
| 1320.2500–1320.7000 | 1320.2500–1320.6875 |
| 1321.0000–1321.8750 | 1321.0000–1321.8750 |
| 1322.3000–1323.2000 | 1322.3125–1323.1875 |
| 1324.3000–1326.8750 | 1324.3125–1326.8750 |
| 1327.6250–1329.7000 | 1327.6250–1329.6875 |
| 1330.0000–1331.8750 | 1330.0000–1331.8750 |
| 1333.0000–1336.3750 | 1333.0000–1336.3750 |

Microwindows below 1300 $cm^{-1}$ are used for all tangent altitudes, while microwindows above 1300 $cm^{-1}$ are used for tangent altitudes above 44.5 km only.

The temperature profile and the 2D-distribution of the temperature field along with the line of sight pointing information from a previous retrieval step in the processing chain (Kiefer et al., 2021) have been used in the retrievals. Interfering species that have been considered in the radiative transfer calculation but not retrieved are $H_2O$, $O_3$, $N_2O$, $CH_4$, $SO_2$, $NO_2$, ClO, OCS, HCN, $C_2H_2$, $C_2H_6$, CFC-11, CFC-12, HCFC-22, $ClONO_2$, $CO_2$, $NH_3$, HOCl, and $H_2O_2$. Information on $CO_2$ abundances has been taken from WACCM (for details see Kiefer et al. (2021)), and for $NH_3$, HOCl, and $H_2O_2$ from our climatological database (Kiefer et al., 2002), while the profiles for all other species have been taken from the previous V5 version. In case of RR MA, UA and NLC retrievals, if profiles for interfering species were not available from V5 RR MA/UA/NLC processing, climatologies were built from V5 RR NOM retrievals and used in the respective latitude bands.

For data versions before V5, a continuum emission, assumed to be mainly made up by aerosols in the stratosphere and far line wings of atmospheric gases, was considered up to 32 km, because it was believed sufficient to cover the Junge aerosol layer (Junge and Manson, 1961). Unlike in these earlier $HNO_3$ data versions, and similar to the V5 data version, the atmospheric continuum is now retrieved up to 58 km altitude (except for the UTLS-1 measurement mode, where the highest altitude of the continuum is 44 km because of the altitude coverage of this observation mode) in order to account for aerosols higher up, e.g. meteoric dust (Neely III et al., 2011).

https://doi.org/10.5194/egusphere-2026-4116
Preprint. Discussion started: 29 July 2026


**Table 3.** Microwindows used in the MIPAS FR and RR $ClONO_2$ retrieval

| Wavenumber ($cm^{-1}$) | Altitude range (km) |
|---|---|
| 779.5–781.0 | 0–120 |
| 1291.0–1293.5 | 34.5–120 |

The retrieval gridwidth is 1 km between 4 and 44 km. Between 44 and 70 km the gridwidth is 2 km. Additional gridpoints are 75.0, 80.0, 90.0, 100.0, and 120.0 km. The retrieval is regularized with a smoothing constraint (see above). The a priori profile is chosen as constant zero over the full altitude range in order not to imprint any altitude structure on the retrieved profile. For the uppermost four altitudes of the retrieval grid, a diagonal term is added to the Tikhonov smoothing regularization matrix which pushes mixing ratios there towards zero. This avoids systematic negative mixing ratios that would often be encountered otherwise and which would propagate downward.

### 3.2 The retrieval of $ClONO_2$

Beyond the pre-retrieved data mentioned in Section 3.1, and $HNO_3$, the retrieval of $CH_4$ along with $N_2O$, and of $NO_2$ precedes that of $ClONO_2$ (Fig. 1). In order to minimize error crosstalk due to spectroscopic inconsistencies, $O_3$ is fitted together with the target gas $ClONO_2$. Resulting $O_3$ mixing ratios, however, are not considered as scientifically useful and are thus discarded. As for $HNO_3$, the continuum is retrieved up to and altitude of 58 km for FR/RR NOM and RR MA measurements, and up to 44 km for RR UTLS-1 measurements.

For the retrieval we use the spectral region from 779.5 to 781.0 $cm^{-1}$ in the MIPAS A band, which contains the Q-branch of the $\nu_4$ band. Above 34 km, the spectral region from 1291.0 to 1293.5 $cm^{-1}$ in the MIPAS B band, which includes the $\nu_2$ band, is now also used for V8, in order to increase the sensitivity at higher altitudes. Interfering gases included in the simulation of the spectra but not fitted are $H_2O$, $CO_2$, $NO_2$, $HNO_3$ in both analysis windows, and additionally $N_2O$ and $CH_4$ in the MIPAS B band. Except for $CO_2$ profiles, which are taken from WACCM, profiles from the preceding steps in the V8 processing chain are used for all other interfering species. Absorption cross-sections by Wagner and Birk (2003) are used for $ClONO_2$.

While for former data versions the same vertical grid was used as described for the retrieval of $HNO_3$, for V8 a finer grid is used in order to avoid an artificial kink in the profiles showing up earlier. The grid width is 1 km up to 60 km altitude. Between 60 and 70 km the grid width is 2 km. Further grid points are 75, 80, 90, 100, and 120 km.

Up to 42 km, the Tikhonov-type regularization matrix is set altitude-constant. Above, the regularization strength is increasing with altitude. In addition, the profile points at 100 and 120 km are regularized with a diagonal term, which serves the purpose to avoid excessive negative mixing ratios due to retrieval instabilities. A constant zero profile is used as a priori.

https://doi.org/10.5194/egusphere-2026-4116
Preprint. Discussion started: 29 July 2026


### 3.3 The retrieval of $HNO_4$

Between the retrieval of $ClONO_2$ and that of $HNO_4$, CFC-12, ClO, CFC-11 along with $COCl_2$ and NO are retrieved (Fig. 1). The V8 retrieval of $HNO_4$ used the same finer vertical grid as $ClONO_2$. The spectral microwindow used for the retrieval is 802.0 to 804.0 $cm^{-1}$, similar to previous data versions, and contains lines of the $\nu_6$ band. Absorption cross-sections used are based on laboratory measurements by May and Friedl (1993) at 220 K. For V8, they are now complemented by additional cross-section spectra at 298 K, using information from Friedl et al. (1994), as documented in Wetzel et al. (2017). To minimize error propagation caused by spectroscopic inconsistencies, $O_3$ and $ClONO_2$ are fitted jointly with the target gas $HNO_4$. Resulting mixing ratios of these gases, however, are not used any further. As for the gases discussed above, the continuum is retrieved up to an altitude of 58 km, except for the UTLS-1 mode where the uppermost altitude is 44 km. Further interferents that are considered in the spectra simulation but not jointly retrieved are $H_2O$, $HNO_3$, ClO, $NO_2$ (from previous steps in the V8 retrieval chain), OCS, HCN, $C_2H_2$, $C_2H_6$, $COF_2$, HCFC-22, $CCl_4$, CFC-113, Acetone, PAN (from V5 retrievals), $CO_2$ (from WACCM), and $NH_3$, $CH_3Cl$, $C_2H_4$, $CHCl_3$, $CH_3OH$, and $BrONO_2$ (from our climatological database). In case of RR MA retrievals, if profiles for interfering species were not available from V5 RR MA processing, climatologies were built from V5 RR NOM retrievals and used in the respective latitude bands, as described above.

To stabilize the retrieval a Tikhonov-type smoothing constraint is used with an equal regularization strength throughout all altitudes. The a priori profile is zero at all altitudes. Similarly as for $ClONO_2$, the regularization matrix contains diagonal elements for the altitudes of 100 and 120 km in order to avoid excessive negative mixing ratios that would trigger unphysical profile oscillations if not suppressed.

### 3.4 The retrieval of $N_2O_5$

The validation of previous $N_2O_5$ data versions remained somewhat inconclusive and left several questions open (see Section 2). In particular, the differences to ACE-FTS measurements above and below the $N_2O_5$ vmr maximum remained a concern. Since another broad-band emitting species in the spectral vicinity of $N_2O_5$ is the $H_2SO_4$ aerosol, and spectroscopic information and a dedicated retrieval approach has become available now (Günther et al., 2018) we included the retrieval of $H_2SO_4$ total aerosol volume densities into the retrieval approach for $N_2O_5$.

With $HNO_4$ mixing ratios available, CO, $C_2H_6$ and HCFC-22 are retrieved before the retrieval of $N_2O_5$ together with $H_2SO_4$ is started (Fig. 1). The spectral window used is 1217.0 – 1276.0 $cm^{-1}$ in MIPAS channel B which covers a larger part of the $\nu_{12}$ band of $N_2O_5$. Spectroscopic information for $N_2O_5$ is from the HITRAN2016 data base (Gordon et al., 2017), while for $H_2SO_4$ total aerosol volume densities, imaginary parts of refractive indices as provided by Niedziela et al. (1999) have been used. Because of their spectral interference, $N_2O$, $CH_4$, and $H_2O$ are fitted along with the target species $N_2O_5$ and $H_2SO_4$. While resulting mixing ratios of $N_2O$, $CH_4$, and $H_2O$ are not used any further, the analysis of resulting $H_2SO_4$ volume densities is interesting in its own right but deferred to a future publication. Further interferents considered in the radiative transfer calculations but not fitted are $O_3$, $HNO_3$, $ClONO_2$, $NO_2$ (from previous steps of the V8 processing chain), $SO_2$, $C_2H_2$, $COF_2$, CFC-113, acetone (from previous V5 retrievals), $CO_2$ (from WACCM), and $NH_3$, HOCl, $H_2O_2$, $CF_4$, and CH3COOH

https://doi.org/10.5194/egusphere-2026-4116
Preprint. Discussion started: 29 July 2026


(from our climatological database). In case of RR MA retrievals, if profiles for interfering species were not available from V5 RR MA processing, climatologies were built from V5 RR NOM retrievals and used in the respective latitude bands.

The continuum is retrieved at altitudes up to 80 km, except for the UTLS-1 mode where it is limited to 44 km. The offset is retrieved against an a priori profile, while the diagonal constraint has been increased by a factor of four, compared to other trace gas retrievals in this wavenumber range, in order to stabilize the retrieval in presence of the exceptionally high-reaching continuum retrieval. For V8, the retrieval of $N_2O_5$ uses the same new vertical grid as used for $ClONO_2$ and $HNO_4$.

Similar to the other gases described above, the retrieval is stabilized with Tikhonov-type smoothing constraints with equal regularization strengths throughout all altitudes, and the a priori profiles are zero at all altitudes. Diagonal terms in the regularization matrices are used for 100 and 120 km altitudes to constrain the retrieved profiles to zero.

## 4 Data characterization

### 4.1 Averaging kernels and vertical resolution

Averaging kernel matrices are an appropriate means to characterize the vertical resolution of a retrieval and its content of prior information (Rodgers, 2000). Figures 2 to 7 show the averaging kernels of $HNO_3$, $ClONO_2$, $HNO_4$, and $N_2O_5$ for one specific profile each, and the vertical resolutions along an example orbit, for the FR NOM, RR NOM, and RR MA observation modes. The vertical resolutions are derived from the full widths at half maximum of the averaging kernel rows.

The vertical resolution of FR NOM $HNO_3$ retrievals varies between 2 and 4 km in the lower and middle stratosphere (Fig. 3). In the upper stratosphere the vertical resolution is around 6 km, with two lower-resolved thin layers in between. The vertical resolution is generally better at altitudes where the vertical grid point is close to a tangent altitude of the measurement, and slightly coarser between two tangent altitudes. Conversely, retrieval noise is larger where a grid point is close to a tangent altitude, because the retrieved value depends largely on this particular measurement; in turn, retrieval noise is smaller for data points between two tangent altitudes, because the retrieved value depends largely on two measurements. This is a feature of all retrievals performed on retrieval grids finer than the tangent altitude spacing. Below 55 km, the averaging kernels peak at the nominal altitudes (Fig. 2). V8 $HNO_3$ from the FR NOM observation mode is recommended for use between 5 and 55 km altitude.

For RR NOM $HNO_3$ retrievals, the vertical resolution is better than for FR NOM in the lower to middle stratosphere, but worse in the mesosphere (Fig. 5). It varies between 2 and 3 km up to 35 km, is around 4 to 6 km up to 55 km, but worse than 8 km above. The averaging kernels peak at the nominal altitudes up to about 60 km (Fig. 4). The recommended altitude range is 5 to 55 km.

V8 RR MA $HNO_3$ profiles start around 16 km and provide a vertical resolution of about 3 to 4 km in the lower to middle stratosphere (Fig. 7). Similar to RR NOM observations, it increases to around 6 km in the upper stratosphere and lower mesosphere, and to beyond 8 km above 60 km. The recommended altitude range is 16 to 55 km.

The behaviour of $ClONO_2$ for the various observation modes is quite similar to that of $HNO_3$, except that the useful altitude range is restricted to below 45 km, and averaging kernels peak typically at their nominal tangent altitude up to 40 km (Figs. 2,

https://doi.org/10.5194/egusphere-2026-4116
Preprint. Discussion started: 29 July 2026


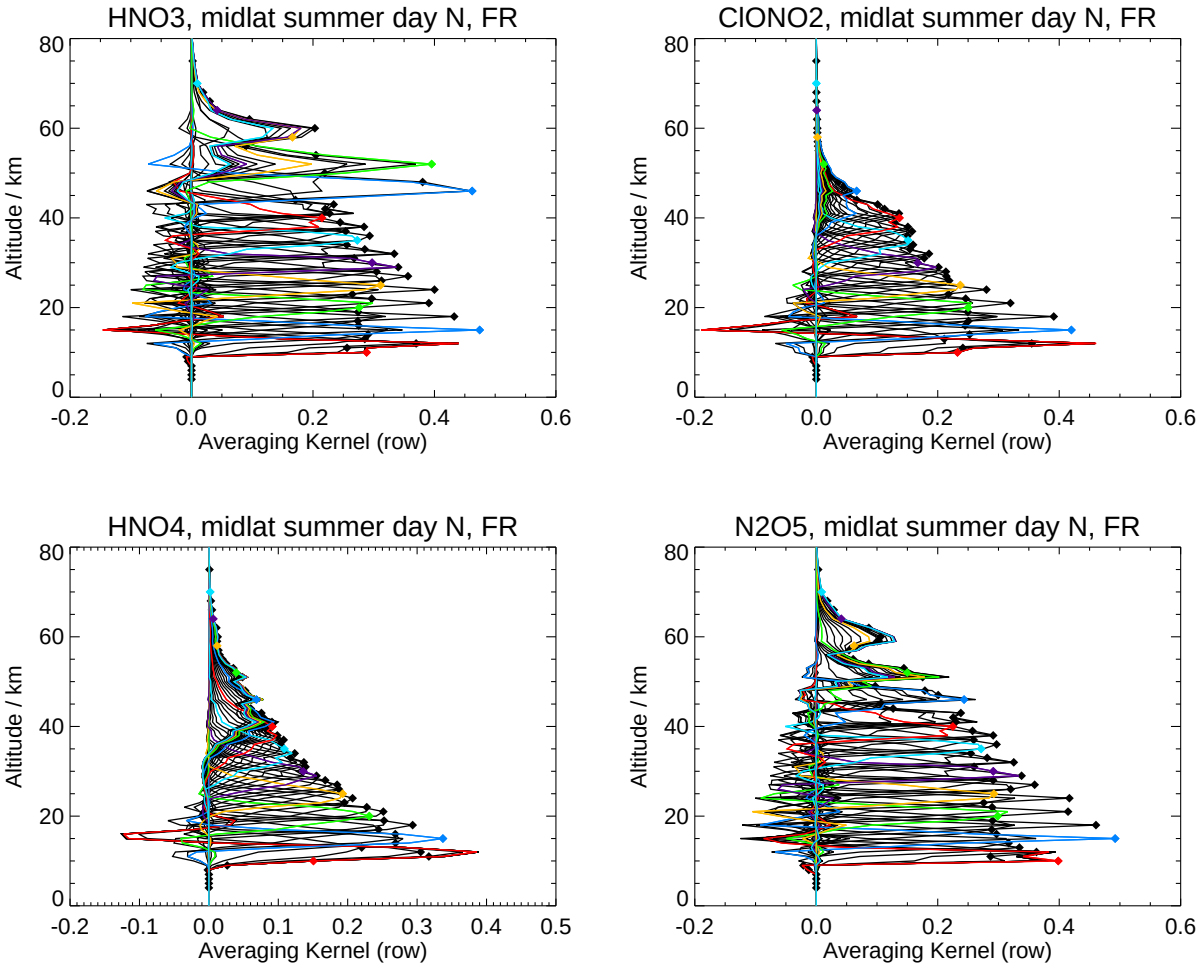


**Figure 2.** Profile averaging kernels of MIPAS $HNO_3$, $ClONO_2$, $HNO_4$, and $N_2O_5$ retrievals from FR NOM spectra. Some of the averaging kernels are coloured to make them easier to distinguish. The averaging kernels refer to a limb sequence recorded at 46.1°N, 41.0°E during Envisat orbit 06974 on 1 July 2003.

https://doi.org/10.5194/egusphere-2026-4116
Preprint. Discussion started: 29 July 2026


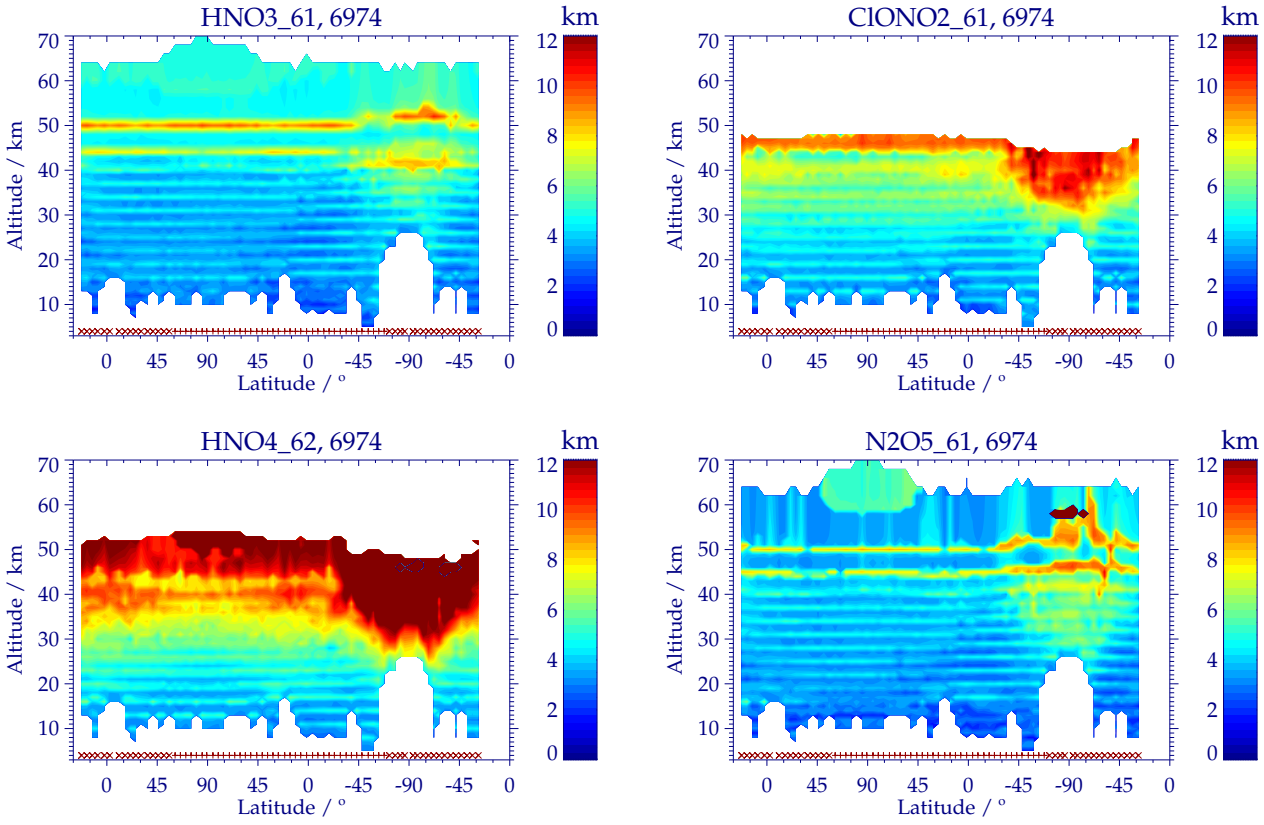


**Figure 3.** Vertical resolution of MIPAS $HNO_3$, $ClONO_2$, $HNO_4$, and $N_2O_5$ retrievals from FR NOM spectra along Envisat orbit 06974 recorded on 1 July 2003. The crosses and plus signs at the bottom of the panels mark the ascending (10 pm) and descending (10 am) orbit legs, respectively.

4, and 6). The vertical resolution in the lower to middle atmosphere up to ∼30 km is typically 3–5 km/2–4.5 km/4–5 km in the FR NOM/RR NOM/RR MA observation modes, and deteriorates to 6–9 km in the upper stratosphere/lower mesosphere for all observation modes (Figs. 3, 5, and 7).

The vertical resolution of $HNO_4$ in the stratosphere below 30 km is 3–5 km/2–4.5 km/4–5 km for the FR NOM/RR NOM/RR MA observation modes (Figs. 3, 5, and 7). Above that altitude, it deteriorates to 8 km and more, with polar winter conditions leading to even stronger deterioration. The averaging kernels peak at their nominal tangent altitudes up to altitudes of 35 km (Figs. 2, 4, and 6). Above about 40 km, no relevant information is available, and we recommend not to use the data above this height.

From the FR NOM observation mode, $N_2O_5$ is retrieved with a vertical resolution of 2 to 5 km over almost the full altitude range up to 60 km, with slightly worse vertical resolution around 6-8 km under polar winter conditions (Fig. 3). For the RR

https://doi.org/10.5194/egusphere-2026-4116
Preprint. Discussion started: 29 July 2026


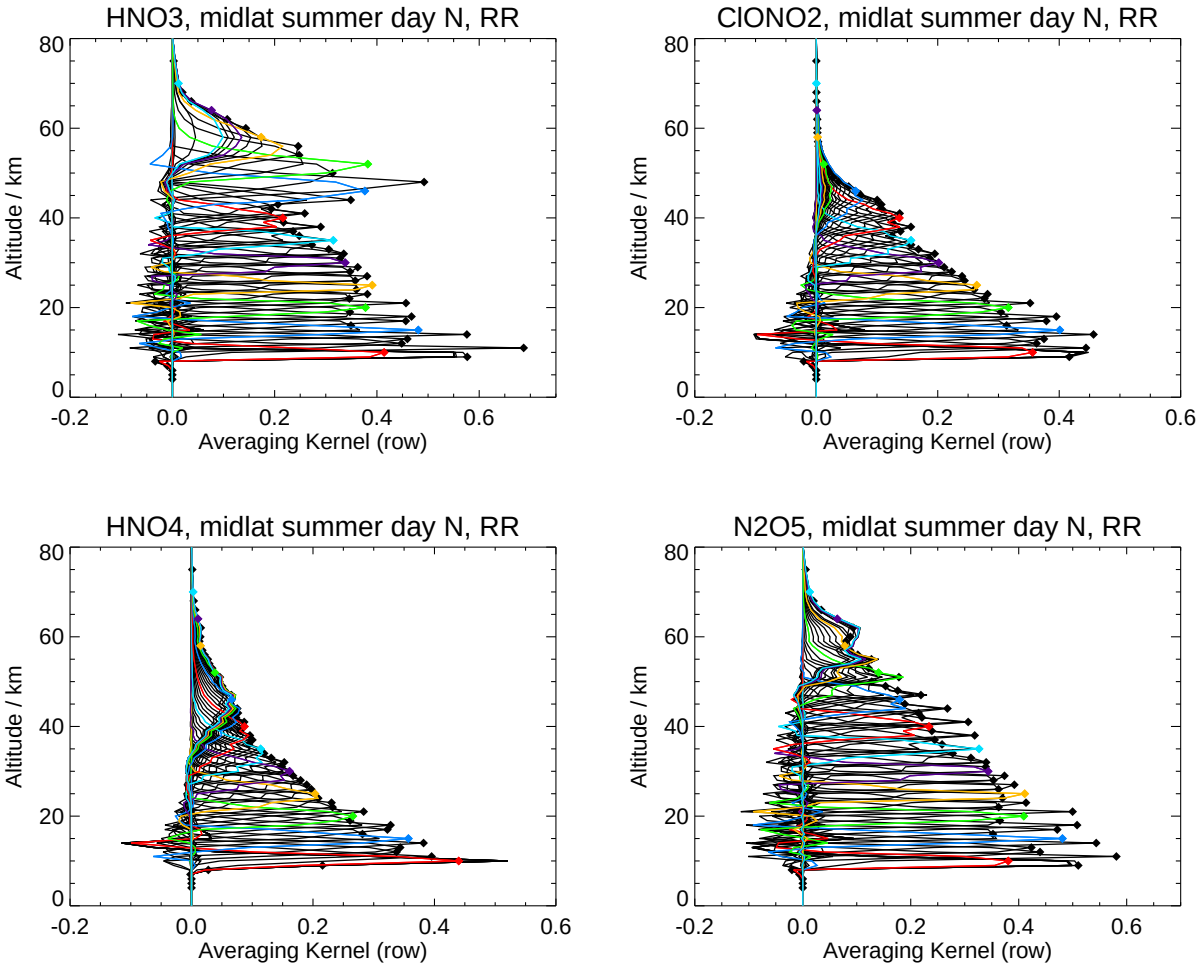


**Figure 4.** Profile averaging kernels of MIPAS $HNO_3$, $ClONO_2$, $HNO_4$, and $N_2O_5$ retrievals from RR NOM spectra. Some of the averaging kernels are coloured to make them easier to distinguish. The averaging kernels refer to a limb sequence recorded at 47.5°N, 103.8°W during Envisat orbit 38371 on 2 July 2009.

https://doi.org/10.5194/egusphere-2026-4116
Preprint. Discussion started: 29 July 2026


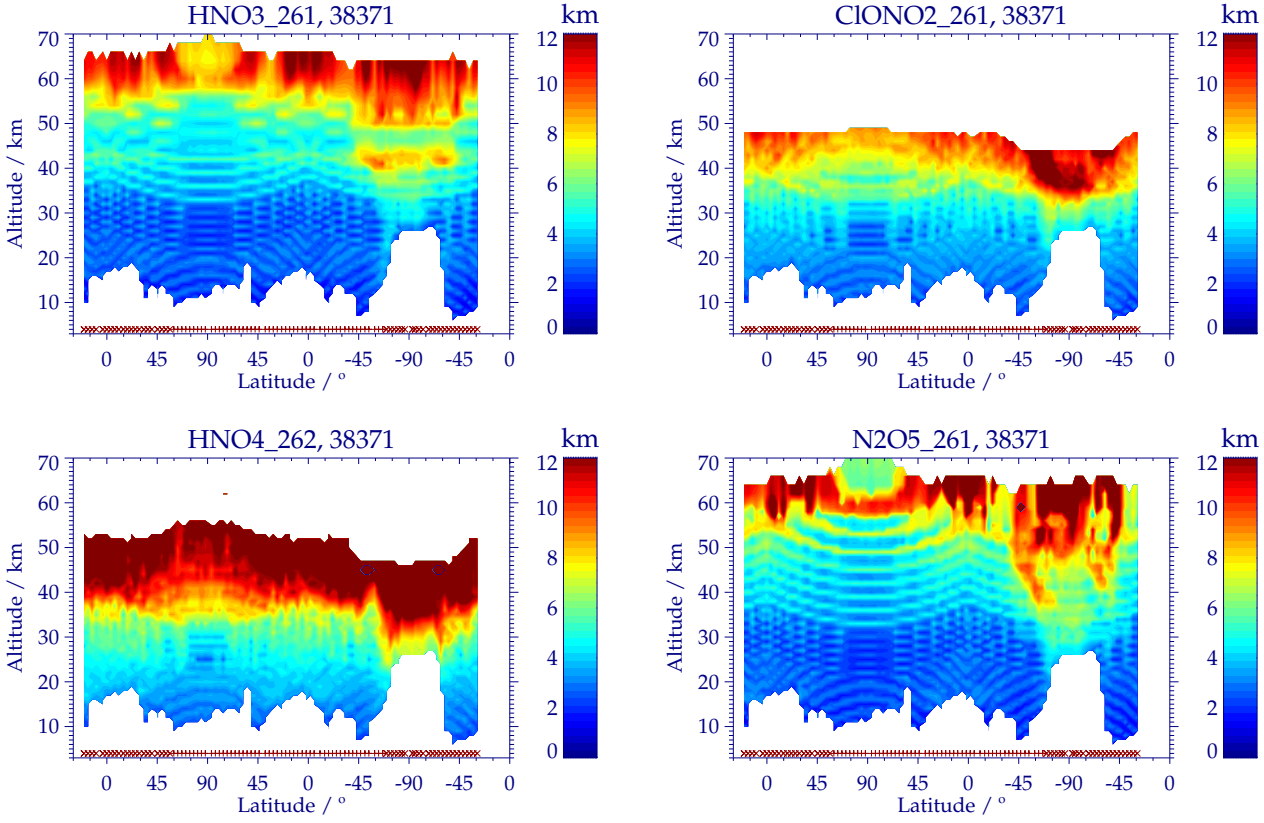


**Figure 5.** Vertical resolution of MIPAS $HNO_3$, $ClONO_2$, $HNO_4$, and $N_2O_5$ retrievals from RR NOM spectra along Envisat orbit 38371 recorded on 2 July 2009. The crosses and plus signs at the bottom of the panels mark the ascending (10 pm) and descending (10 am) orbit legs, respectively.

NOM observation mode, the vertical resolution is better than 3.5 km below 30 km altitude, 4 to 6 km in the upper stratosphere, and beyond 8 km in the mesosphere (Fig. 5). For the RR MA mode, the vertical resolution is 3 to 5 km up to about 45 km, better than 8 km up to 55 km, and beyond 8 km above (Fig. 7). For all observation modes, the averaging kernels peak at their nominal tangent altitudes up to about 60 km (Figs. 2, 4, and 6). The use of V8 $N_2O_5$ data is therefore recommended between 5 and 60 km.

### 4.2 Horizontal information smearing and displacement

For the characterization of the horizontal smearing and displacement of information, we use the horizontal averaging kernel matrix, following the concept proposed by von Clarmann et al. (2009a). The horizontal distance between the averaging-kernel-weighted mean of the horizontal coordinate and the nominal geolocation of the limb scan (set at 30 km for FR NOM and RR

https://doi.org/10.5194/egusphere-2026-4116
Preprint. Discussion started: 29 July 2026


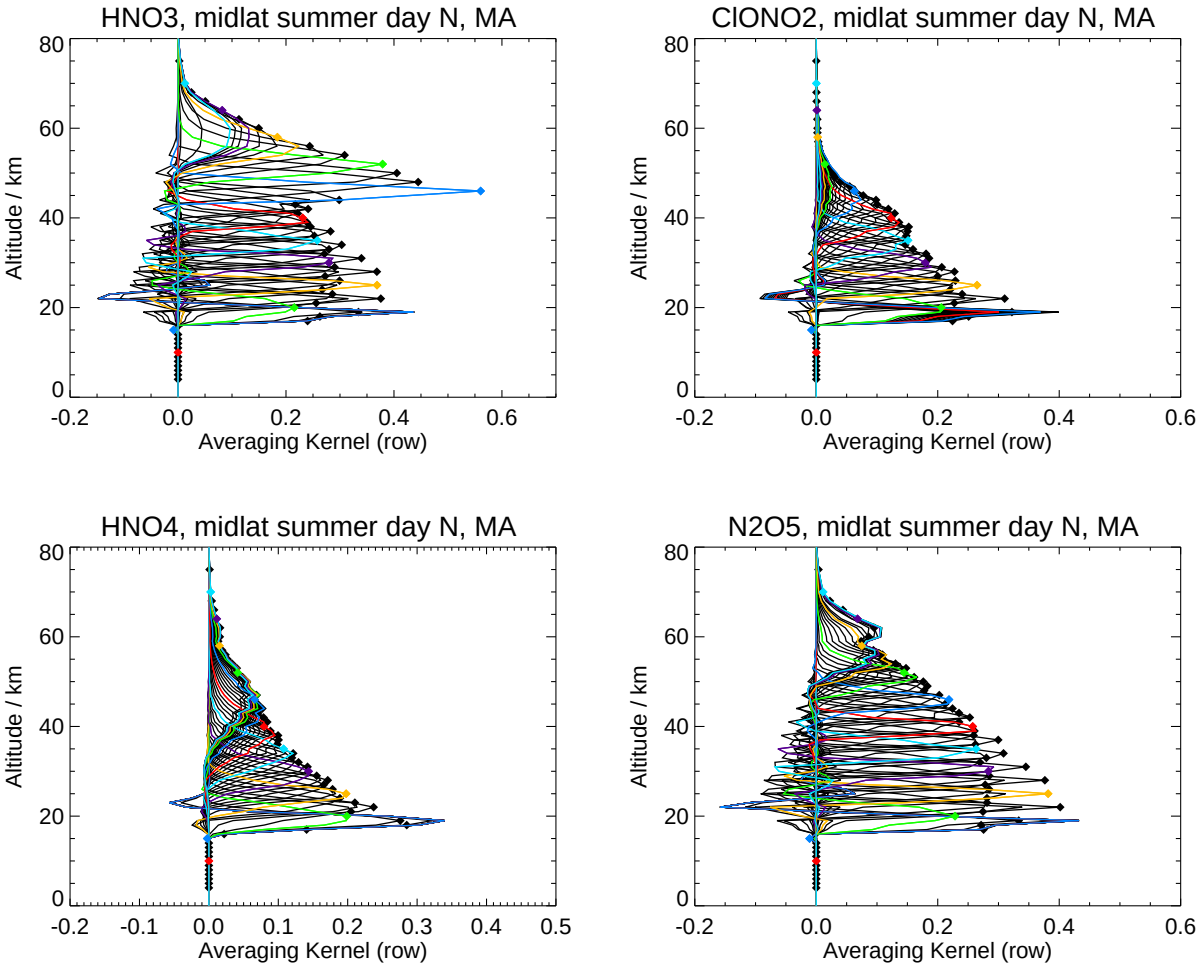


**Figure 6.** Profile averaging kernels of MIPAS $HNO_3$, $ClONO_2$, $HNO_4$, and $N_2O_5$ retrievals from RR MA spectra. Some of the averaging kernels are coloured to make them easier to distinguish. The averaging kernels refer to a limb sequence recorded at 45.6°N, 74.1°E during Envisat orbit 38550 on 15 July 2009.

https://doi.org/10.5194/egusphere-2026-4116
Preprint. Discussion started: 29 July 2026


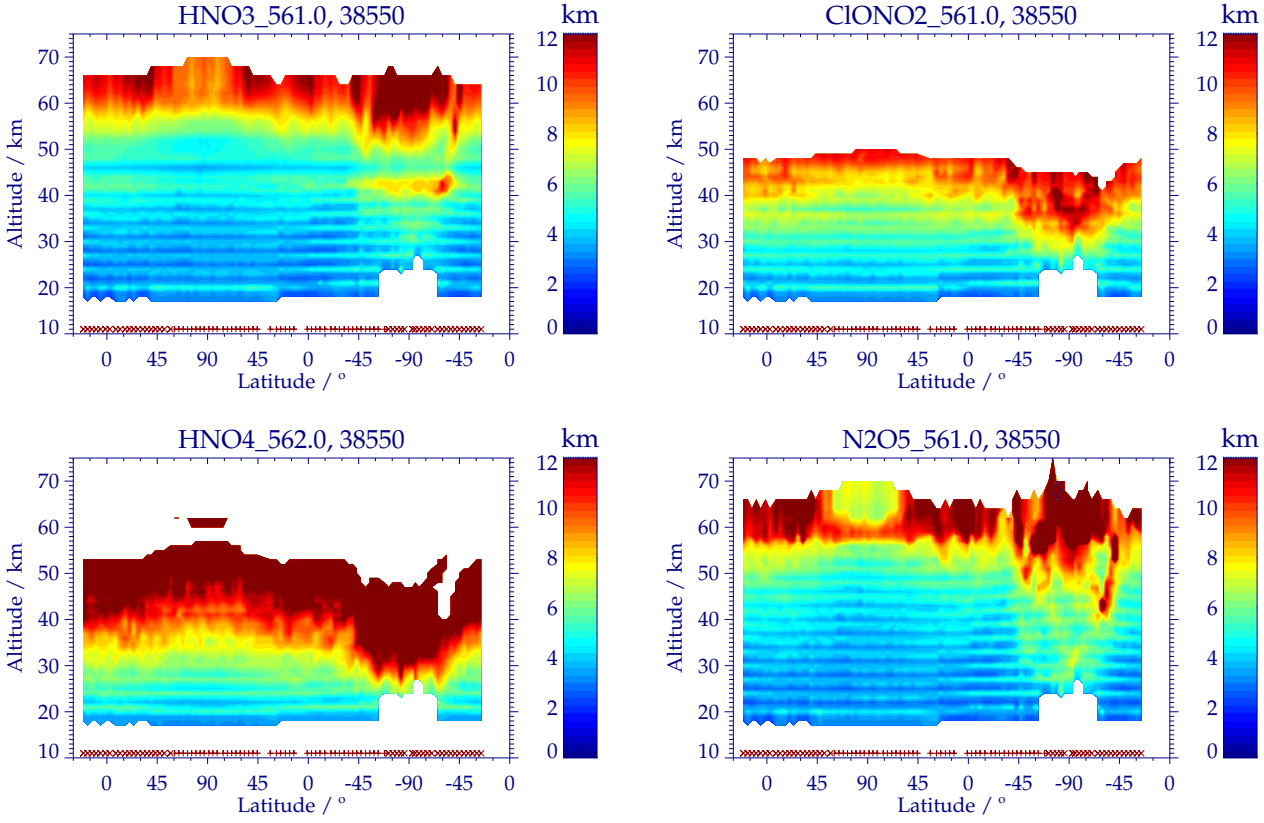


**Figure 7.** Vertical resolution of MIPAS $HNO_3$, $ClONO_2$, $HNO_4$, and $N_2O_5$ retrievals from RR MA spectra along Envisat orbit 38550 recorded on 2 July 2009. The crosses and plus signs at the bottom of the panels mark the ascending (10 pm) and descending (10 am) orbit legs, respectively.

NOM modes, and at 60 km for the RR MA mode) is used as a metric of the horizontal information displacement. Positive signs indicate information displacements towards the satellite. The respective standard deviation multiplied by $2\sqrt{2\ln 2}$ is used as a metric of information smearing. As long as the information distribution follows a normal distribution, this metric is equivalent with the full width at half maximum of the vertically integrated 2D averaging kernels. It is, however, much more robust for bi- or multi-modal information distributions.

In Tables 4–6, the information displacements for the target gases are shown for an FR NOM (orbit 6075, 47.9°S, 39.8°W, 29 April 2003, 22° solar elevation) an RR NOM (orbit 39483, 57.1°S, 176.1°W, 18 September 2009, -32.5° solar elevation), and an RR MA (orbit 39520, 45.0°N, 15.1°W, 20 September 2009, -39.0° solar elevation) measurement. Tables 7–9 show the horizontal information smearing for the measurements mentioned above.

https://doi.org/10.5194/egusphere-2026-4116
Preprint. Discussion started: 29 July 2026


**Table 4.** Information displacement, FR NOM observation mode. Positive values mean displacement towards the satellite.

| Altitude /km | $HNO_3$ /km | $ClONO_2$ /km | $HNO_4$ /km | $N_2O_5$ /km |
|---|---|---|---|---|
| 60 | | | | -126.2 |
| 54 | -126.6 | | | -122.3 |
| 50 | -112.7 | | | -113.0 |
| 44 | -86.6 | -75.9 | | -87.3 |
| 40 | -68.2 | -60.1 | -48.4 | -70.0 |
| 35 | -21.5 | -22.9 | -18.2 | -22.0 |
| 30 | 17.0 | 14.1 | 14.5 | 18.2 |
| 25 | 56.0 | 54.0 | 52.5 | 58.4 |
| 20 | 94.2 | 90.9 | 89.6 | 89.9 |
| 15 | 124.0 | 121.9 | 119.1 | 123.5 |
| 10 | 148.9 | 143.9 | 142.4 | 169.9 |

**Table 5.** Information displacement, RR NOM observation mode. Positive values mean displacement towards the satellite.

| Altitude /km | $HNO_3$ /km | $ClONO_2$ /km | $HNO_4$ /km | $N_2O_5$ /km |
|---|---|---|---|---|
| 60 | | | | -64.4 |
| 54 | -62.2 | | | -59.1 |
| 50 | -57.6 | | | -57.3 |
| 44 | -42.4 | -41.8 | | -49.5 |
| 40 | -28.9 | -34.7 | -30.9 | -35.9 |
| 35 | -21.6 | -16.6 | -17.1 | -24.4 |
| 30 | 2.6 | 1.8 | 1.6 | 1.1 |
| 25 | 23.5 | 21.5 | 25.6 | 25.1 |
| 20 | 58.8 | 53.7 | 56.8 | 60.8 |
| 15 | 88.9 | 83.7 | 84.3 | 97.5 |
| 10 | 105.4 | 100.6 | 104.1 | 126.2 |

https://doi.org/10.5194/egusphere-2026-4116
Preprint. Discussion started: 29 July 2026


**Table 6.** Information displacement, RR MA observation mode. Positive values mean displacement towards the satellite.

| Altitude /km | $HNO_3$ /km | $ClONO_2$ /km | $HNO_4$ /km | $N_2O_5$ /km |
|---|---|---|---|---|
| 60 | | | | 18.4 |
| 54 | 25.2 | | | 27.6 |
| 50 | 37.0 | | | 37.7 |
| 44 | 52.5 | 57.2 | | 53.2 |
| 40 | 68.3 | 67.1 | 70.9 | 68.7 |
| 35 | 77.8 | 77.9 | 80.5 | 77.5 |
| 30 | 89.7 | 88.4 | 91.1 | 89.0 |
| 25 | 107.3 | 104.9 | 103.6 | 105.7 |
| 20 | 117.4 | 114.5 | 113.3 | 116.2 |

**Table 7.** Information smearing, FR NOM observation mode.

| Altitude /km | $HNO_3$ /km | $ClONO_2$ /km | $HNO_4$ /km | $N_2O_5$ /km |
|---|---|---|---|---|
| 60 | | | | 480.8 |
| 54 | 474.9 | | | 479.2 |
| 50 | 425.1 | | | 483.7 |
| 44 | 399.5 | 506.8 | | 432.1 |
| 40 | 363.1 | 505.4 | 521.5 | 381.2 |
| 35 | 330.3 | 434.8 | 483.0 | 336.8 |
| 30 | 328.6 | 358.4 | 399.2 | 331.1 |
| 25 | 347.7 | 328.9 | 352.2 | 335.1 |
| 20 | 359.1 | 320.3 | 328.0 | 329.8 |
| 15 | 374.7 | 330.9 | 307.0 | 339.4 |
| 10 | 376.7 | 353.3 | 310.8 | 357.4 |

For all species and for FR and RR NOM observation modes, information is displaced towards the satellite for altitudes up to above 30 km, and beyond the tangent altitude above. The displacement is generally larger for FR NOM measurements than for RR NOM measurements. Largest values are found for FR NOM $N_2O_5$ (170 km at 10 km altitude). All information displacement values are significantly smaller than the horizontal sampling of MIPAS (FR NOM: 510 km; RR NOM; 410 km; RR MA: 430 km). For the RR MA mode, all displacements are positive, i.e. towards the satellite. This is because the nominal geolocation of RR MA limb scans refers to a tangent point at about 60 km altitude. As for FR and RR NOM modes, the information displacement values are again far smaller than the horizontal sampling.

The information smearing takes values between 290 km (RR NOM $HNO_4$ at 10 km) and 535 km (RR NOM $HNO_4$ at 40 km). In some cases, the information smearing exceeds the horizontal sampling. However, in the lower stratosphere the horizontal resolution is still dominated by the horizontal sampling and not by the information smearing.

https://doi.org/10.5194/egusphere-2026-4116
Preprint. Discussion started: 29 July 2026


**Table 8.** Information smearing, RR NOM observation mode.

| Altitude /km | $HNO_3$ /km | $ClONO_2$ /km | $HNO_4$ /km | $N_2O_5$ /km |
|---|---|---|---|---|
| 60 | | | | 458.4 |
| 54 | 458.0 | | | 476.9 |
| 50 | 403.5 | | | 449.1 |
| 44 | 369.7 | 501.8 | | 361.9 |
| 40 | 375.8 | 513.1 | 535.0 | 362.0 |
| 35 | 324.3 | 455.0 | 503.4 | 330.7 |
| 30 | 313.9 | 378.4 | 423.0 | 324.5 |
| 25 | 310.7 | 344.3 | 366.7 | 308.9 |
| 20 | 312.8 | 314.5 | 326.3 | 301.0 |
| 15 | 308.1 | 305.7 | 304.9 | 320.3 |
| 10 | 294.6 | 290.0 | 289.8 | 324.4 |

**Table 9.** Information smearing, RR MA observation mode.

| Altitude /km | $HNO_3$ /km | $ClONO_2$ /km | $HNO_4$ /km | $N_2O_5$ /km |
|---|---|---|---|---|
| 60 | | | | 418.2 |
| 54 | 407.8 | | | 424.8 |
| 50 | 356.0 | | | 387.8 |
| 44 | 338.2 | 497.7 | | 336.5 |
| 40 | 338.6 | 489.8 | 515.8 | 331.3 |
| 35 | 318.7 | 418.2 | 461.5 | 324.3 |
| 30 | 314.5 | 358.8 | 395.2 | 323.0 |
| 25 | 327.8 | 332.2 | 365.1 | 330.3 |
| 20 | 337.8 | 311.6 | 315.0 | 335.2 |

### 4.3 Error budget

MIPAS errors have been analyzed following the recommendations published by the "Atmospheric Processes And their Role in Climate – Towards Unified Error Reporting (APARC-TUNER)" activity (von Clarmann et al., 2020) and described by von Clarmann et al. (2022). Random and systematic uncertainties are calculated for classes of atmospheric conditions that are set up from latitude bands, seasons and day-and-night conditions for all relevant observation modes, on basis of a subset of representative observations for each class (see Supplements for the list of classes). In the data repository, every profile is assigned to one of the classes, and respective uncertainties are provided for the profiles, including scaling to the actual profile values in case the uncertainties are of relative nature. In the following, we provide a species-by-species discussion of the ingoing uncertainties and the resulting error components for the example class of RR NOM Southern polar winter night

https://doi.org/10.5194/egusphere-2026-4116
Preprint. Discussion started: 29 July 2026


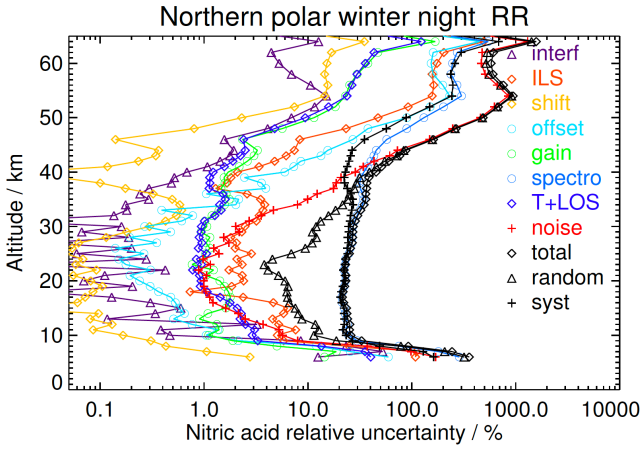


**Figure 8.** $HNO_3$ error budget for RR NOM Northern polar winter night conditions.

measurements. The error information for all other classes and observation modes, in terms of tables and figures, are collected in the supplements for all species separately.

### 4.3.1 The $HNO_3$ error budget

Error sources affecting the retrieval of $HNO_3$ are summarized and quantified in Table 10 for the RR NOM observation mode. Similar tables for the FR NOM and RR MA observation modes are presented in the Supplement.

Figure 8 presents the resulting error budget of $HNO_3$ for RR NOM Northern polar winter night observations. Error budgets for all other atmospheric conditions and observation modes are collected in the Supplement. Below 10 km altitude the random error, dominated by measurement noise, and the systematic error, dominated by spectroscopic uncertainty, contribute roughly equally to a total error of far beyond 100%. In the altitude range of the stratospheric $HNO_3$ maximum, the total random error amounts to 3 to 10%, while the systematic error, again dominated by spectroscopic uncertainty, increases the total (random + systematic) error to about 20 – 30%. Above 40 km, the $HNO_3$ total error increases strongly, mainly due to measurement noise. This means that while the absolute stratospheric $HNO_3$ abundances below 40 km are rather uncertain and may be biased, variability studies will benefit from the rather good precision of the observations.

### 4.3.2 The $ClONO_2$ error budget

Ingoing uncertainties used for the $ClONO_2$ error analysis are compiled in Table 11 for the RR NOM observation mode. Similar Tables for the MIPAS FR NOM and RR MA observation modes are presented in the Supplement.

Figure 9 presents the resulting error budget of $ClONO_2$ for RR NOM Northern polar winter night observations. Error budgets for all other atmospheric conditions and observation modes are collected in the Supplement. The leading uncertainty in the troposphere below 10 km is the measurement noise. In the stratosphere, below 35 km, the total (random + systematic)

https://doi.org/10.5194/egusphere-2026-4116
Preprint. Discussion started: 29 July 2026


**Table 10.** Assumed $1\sigma$ uncertainties affecting the retrieval of $HNO_3$ (RR NOM)

| Type of Uncertainty | Value / typical value[1] | Source[2] | Propagation Method[3] |
|---|---|---|---|
| noise (A band) | 20 nW/(cm$^2$ sr cm$^{-1}$) | Kleinert et al. (2018) | G(16) |
| noise (B band) | 10 nW/(cm$^2$ sr cm$^{-1}$) | Kleinert et al. (2018) | G(16) |
| offset (A band) | 3 nW/ (cm$^2$ sr cm$^{-1}$) | Kleinert et al. (2018) | G(5;13) |
| offset (B band) | 1.5 nW/ (cm$^2$ sr cm$^{-1}$) | Kleinert et al. (2018) | G(5;13) |
| gain random (A and B band) | 0.21% | Kleinert et al. (2018) | P(21;22) |
| gain systematic (A band) | 1.15% | Kleinert et al. (2018) | P(21;22) |
| gain systematic (B band) | 1.03% | Kleinert et al. (2018) | P(21;23) |
| spectral shift | 0.00029 cm$^{-1}$ | preceding V8 retrieval (Kiefer et al., 2021) | P(7) |
| ILS | 3% | Hase (2000, 2003) | P(7;14;15) |
| Temp., noise | 0.22 - 1.23 K | preceding V8 retrieval Kiefer et al. (2021) | G(6) |
| Tang. alt., noise | 29 - 52 m | preceding V8 retrieval Kiefer et al. (2021) | G(6) |
| Temp. spectral shift | 0.01 - 0.10 K | preceding V8 retrieval Kiefer et al. (2021) | P(17) |
| Tang. alt., spectral shift | 1 - 15 m | preceding V8 retrieval Kiefer et al. (2021) | P(17) |
| Temp., offset | 0.03 - 0.45 K | preceding V8 retrieval Kiefer et al. (2021) | P(7) |
| Tang. alt., offset | 8 - 16 m | preceding V8 retrieval Kiefer et al. (2021) | P(7) |
| Temp., ILS | 0.05 - 1.16 K | preceding V8 retrieval Kiefer et al. (2021) | P(7) |
| Tang. alt., ILS | 8 - 113 m | preceding V8 retrieval Kiefer et al. (2021) | P(7) |
| Temp., $CO_2$ intensities | 0.03 - 0.18 K | preceding V8 retrieval Kiefer et al. (2021) | P(7;26;27) |
| Tang. alt., $CO_2$ intensities | 26 - 34 m | preceding V8 retrieval Kiefer et al. (2021) | P(7;26;27) |
| Temp., $CO_2$ broadening | 0.14 - 1.47 K | preceding V8 retrieval Kiefer et al. (2021) | P(7;28;29) |
| Tang. alt., $CO_2$ broadening | 198 - 252 m | preceding V8 retrieval Kiefer et al. (2021) | P(7;28;29) |
| Temp., gain, syst. | 0.22 - 0.81 K | preceding V8 retrieval Kiefer et al. (2021) | P(21) |
| Tang. alt., gain, syst. | 1 - 49 m | preceding V8 retrieval Kiefer et al. (2021) | P(21) |
| Temp., gain, random | 0.04 - 0.15 K | preceding V8 retrieval Kiefer et al. (2021) | P(21) |
| Tang. alt., gain, random | 0.2 - 9 m | preceding V8 retrieval Kiefer et al. (2021) | P(21) |
| vmr($C_2H_2$) | 3.22E-06 - 9.55E-06 ppmv | V5 retrieval (Wiegele et al., 2012) | G(6) |
| vmr($C_2H_6$) | 2.77E-07 - 7.56E-05 ppmv | V5 retrieval (Wiegele et al., 2012) | G(6) |
| vmr($CH_4$) | 1.03E-02 - 1.44E-01 ppmv | V5 retrieval (Plieninger et al., 2015) | G(6) |
| vmr($CO_2$) | 7.56E-01 - 7.51E+00 ppmv | WACCM model calc. (Kiefer et al., 2021) | P(20) |
| vmr(ClO) | 1.50E-05 - 6.60E-04 ppmv | V5 retrieval (von Clarmann et al., 2013) | G(6) |
| vmr(HCN) | 1.54E-05 - 4.41E-05 ppmv | V5 retrieval (Wiegele et al., 2012) | G(6) |
| vmr($H_2O_2$) | 3.03E-06 - 1.12E-04 ppmv | database (Kiefer et al., 2002) | P(7;11) |
| vmr($H_2O$) | 1.87E-01 - 2.24E-00 ppmv | preceding V8 retrieval (Kiefer et al., 2024) | G(6) |
| vmr(HOCl) | 2.12E-06 - 7.27E-05 ppmv | database (Kiefer et al., 2002) | P(7;11) |
| vmr($O_3$) | 2.48E-02 - 8.52E-02 ppmv | preceding V8 retrieval (Kiefer et al., 2023) | G(6) |
| vmr($N_2O$) | 3.14E-04 - 1.59E-02 ppmv | V5 retrieval (Plieninger et al., 2015) | G(6) |
| vmr($SO_2$) | 5.95E-05 - 4.24E-04 ppmv | V5 retrieval (Höpfner et al., 2015) | G(6) |
| vmr($NH_3$) | 7.18E-12 - 3.75E-05 ppmv | database (Kiefer et al., 2002) | P(7;11) |
| vmr($NO_2$) | 7.49E-08 - 3.77E-04 ppmv | V5 retrieval (Funke et al., 2005b) | G(6) |
| vmr(OCS) | 3.37E-05 - 2.14E-04 ppmv | V5 retrieval (Glatthor et al., 2017) | G(6) |
| vmr(CFC-11) | 2.64E-08 - 5.94E-06 ppmv | V5 retrieval (Kellmann et al., 2012) | G(6) |
| vmr(CFC-12) | 1.09E-05 - 1.57E-04 ppmv | V5 retrieval (Kellmann et al., 2012) | G(6) |
| vmr(HCFC-22) | 4.78E-06 - 1.46E-05 ppmv | V5 retrieval (Chirkov et al., 2016) | G(6) |
| vmr($ClONO_2$) | 7.38E-06 - 1.04E-04 ppmv | V5 retrieval (von Clarmann et al., 2013) | G(6) |
| line intensities | 25% | Flaud et al. (2015); Rothman et al. (2009) | P(7) |
| broadening coeff. | 7.5% | Flaud et al. (2015); Rothman et al. (2009) | P(7) |

[1] For variable uncertainties typical values are reported. Some errors in Kleinert et al. (2018) given in terms of $2\sigma$ were re-scaled them to $1\sigma$. [2] In some cases unpublished V5 data were used. In these cases, reference to an earlier data version is made. [3] Temperature and tangent altitude errors due to noise, spectral shift, and offset are propagated separately. The notation is as follows: "G" refers to generalized Gaussian error propagation in a matrix formalism, while "P" refers to perturbation studies. The numbers in parentheses are the respective equation numbers in von Clarmann et al. (2022).

https://doi.org/10.5194/egusphere-2026-4116
Preprint. Discussion started: 29 July 2026


**Table 11.** Assumed $1\sigma$ uncertainties affecting the retrieval of $ClONO_2$ (RR NOM)

| Type of Uncertainty | Value / typical value[1] | Source[2] | Propagation Method[3] |
|---|---|---|---|
| noise (A band) | 20 nW/(cm$^2$ sr cm$^{-1}$) | Kleinert et al. (2018) | G(16) |
| noise (B band) | 10 nW/(cm$^2$ sr cm$^{-1}$) | Kleinert et al. (2018) | G(16) |
| offset (A band) | 3 nW/ (cm$^2$ sr cm$^{-1}$) | Kleinert et al. (2018) | G(5;13) |
| offset (B band) | 1.5 nW/ (cm$^2$ sr cm$^{-1}$) | Kleinert et al. (2018) | G(5;13) |
| gain random (A and B band) | 0.21% | Kleinert et al. (2018) | P(21;22) |
| gain systematic (A band) | 1.15% | Kleinert et al. (2018) | P(21;22) |
| gain systematic (B band) | 1.03% | Kleinert et al. (2018) | P(21;23) |
| spectral shift | 0.00029 cm$^{-1}$ | preceding V8 retrieval (Kiefer et al., 2021) | P(7) |
| ILS | 3% | Hase (2000, 2003) | P(7;14;15) |
| Temp., noise | 0.22 - 1.23 K | preceding V8 retrieval Kiefer et al. (2021) | G(6) |
| Tang. alt., noise | 29 - 52 m | preceding V8 retrieval Kiefer et al. (2021) | G(6) |
| Temp., spectral shift | 0.01 - 0.10 K | preceding V8 retrieval Kiefer et al. (2021) | P(17) |
| Tang. alt., spectral shift | 1 - 15 m | preceding V8 retrieval Kiefer et al. (2021) | P(17) |
| Temp., offset | 0.03 - 0.45 K | preceding V8 retrieval Kiefer et al. (2021) | P(7) |
| Tang. alt., offset | 8 - 16 m | preceding V8 retrieval Kiefer et al. (2021) | P(7) |
| Temp., ILS | 0.05 - 1.16 K | preceding V8 retrieval Kiefer et al. (2021) | P(7) |
| Tang. alt., ILS | 8 - 113 m | preceding V8 retrieval Kiefer et al. (2021) | P(7) |
| Temp., $CO_2$ intensities | 0.03 - 0.18 K | preceding V8 retrieval Kiefer et al. (2021) | P(7;26;27) |
| Tang. alt., $CO_2$ intensities | 26 - 34 m | preceding V8 retrieval Kiefer et al. (2021) | P(7;26;27) |
| Temp., $CO_2$ broadening | 0.14 - 1.47 K | preceding V8 retrieval Kiefer et al. (2021) | P(7;28;29) |
| Tang. alt., $CO_2$ broadening | 198 - 252 m | preceding V8 retrieval Kiefer et al. (2021) | P(7;28;29) |
| Temp., gain, syst. | 0.22 - 0.81 K | preceding V8 retrieval Kiefer et al. (2021) | P(21) |
| Tang. alt., gain, syst. | 1 - 49 m | preceding V8 retrieval Kiefer et al. (2021) | P(21) |
| Temp., gain, random | 0.04 - 0.15 K | preceding V8 retrieval Kiefer et al. (2021) | P(21) |
| Tang. alt., gain, random | 0.2 - 9 m | preceding V8 retrieval Kiefer et al. (2021) | P(21) |
| vmr($CH_4$) | 7.76E-03 - 9.78E-02 ppmv | preceding V8 retrieval (Glatthor et al., 2024a) | G(6) |
| vmr($CO_2$) | 7.56E-01 - 7.51E+00 ppmv | WACCM model calc. (Kiefer et al., 2021) | P(20) |
| vmr($H_2O$) | 1.87E-01 - 2.24E+00 ppmv | preceding V8 retrieval (Kiefer et al., 2024) | G(6) |
| vmr($N_2O$) | 3.73E-04 - 1.03E-02 ppmv | preceding V8 retrieval (Glatthor et al., 2024a) | G(6) |
| vmr($NO_2$) | 2.03E-07 - 2.88E-04 ppmv | preceding V8 retrieval (Funke et al., 2026) | G(6) |
| vmr($HNO_3$) | 5.54E-05 - 4.51E-04 ppmv | preceding V8 retrieval (this paper) | G(6) |
| spectroscopic data | 2.5% | Wagner and Birk (2003) | P(7) |

[1] For variable uncertainties typical values are reported. Some errors in Kleinert et al. (2018) are given in terms of $2\sigma$; we have re-scaled them to $1\sigma$. [2] In some cases V5 data were used of which no journal publication is available. In these cases, reference to an earlier data version is made. [3] Temperature and tangent altitude errors due to noise, spectral shift, and offset are propagated separately. The notation is as follows: "G" refers to generalized Gaussian error propagation in a matrix formalism, while "P" refers to perturbation studies. The numbers in parentheses are the respective equation numbers in von Clarmann et al. (2022).

uncertainty of $ClONO_2$ is between 6 and about 15 %. Below about 20 km, random uncertainties, dominated by measurement noise, result in the leading error contributions. Between 20 and 35 km, both random and systematic uncertainties, the latter dominated by spectroscopic uncertainties, contribute about equally to the total error budget. Above 35 km, the total error is again largely dominated by measurement noise. Overall, with random errors dominating the error budget below 20 and above 35 km, $ClONO_2$ uncertainties can be favourably reduced by averaging, without introducing a significant bias.

https://doi.org/10.5194/egusphere-2026-4116
Preprint. Discussion started: 29 July 2026


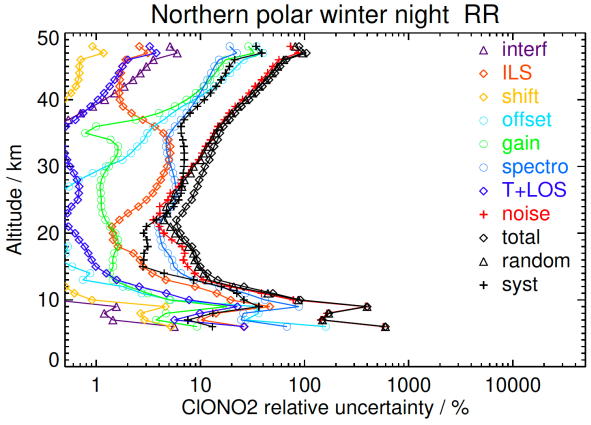


**Figure 9.** $ClONO_2$ error budget for RR NOM Northern polar winter night conditions.

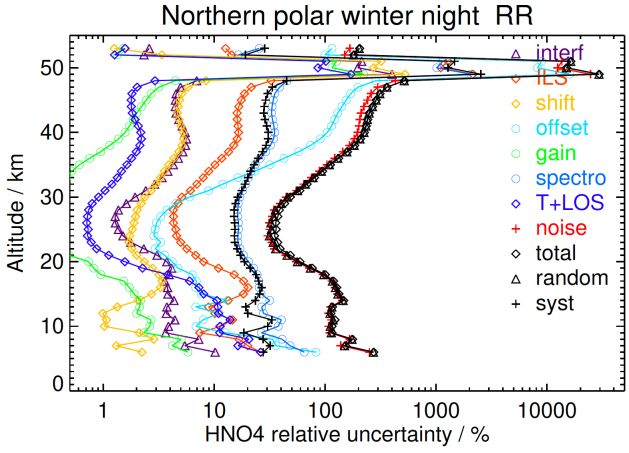


**Figure 10.** $HNO_4$ error budget for RR NOM Northern polar winter night conditions.

### 4.3.3 The $HNO_4$ error budget

$HNO_4$ error estimation relies on estimates of ingoing uncertainties as listed in Table 12 for the RR NOM observation mode. Similar Tables for the MIPAS FR NOM and RR MA observation modes are presented in the Supplement.

We discuss the total error budget of $HNO_4$ at the example of RR NOM Northern polar winter night conditions (Fig. 10 (for all other atmospheric conditions and observation modes see the Supplement). The total error budget is dominated by measurement noise over the entire altitude range. The uncertainty is lowest with about 40 % in the altitude range between 20 and 30 km and increases to more than 100 % above and below. The systematic error, dominated by spectroscopic uncertainties, contributes with about 10 to 20 % to the total error budget.

https://doi.org/10.5194/egusphere-2026-4116
Preprint. Discussion started: 29 July 2026


**Table 12.** Assumed $1\sigma$ uncertainties affecting the retrieval of $HNO_4$ (RR NOM)

| Type of Uncertainty | Value / typical value[1] | Source[2] | Propagation Method[3] |
|---|---|---|---|
| noise (A band) | 20 nW/(cm$^2$ sr cm$^{-1}$) | Kleinert et al. (2018) | G(16) |
| offset (A band) | 3 nW/ (cm$^2$ sr cm$^{-1}$) | Kleinert et al. (2018) | G(5;13) |
| gain random (A band) | 0.21% | Kleinert et al. (2018) | P(21;22) |
| gain systematic (A band) | 1.15% | Kleinert et al. (2018) | P(21;22) |
| spectral shift | 0.00029 cm$^{-1}$ | preceding V8 retrieval (Kiefer et al., 2021) | P(7) |
| ILS | 3% | Hase (2000, 2003) | P(7;14;15) |
| Temp., noise | 0.22 - 1.23 K | preceding V8 retrieval Kiefer et al. (2021) | G(6) |
| Tang. alt., noise | 29 - 52 m | preceding V8 retrieval Kiefer et al. (2021) | G(6) |
| Temp., spectral shift | 0.01 - 0.10 K | preceding V8 retrieval Kiefer et al. (2021) | P(17) |
| Tang. alt., spectral shift | 1 - 15 m | preceding V8 retrieval Kiefer et al. (2021) | P(17) |
| Temp., offset | 0.03 - 0.45 K | preceding V8 retrieval Kiefer et al. (2021) | P(7) |
| Tang. alt., offset | 8 - 16 m | preceding V8 retrieval Kiefer et al. (2021) | P(7) |
| Temp., ILS | 0.05 - 1.16 K | preceding V8 retrieval Kiefer et al. (2021) | P(7) |
| Tang. alt., ILS | 8 - 113 m | preceding V8 retrieval Kiefer et al. (2021) | P(7) |
| Temp., $CO_2$ intensities | 0.03 - 0.18 K | preceding V8 retrieval Kiefer et al. (2021) | P(7;26;27) |
| Tang. alt., $CO_2$ intensities | 26 - 34 m | preceding V8 retrieval Kiefer et al. (2021) | P(7;26;27) |
| Temp., $CO_2$ broadening | 0.14 - 1.47 K | preceding V8 retrieval Kiefer et al. (2021) | P(7;28;29) |
| Tang. alt., $CO_2$ broadening | 198 - 252 m | preceding V8 retrieval Kiefer et al. (2021) | P(7;28;29) |
| Temp., gain, syst. | 0.22 - 0.81 K | preceding V8 retrieval Kiefer et al. (2021) | P(21) |
| Tang. alt., gain, syst. | 1 - 49 m | preceding V8 retrieval Kiefer et al. (2021) | P(21) |
| Temp., gain, random | 0.04 - 0.15 K | preceding V8 retrieval Kiefer et al. (2021) | P(21) |
| Tang. alt., gain, random | 0.2 - 9 m | preceding V8 retrieval Kiefer et al. (2021) | P(21) |
| vmr($BrONO_2$) | 3.73E-18 - 5.16E-06 ppmv | climatology Höpfner et al. (2021) | P(7;11) |
| vmr($C_2H_2$) | 3.22E-06 - 9.55E-06 ppmv | V5 retrieval (Glatthor et al., 2007) | G(6) |
| vmr($C_2H_4$) | 1.00E-24 - 1.32E-06 ppmv | database Kiefer et al. (2002) | P(7;11) |
| vmr($C_2H_6$) | 2.77E-07 - 7.56E-05 ppmv | V5 retrieval (Glatthor et al., 2007) | G(6) |
| vmr($CCl_4$) | 3.05E-08 - 2.41E-06 ppmv | V5 retrieval (Eckert et al., 2017) | G(6) |
| vmr($COF_2$) | 7.02E-07 - 3.70E-05 ppmv | V5 FR climatology (unpublished data) | G(6) |
| vmr($CHCl_3$) | 3.19E-14 - 5.56E-05 ppmv | database Kiefer et al. (2002) | P(7;11) |
| vmr($CH_3Cl$) | 4.05E-07 - 5.88E-04 ppmv | database Kiefer et al. (2002) | P(7;11) |
| vmr($CH_3OH$) | 1.00E-24 - 2.95E-04 ppmv | database Kiefer et al. (2002) | P(7;11) |
| vmr($CO_2$) | 7.56E-01 - 7.51E+00 ppmv | WACCM model calc. (Kiefer et al., 2021) | P(20) |
| vmr(ClO) | 7.42E-05 - 6.51E-04 ppmv | preceding V8 retrieval(Glatthor et al., 2024b) | G(6) |
| vmr(HCN) | 1.54E-05 - 4.41E-05 ppmv | V5 retrieval (Glatthor et al., 2009) | G(6) |
| vmr($H_2O$) | 1.87E-01 - 2.24E+00 ppmv | preceding V8 retrieval (Kiefer et al., 2024) | G(6) |
| vmr($HNO_3$) | 5.54E-05 - 4.51E-04 ppmv | preceding V8 retrieval (this paper) | G(6) |
| vmr($NH_3$) | 7.18E-12 - 3.75E-05 ppmv | database Kiefer et al. (2002) | P(7;11) |
| vmr($NO_2$) | 2.03E-07 - 2.88E-04 ppmv | preceding V8 retrieval (Funke et al., 2026) | G(6) |
| vmr(OCS) | 3.37E-05 - 2.14E-04 ppmv | V5 retrieval (Glatthor et al., 2017) | G(6) |
| vmr(acetone) | 5.01E-07 - 8.07E-05 ppmv | V5 retrieval (unpublished data) | G(6) |
| vmr(PAN) | 5.92E-07 - 1.55E-05 ppmv | V5 retrieval (Glatthor et al., 2007) | G(6) |
| vmr(CFC-113) | 2.26E-07 - 1.14E-05 ppmv | V5 retrieval (unpublished data) | G(6) |
| vmr(HCFC-22) | 4.78E-06 - 1.46E-05 ppmv | V5 retrieval (Chirkov et al., 2016) | G(6) |
| spectroscopic data | 15% | May and Friedl (1993) | P(7) |

[1] For variable uncertainties typical values are reported. Some errors in Kleinert et al. (2018) are given in terms of $2\sigma$; we have re-scaled them to $1\sigma$. [2] In some cases V5 data were used of which no journal publication is available. In these cases, reference to an earlier data version is made. [3] Temperature and tangent altitude errors due to noise, spectral shift, and offset are propagated separately. The notation is as follows: "G" refers to generalized Gaussian error propagation in a matrix formalism, while "P" refers to perturbation studies. The numbers in parentheses are the respective equation numbers in von Clarmann et al. (2022).

https://doi.org/10.5194/egusphere-2026-4116
Preprint. Discussion started: 29 July 2026


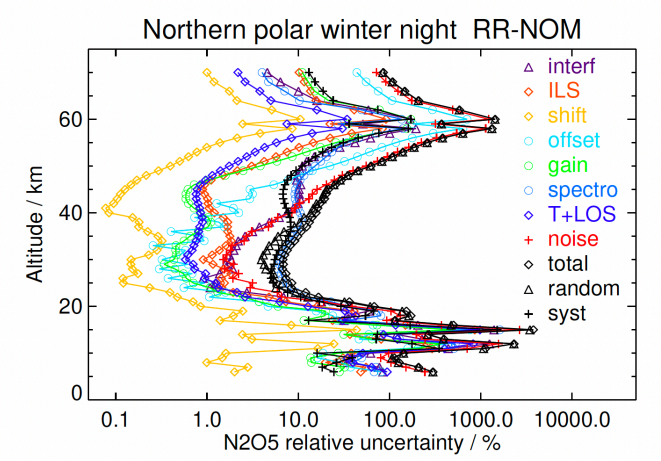


**Figure 11.** $N_2O_5$ error budget for RR NOM Northern polar winter night conditions.

#### 4.3.4 The $N_2O_5$ error budget

Assumed uncertainties used for the error propagation of the $N_2O_5$ retrievals are listed in Table 13 for the RR NOM observation mode. Similar Tables for the MIPAS FR NOM and RR MA observation modes are presented in the Supplement.

Figure 11 presents the resulting error budget of $N_2O_5$ for RR NOM Northern polar winter night observations. Error budgets for all other atmospheric conditions and observation modes are collected in the Supplement. In the relevant altitude range between 20 and 40 km, the total error budget of $N_2O_5$ is dominated by a number of sources that all contribute to significant amounts. The spectroscopic uncertainty contributes with about 7 to 12 % to the overall uncertainty of 8 to 20 %. Other contributions in this altitude range come from measurement noise (1 to 5 %), interfering species (<1 to 5 %), and the uncertainties of the instrumental line shape and the offset. Among the interfering species, the $COF_2$ uncertainty contributes most to the error budget. In hindsight, it would have been better to jointly fit this trace gas with $N_2O_5$. Above 40 km, the measurement noise is again the dominating contribution to the total error budget. For some atmospheric conditions, large $COF_2$ uncertainties contribute as well to a significant amount. Below 20 km, measurement noise, spectroscopic uncertainties, temperature and line-of-sight uncertainties, and gain and offset uncertainties contribute almost equally to the total error that is in the 100 to 1000 % range there.

## 5 Generation of the $NO_y$ data product

The total concentration of $[NO_y]$ is computed from the sum $[HNO_3] + [ClONO_2] + [NO] + [NO_2] + 2\times[N_2O_5] + [HNO_4]$, thus considering six of the most abundant reactive nitrogen constituents ("Big 6"). The retrieval and description of the NO data product can be found in Funke et al. (2023), while the $NO_2$ retrieval and data product is described by Funke et al. (2026). Uncertainties of individual components are considered uncorrelated for both random and systematic contributions. This assumption is justified because random uncertainties of all constituents are dominated by measurement noise, while

https://doi.org/10.5194/egusphere-2026-4116
Preprint. Discussion started: 29 July 2026


**Table 13.** Assumed $1\sigma$ uncertainties affecting the retrieval of $N_2O_5$ (RR NOM)

| Type of Uncertainty | Value / typical value[1] | Source[2] | Propagation Method[3] |
|---|---|---|---|
| noise (B band) | 10 nW/(cm$^2$ sr cm$^{-1}$) | Kleinert et al. (2018) | G(16) |
| offset (B band) | 1.5 nW/ (cm$^2$ sr cm$^{-1}$) | Kleinert et al. (2018) | G(5;13) |
| gain random (B band) | 0.21% | Kleinert et al. (2018) | P(21;23) |
| gain systematic (B band) | 1.03% | Kleinert et al. (2018) | P(21;23) |
| spectral shift | 0.00029 cm$^{-1}$ | preceding V8 retrieval (Kiefer et al., 2021) | P(7) |
| ILS | 3% | Hase (2000, 2003) | P(7;14;15) |
| Temp., noise | 0.22 - 1.23 K | preceding V8 retrieval Kiefer et al. (2021) | G(6) |
| Tang. alt., noise | 29 - 52 m | preceding V8 retrieval Kiefer et al. (2021) | G(6) |
| Temp., spectral shift | 0.01 - 0.10 K | preceding V8 retrieval Kiefer et al. (2021) | P(17) |
| Tang. alt., spectral shift | 1 - 15 m | preceding V8 retrieval Kiefer et al. (2021) | P(17) |
| Temp., offset | 0.03 - 0.45 K | preceding V8 retrieval Kiefer et al. (2021) | P(7) |
| Tang. alt., offset | 8 - 16 m | preceding V8 retrieval Kiefer et al. (2021) | P(7) |
| Temp., ILS | 0.05 - 1.16 K | preceding V8 retrieval Kiefer et al. (2021) | P(7) |
| Tang. alt., ILS | 8 - 113 m | preceding V8 retrieval Kiefer et al. (2021) | P(7) |
| Temp., $CO_2$ intensities | 0.03 - 0.18 K | preceding V8 retrieval Kiefer et al. (2021) | P(7;26;27) |
| Tang. alt., $CO_2$ intensities | 26 - 34 m | preceding V8 retrieval Kiefer et al. (2021) | P(7;26;27) |
| Temp., $CO_2$ broadening | 0.14 - 1.47 K | preceding V8 retrieval Kiefer et al. (2021) | P(7;28;29) |
| Tang. alt., $CO_2$ broadening | 198 - 252 m | preceding V8 retrieval Kiefer et al. (2021) | P(7;28;29) |
| Temp., gain, syst. | 0.22 - 0.81 K | preceding V8 retrieval Kiefer et al. (2021) | P(19) |
| Tang. alt., gain, syst. | 1 - 49 m | preceding V8 retrieval Kiefer et al. (2021) | P(19) |
| Temp., gain, random | 0.04 - 0.15 K | preceding V8 retrieval Kiefer et al. (2021) | P(19) |
| Tang. alt., gain, random | 0.2 - 9 m | preceding V8 retrieval Kiefer et al. (2021) | P(19) |
| vmr($C_2H_2$) | 3.22E-06 - 9.55E-06 ppmv | V5 retrieval (Glatthor et al., 2007) | G(6) |
| vmr($CH_3COOH$) | 1.00E-24 - 2.01E-04 ppmv | database (Kiefer et al., 2002) | P(7;11) |
| vmr($ClONO_2$) | 9.99E-06 - 8.28E-05 ppmv | preceding V8 retrieval (this paper) | G(6) |
| vmr($COF_2$) | 7.02E-07 - 3.79E-04 ppmv | V5 FR climatology (unpublished data) | G(6) |
| vmr($CO_2$) | 7.56E-01 - 7.51E+00 ppmv | WACCM model calc. (Kiefer et al., 2021) | P(20) |
| vmr($H_2O_2$) | 3.03E-06 - 1.12E-04 ppmv | database (Kiefer et al., 2002) | P(7;11) |
| vmr($HNO_3$) | 5.54E-05 - 4.51E-04 ppmv | preceding V8 retrieval (this paper) | G(6) |
| vmr(HOCl) | 2.12E-06 - 7.27E-05 ppmv | database (Kiefer et al., 2002) | P(7;11) |
| vmr($NH_3$) | 7.18E-12 - 3.75E-05 ppmv | database (Kiefer et al., 2002) | P(7;11) |
| vmr($NO_2$) | 2.03E-07 - 2.88E-04 ppmv | preceding V8 retrieval (Funke et al., 2026) | G(6) |
| vmr($O_3$) | 2.48E-02 - 8.52E-02 ppmv | preceding V8 retrieval (Kiefer et al., 2023) | G(6) |
| vmr($SO_2$) | 5.95E-05 - 4.24E-04 ppmv | V5 retrieval (Höpfner et al., 2015) | G(6) |
| vmr(acetone) | 5.01E-07 - 8.07E-05 ppmv | V5 retrieval (unpublished data) | G(6) |
| vmr($CF_4$) | 5.51E-06 - 1.33E-05 ppmv | database Kiefer et al. (2002) | P(7;11) |
| vmr(CFC-113) | 2.26E-07 1.14E-05 ppmv | V5 retrieval (unpublished data) | G(6) |
| spectroscopic data ($N_2O_5$) | 5% | Wagner and Birk (2003) | P(7) |

[1] For variable uncertainties typical values are reported. Some errors in Kleinert et al. (2018) are given in terms of $2\sigma$; we have re-scaled them to $1\sigma$. [2] In some cases V5 data were used of which no journal publication is available. In these cases, reference to an earlier data version is made. [3] Temperature and tangent altitude errors due to noise, spectral shift, and offset are propagated separately. The notation is as follows: "G" refers to generalized Gaussian error propagation in a matrix formalism, while "P" refers to perturbation studies. The numbers in parentheses are the respective equation numbers in von Clarmann et al. (2022).

https://doi.org/10.5194/egusphere-2026-4116
Preprint. Discussion started: 29 July 2026


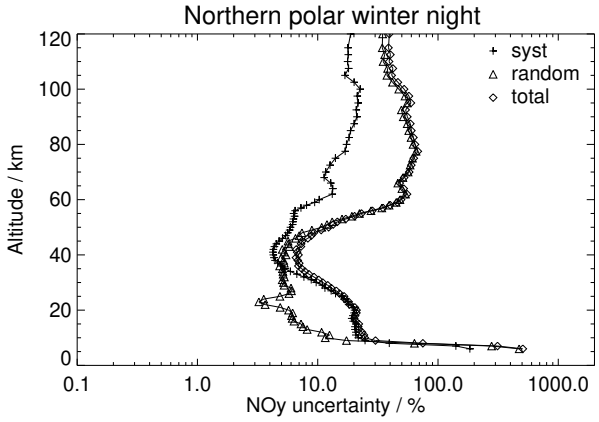


**Figure 12.** $NO_y$ error budget (total random, total systematic, and total error) for RR NOM Northern polar winter night conditions.

systematic uncertainties are dominated by either spectroscopic or – in the case of nitric oxide - non-LTE errors. Reported $NO_y$ uncertainty estimates (random, systematic and total) have been calculated from the quadratic sum of those of all contributing constituents (see Fig. 12), similarly as described in Funke et al. (2014b). For the vertical resolution $\epsilon$, however, we use a slightly revised approach

$$\epsilon = \left[ \frac{\sum_i {\epsilon_i}^{-1} \mathrm{VMR}_i}{\sum_i \mathrm{VMR}_i} \right]^{-1}, \quad (1)$$

considering that the resolution is inversely proportional to the averaging kernel diagonal.

## 6 Comparison to the V5 data version

In this section, we compare the new version 8 data to previous data versions in the sense of a 'delta validation'. MIPAS data products of nitrogen species of previous data versions have already been compared to data from independent measurement systems. Thus, we do not provide a full validation to reference data here. Instead, we check if the differences between MIPAS V8 and MIPAS V5 data help to remove the issues identified in the validation studies of preceding MIPAS data versions.

### 6.1 $HNO_3$

Compared to the previous data version of $HNO_3$, V5H/R_HNO3_22/224/225, the new V8 data version provides higher volume mixing ratios for large latitude regions at almost all altitudes (Fig. 13). The vmrs are increased by less than 5% over most areas, but by up to 20% around the tropical tropopause, where, however, the absolute abundances are rather low (see Fig. 13 and Fig. 22, top left panel, in the next section). Below 25 km, reduced abundances in V8 data are found for the Northern tropics and mid-latitudes during the FR period (Fig. 13, middle panel), in Northern and Southern mid-latitudes during hemispheric winters, and Antarctic polar winters. For Southern subpolar latitudes (50 to 80°S) at 35 km, above the main stratospheric $HNO_3$

https://doi.org/10.5194/egusphere-2026-4116
Preprint. Discussion started: 29 July 2026


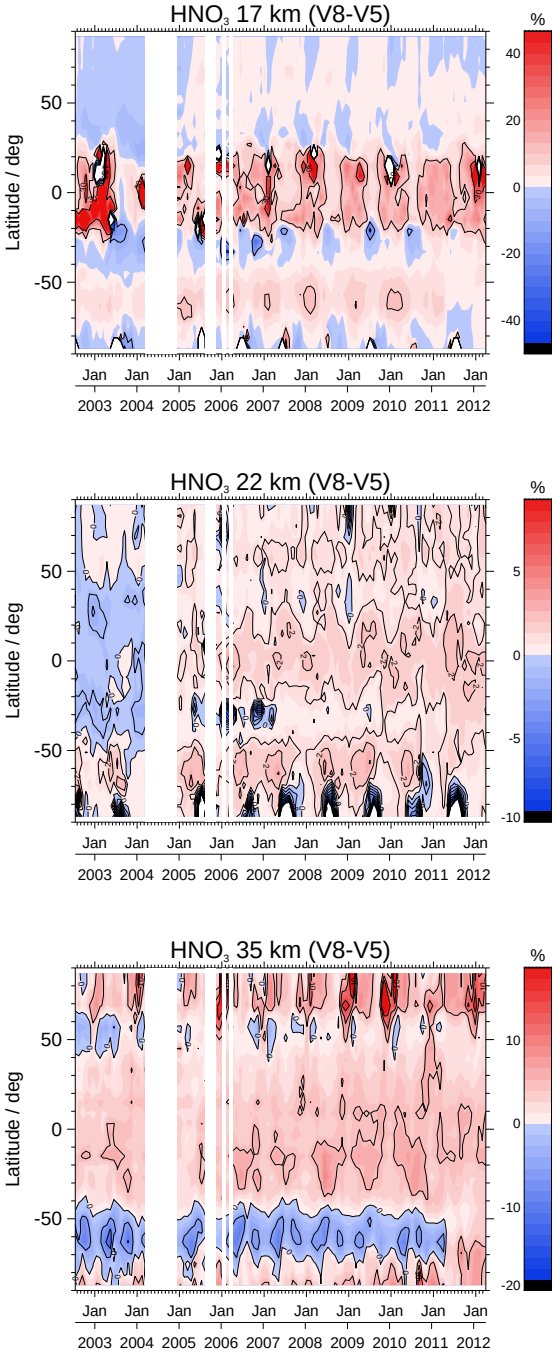


**Figure 13.** Time series of relative differences between V8 and V5 $HNO_3$ data (in terms of (V8-V5)/V5) over all latitudes at 17 km (top), 22 km (middle) and 35 km altitude (bottom) (FR and RR NOM data only). White areas are missing data due to clouds and polar stratospheric clouds (PSCs), or due to filter criteria. White stripes are missing data due to inactivity of MIPAS.

https://doi.org/10.5194/egusphere-2026-4116
Preprint. Discussion started: 29 July 2026


maximum, the V8 $HNO_3$ vmrs are lower than V5 all year round (see Fig. 13, bottom panel). The reduced concentrations in the FR period compared to the enhanced concentrations during the RR period in the Northern hemispheric lower stratosphere make the time series in this altitude range more consistent than they were before.

MIPAS V5 data of $HNO_3$ were intercompared to other satellite data on a zonal mean basis by Hegglin and Tegtmeier (2017). They were found to have a negative bias (up to -20%) in the tropics up to $\pm 30°$ below 20 hPa and a positive bias up to 10% elsewhere. The negative bias in the tropical lower stratosphere seems to be reduced by the new V8 data, while the high bias elsewhere has rather increased. An assessment in the polar winter regions was found to be difficult due to sampling effects on MIPAS data caused by polar stratospheric clouds.

Compared to the previous validation of MIPAS V5 $HNO_3$ versus ACE-FTS v3.5 data based on coincident profiles, the new data version appears to further reduce some of the differences observed previously, which were, however, already small. Sheese et al. (2016, 2017) found almost perfect agreement for the two data sets between 20 and 28 km, and a negative bias of MIPAS versus ACE-FTS of less than 10% for 8 to 20 km and 28 to 40 km altitude. While the agreement around the stratospheric $HNO_3$ maximum might now be a little worse (with a MIPAS positive bias of 2 to 4%), the negative bias in the flanks of the stratospheric maximum seems to be reduced to almost zero. However, a proper validation would require a comparison to the most recent data version of ACE-FTS, and other satellite data. This is beyond the scope of this paper.

### 6.2 $ClONO_2$

Compared to the previous data version, V5H_CLONO2_21, the new V8 FR $ClONO_2$ abundances at 20 km are lower by about 5% in the Northern and Southern mid-latitudes and the Northern Arctic without any seasonal variation, and higher by 5 to 20% in the tropics and polewards of 50°S (Fig. 14, top panel). During the RR phase from 2005 on, the new V8 $ClONO_2$ mixing ratios show about the same behavior, except that they are higher in the Arctic region as well, by up to 5%. For higher altitudes (25 and 40 km, Fig. 14, middle and bottom panels), the different behaviour for the FR and RR phases is remarkable: while the retrieved $ClONO_2$ amounts have decreased for the FR phase over large latitude regions (except in polar regions at 25 km and partly in the tropics at 40 km), they have increased for RR NOM by up to 5% over almost all latitudes except polar winters at 25 km. At 40 km, they increased for RR NOM by up to 50% for low to mid-latitudes and more than 100% in polar summers, but not in polar winters, in both hemispheres. As shown in the next section in Figs. 23 and 24 (top right panels), these opposite changes bring the complete time series from 2002 to 2012 in better consistency and reduce the step between the two periods that was observed previously.

With respect to profile-by-profile validation against ACE-FTS version 3.5 data (Sheese et al., 2016), the changes between the V5 and V8 data versions result generally in enlarged discrepancies. V5 data had a high bias between 17 and 35 km relative to ACE-FTS in the order of 10% that is now further increased, at least in the RR phase, by 5 to 50%. Below 20 km, where MIPAS V5 data had a low bias of up to 35% with respect to ACE-FTS, this low bias is now considerably reduced (not shown). In the comparison of zonal mean data by Hegglin and Tegtmeier (2017), MIPAS V5 and ACE-FTS v2.2 data showed a general agreement within $\pm$ 10% in the lower to middle stratosphere with a tendency of MIPAS providing larger values. Only in the lower stratosphere, where $ClONO_2$ vmrs become small, the relative differences were larger. With respect to this comparison,

https://doi.org/10.5194/egusphere-2026-4116
Preprint. Discussion started: 29 July 2026


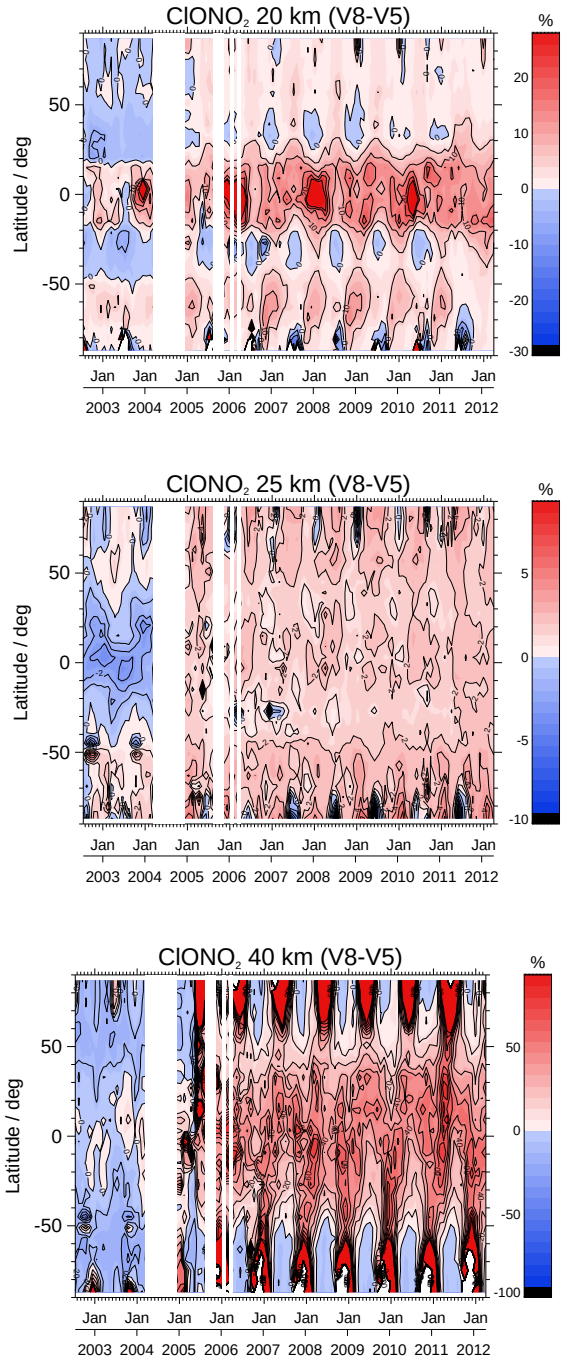


**Figure 14.** Time series of relative differences between V8 and V5 $ClONO_2$ data (in terms of (V8-V5)/V5) over all latitudes at 20 km (top), 25 km (middle) and 40 km altitude (bottom) (FR and RR NOM data only). White areas are missing data due to clouds and polar stratospheric clouds (PSCs), or due to filter criteria. White stripes are missing data due to inactivity of MIPAS.

https://doi.org/10.5194/egusphere-2026-4116
Preprint. Discussion started: 29 July 2026


the new V8 $ClONO_2$ data set seems to increase the differences to ACE-FTS v2.2 zonal mean data previously identified. While these comparisons may provide a first hint on the consistency with other satellite data sets, a proper validation – that is beyond the scope of this paper – should be done with the most recent data version of ACE-FTS.

### 6.3 $HNO_4$

For both FR and RR data, V8 $HNO_4$ vmrs are smaller than the respective V5 data in the stratospheric $HNO_4$ maximum at 25 km and below over almost all latitudes and seasons. The only exception are the late springs/early polar winters in both hemispheres, for which slightly increased vmrs, up to 10%, are retrieved in version V8 (Fig 15, top panel). Slightly above the stratospheric maximum, around 30 km, V8 FR NOM data are lower than V5 data, while V8 RR NOM data are higher by up to 15% (Fig 15, middle panel). Together with the reduction in and below the stratospheric maximum, this indicates a shift of the retrieved altitude of the stratospheric $HNO_4$ layer to slightly higher altitudes in V8 for the MIPAS RR period. Above the $HNO_4$ layer, around 40 km, we observe a strong reduction of $HNO_4$ vmrs, by appr. 60% during the FR period, and around 80% during the RR period. This reduction is due to an unphysical feature in V5 data with strongly enhanced values in this altitude range. This unphysical feature was first identified in MIPAS $HNO_4$ V5 data for nighttime observations by Hegglin and Tegtmeier (2017). We assign it to a less than optimal handling of spectral continua in the V5 retrievals, e.g. from aerosols. Hegglin and Tegtmeier (2017) found in their comparisons that V5 $HNO_4$ monthly zonal mean data from MIPAS were generally higher than ACE-FTS v2.2 data by up to 50%, also in the stratospheric main layer. This comparison was performed below 10 hPa in order to avoid the effects of the diurnal cycle of $HNO_4$. With respect to this comparison, the MIPAS V8 $HNO_4$ data for the RR period seem to have increased the differences to ACE-FTS between 25 and 30 km altitude, and have reduced them below 25 km. A full validation should be carried out with the most recent data version of ACE-FTS, which, however, is beyond the scope of this paper.

It should be noted that the current data version has an issue after the interruption of MIPAS' operation in 2004 until end of May of 2005. Icing of the detectors during the interruption led to increasing detector noise over this period which resulted in inferior retrieval quality with increased noise error and reduced vertical resolution. Detector decontamination at the end of May 2005 resolved this problem, but the consequences of this deterioration can be seen in the retrieval results above the main $HNO_4$ layer in the stratosphere (Fig. 16). The main stratospheric layer of $HNO_4$ and the data below seem not to be affected (see Figs. 22, 23, and 24).

### 6.4 $N_2O_5$

Figure 17 presents typical relative zonal mean differences between the previous data version, V5H/R_N2O5_21_222_223, and the new V8 data version for a NH late winter situation. With the V8 data version, the stratospheric vmrs at NH polar winter become larger by up to 20%, while at SH polar summer, they are reduced by up to -60%. In the reverse situation (polar summer in the NH, polar winter in the SH), we observe the decrease in the polar summer situation as well, but not the increase for polar winter (not shown). Below the main stratospheric $N_2O_5$ layer, the stratospheric V8 values become considerably larger than V5, while the tropospheric values decrease on average. The V8 $N_2O_5$ values at the $N_2O_5$ maximum around 30 km and above

https://doi.org/10.5194/egusphere-2026-4116
Preprint. Discussion started: 29 July 2026


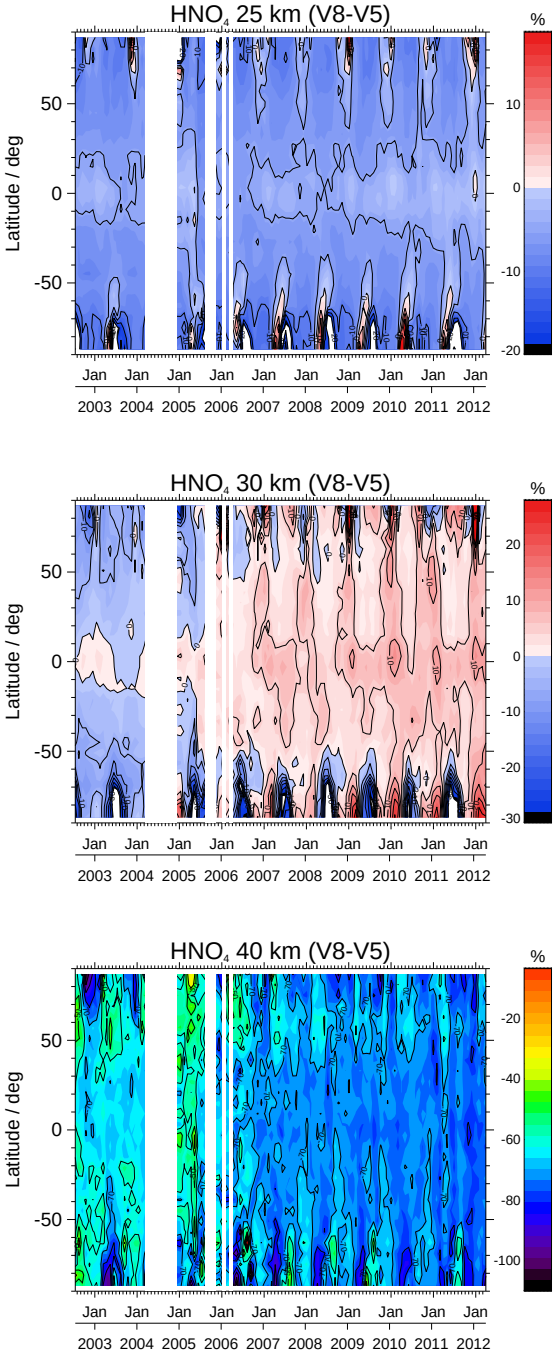


**Figure 15.** Time series of relative differences between V8 and V5 $HNO_4$ data (in terms of (V8-V5)/V5) over all latitudes at 25 km (top), 30 km (middle) and 40 km altitude (bottom) (FR and RR NOM data only). White areas are missing data due to clouds and polar stratospheric clouds (PSCs), or due to filter criteria. White stripes are missing data due to inactivity of MIPAS. Please note that in the bottom panel only negative deviations are shown.

https://doi.org/10.5194/egusphere-2026-4116
Preprint. Discussion started: 29 July 2026


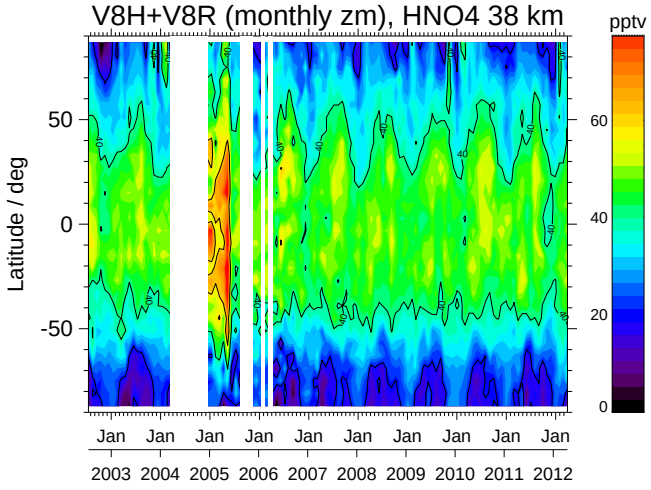


**Figure 16.** Time series of retrieved $HNO_4$ at 38 km altitude over all latitudes. After the interruption of operation in 2004, irregular high $HNO_4$ vmrs are observed until end of May 2005. This artifact in the data is caused by high detector noise and reduced vertical resolution, and fully covered by the increased uncertainties during this time.

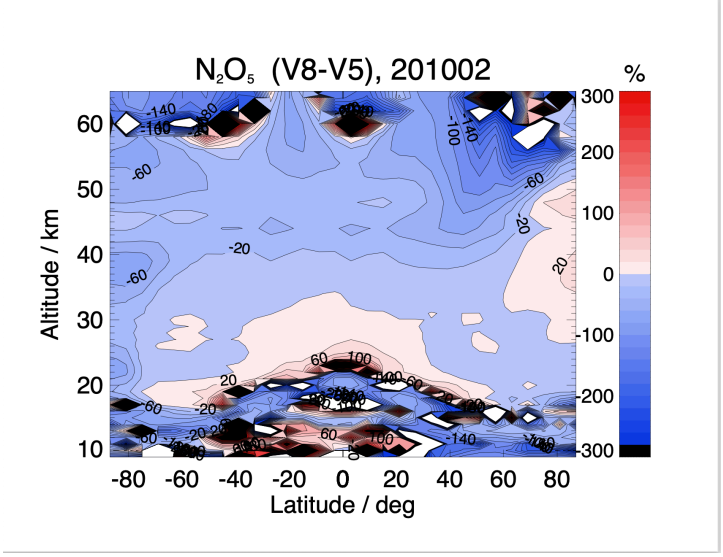


**Figure 17.** Zonal mean distribution of relative differences between MIPAS V8 and V5 $N_2O_5$ data (in terms of (V8-V5)/V5) for a NH late winter situation (February 2010). White areas are missing data.

https://doi.org/10.5194/egusphere-2026-4116
Preprint. Discussion started: 29 July 2026


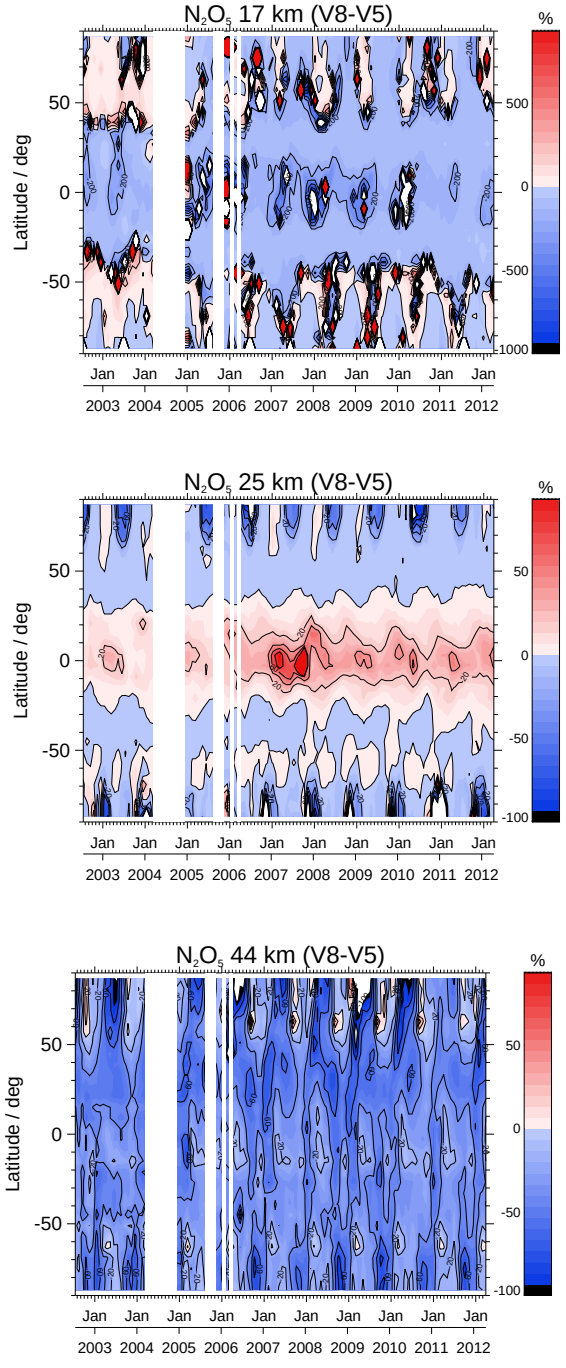


**Figure 18.** Time series of relative differences between V8 and V5 $N_2O_5$ data (in terms of (V8-V5)/V5) over all latitudes at 17 km (top), 25 km (middle) and 44 km altitude (bottom). White areas are missing data due to clouds and polar stratospheric clouds (PSCs), or due to filter criteria. White stripes are missing data due to inactivity of MIPAS.

https://doi.org/10.5194/egusphere-2026-4116
Preprint. Discussion started: 29 July 2026


change in the order of +5% at the lower part to -20% at the higher part, indicating a downward shift of the stratospheric $N_2O_5$ layer in the V8 data.

Figure 18 shows time series of relative differences between MIPAS V5 and V8 (in terms of (V8-V5)/V5) for all latitudes at 17 km (top), 25 km (middle), and 44 km (bottom). At 17 km, the differences (decreases in the low and mid-latitudes and in polar summers, increases during polar winters ) are dramatic, up to -1000 and +200%, however, the absolute vmrs are very low at this altitude. A specific artifact in V5 data related to volcanic sulphate emissions has now been removed. In version 5 data, sulphate aerosol signatures in the spectra not accounted for (due to not joint-fitting $H_2SO_4$) caused strongly negative $N_2O_5$ vmrs erroneously retrieved in the upper troposphere - lower stratosphere region. The strong artifacts appearing particularly after volcanic eruptions have now been removed, demonstrated by positive differences between V8 and V5 $N_2O_5$ vmrs (see Fig. 19, upper panel). The strongest differences appear at latitudes and times similar to $SO_2$ enhancements previously related to volcanic emissions (Höpfner et al., 2015) (see Fig. 19, lower panel).

At 25 km, V8 is higher than V5 in the tropics by up to 40% on average, and around 50 – 70° S by up to 10%. In 2007, there is a unique enhancement in the tropics where V8 vmrs are higher than V5 by up to 100%, the cause of which is not yet known. In polar summers, the V8 $N_2O_5$ vmrs are lower than the V5 data by 40 to more than 100%. Differences between V5 and V8 are consistent for the FR and RR period of MIPAS observations.

At 44 km, we see a seasonal pattern of positive differences between V8 and V5 data during early polar winters when enhanced $NO_x$ is subsiding into the polar vortex from above and $N_2O_5$ forms. These events appear to be stronger in the V8 data than before. At other latitudes and seasons, the changes between V8 and V5 are mostly negative and range from 0 to -100% (V8 being lower than V5). They are strongest negative during NH polar summer and SH polar spring.

The only comparison to other satellite data that was available so far was to ACE-FTS data of version 3.5 (Sheese et al., 2016) and version 2.2 (Hegglin and Tegtmeier, 2017). The zonal-mean comparisons by Hegglin and Tegtmeier (2017) were complicated by the diurnal cycle of $N_2O_5$ and difficult to interpret. Sheese et al. (2016) found agreement between ACE-FTS sunrise data and MIPAS am and pm data in the order of 10% between 22 and 40 km, with MIPAS having a slight high bias versus ACE-FTS. Below and above this altitude range, ACE-FTS was higher than MIPAS by 30% and more, in particular in the lower stratosphere. ACE-FTS sunset data were far off which was explained by a low signal-to-noise ratio of these observations with very low $N_2O_5$ data because of their diurnal cycle. The negative changes towards MIPAS V8 data in the lower stratosphere described above seem to further worsen the discrepancy with ACE-FTS version 3.5 data. With V8 changes by +5 to -20% in the range of the stratospheric $N_2O_5$ layer it is difficult to assess if the new data version provides an improvement of the agreement with ACE-FTS. A dedicated validation, using most recent ACE-FTS data, is required, that is, however, beyond the scope of this paper.

### 6.5 $NO_y$

Figure 20 shows time series of relative differences between MIPAS V5 and V8 (in terms of (V8-V5)/V5) for all latitudes at 25 km, 40 km, and 55 km. Below approximately 30 km, V8 data are about 2-10% larger than V5 data with largest differences

https://doi.org/10.5194/egusphere-2026-4116
Preprint. Discussion started: 29 July 2026


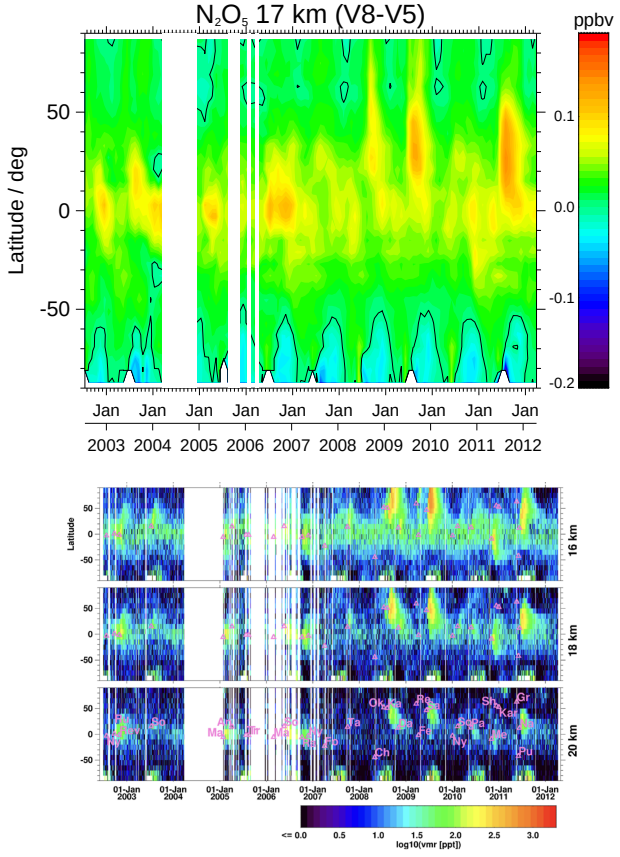


**Figure 19.** Upper panel: Time series of absolute differences between MIPAS V5 and V8 (in terms of (V8 - V5)) for all latitudes at 17 km altitude. Lower panel: Time series of MIPAS V5 SO2 vmrs (Höpfner et al., 2015) over all latitudes at 16, 18, and 20 km altitude. Triangle symbols mark the latitude and time of major volcanic eruptions. For more details, see Höpfner et al. (2015) (their Table 3) White areas are missing data.

found in the tropics. Above, V8 is generally lower by the same amount (except for the FR period where V8-V5 differences remain positive). Around the stratopause and above, V8 polar $NO_y$ is on average larger again compared to V5.

Although individual $NO_y$ compounds exhibit pronounced diurnal variability due to fast photochemistry, $NO_y$ itself is chemically very stable in the stratosphere. The most important sink is NO photolysis which is relevant only above approximately 50 km. Therefore, $NO_y$ is an excellent dynamical tracer in the stratosphere. Here, we use the chemical stability of stratospheric $NO_y$ to test the self-consistency of MIPAS V8 data by comparing observations taken during morning (am) and evening (pm) overpasses which should give similar $NO_y$ concentrations despite the differences of the partitioning of the individual compounds. Figure 21 (upper panel) shows the absolute am-pm differences for V8 $NO_y$, which are mostly well below 1 ppbv in the 20-50 km range. In the stratosphere around 40 km, V5 (see Fig. 21, lower panel) exhibits significantly larger am-pm dif-

https://doi.org/10.5194/egusphere-2026-4116
Preprint. Discussion started: 29 July 2026


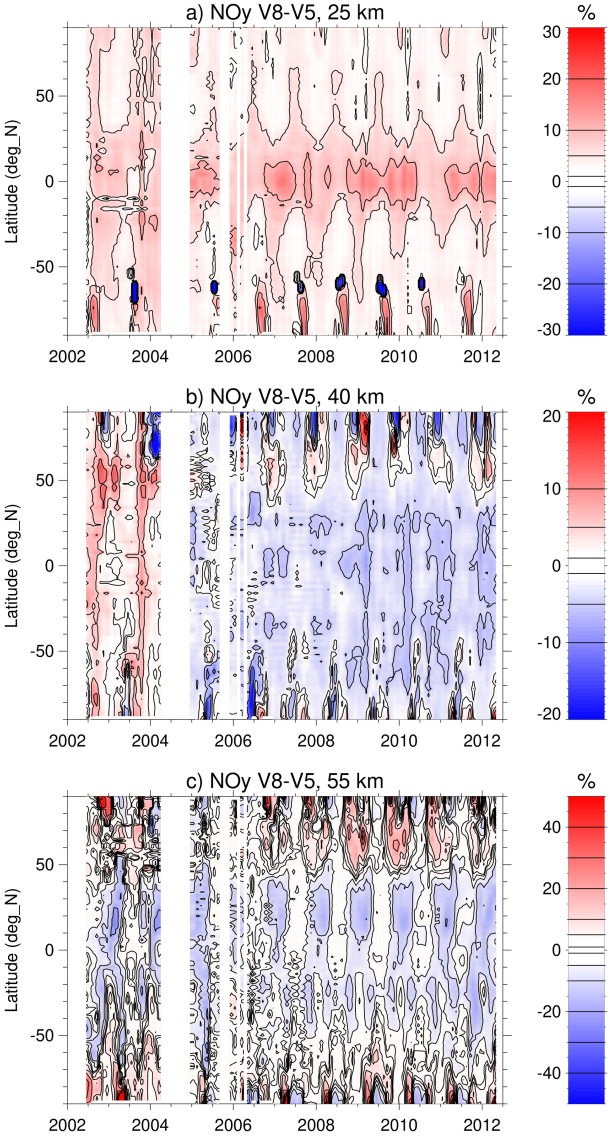


**Figure 20.** Time series of relative differences between V8 and V5 $NO_y$ data (in terms of (V8-V5)/V5) over all latitudes at (a) 25 km, (b) 40 km and (c) 55 km altitude (bottom). White areas are missing data due to clouds and polar stratospheric clouds (PSCs), or due to filter criteria. White stripes are missing data due to inactivity of MIPAS.

ferences, indicative for inconsistencies of the retrieved individual $NO_y$ compounds, compared to the new version 8. Therefore, we conclude that V8 retrievals are more self-consistent than previous versions.

https://doi.org/10.5194/egusphere-2026-4116
Preprint. Discussion started: 29 July 2026


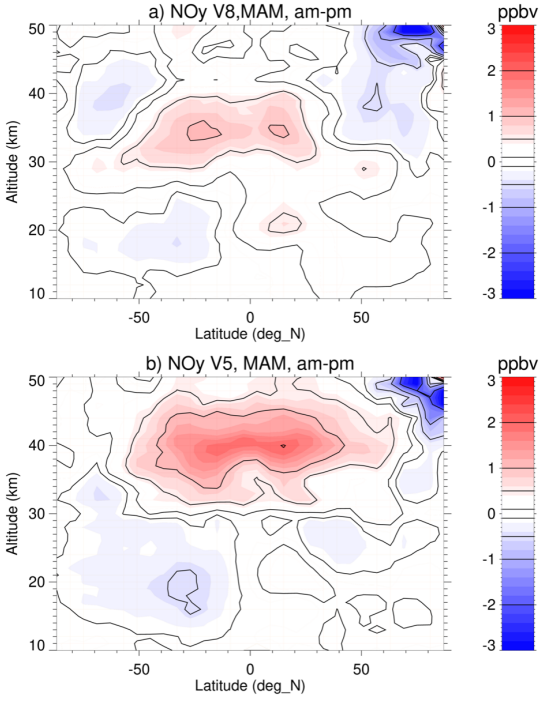


**Figure 21.** (a) Absolute differences between morning (am) and evening (pm) V8 $NO_y$ observations taken in the NH spring season (March-April-May, MAM) during 2002-2012. (b) as (a) but for MIPAS V5 $NO_y$.

## 7 Results

In this section we provide a number of examples for zonal mean distributions and time series of the four nitrogen reservoir gases and the $NO_y$ budget.

Figure 22 presents the monthly zonal mean altitude-latitude cross-sections of the four gases and $NO_y$ for August 2010, which is representative for an Austral midwinter case. All four gases exhibit a moderate diurnal cycle in the middle and upper stratosphere. However, here we present, as an overview, altitude-latitude cross-sections and time series constructed from monthly zonal means averaged over all existing illumination conditions. It is to be noted, however, that polar night conditions are present poleward of about 70°S.

The zonal mean distribution of $HNO_3$ (see Fig. 22, top left panel) for Antarctic polar midwinter reveals the denitrification in the core of the Southern polar vortex due to the uptake of reactive nitrogen in polar stratospheric clouds (low $HNO_3$ values between 90 and 70°S around 20 km) (e.g. Salawitch et al., 1989), the collar of high $HNO_3$ values at the vortex edge and outside of the vortex (e.g. Roche et al., 1993) and enhanced abundances of $HNO_3$ above the altitude range of active ozone depletion (at and above 30 km). In the altitude range between 10 and 15 km between 80 and 70°S some enhancement of $HNO_3$ is also detectable which comes from sedimentation and re-evaporation of $HNO_3$-loaded PSC particles (e.g. Khosrawi et al., 2018). The enhanced values above 30 km stem from $HNO_3$ production following high amounts of $NO_x$ being continuously

https://doi.org/10.5194/egusphere-2026-4116
Preprint. Discussion started: 29 July 2026


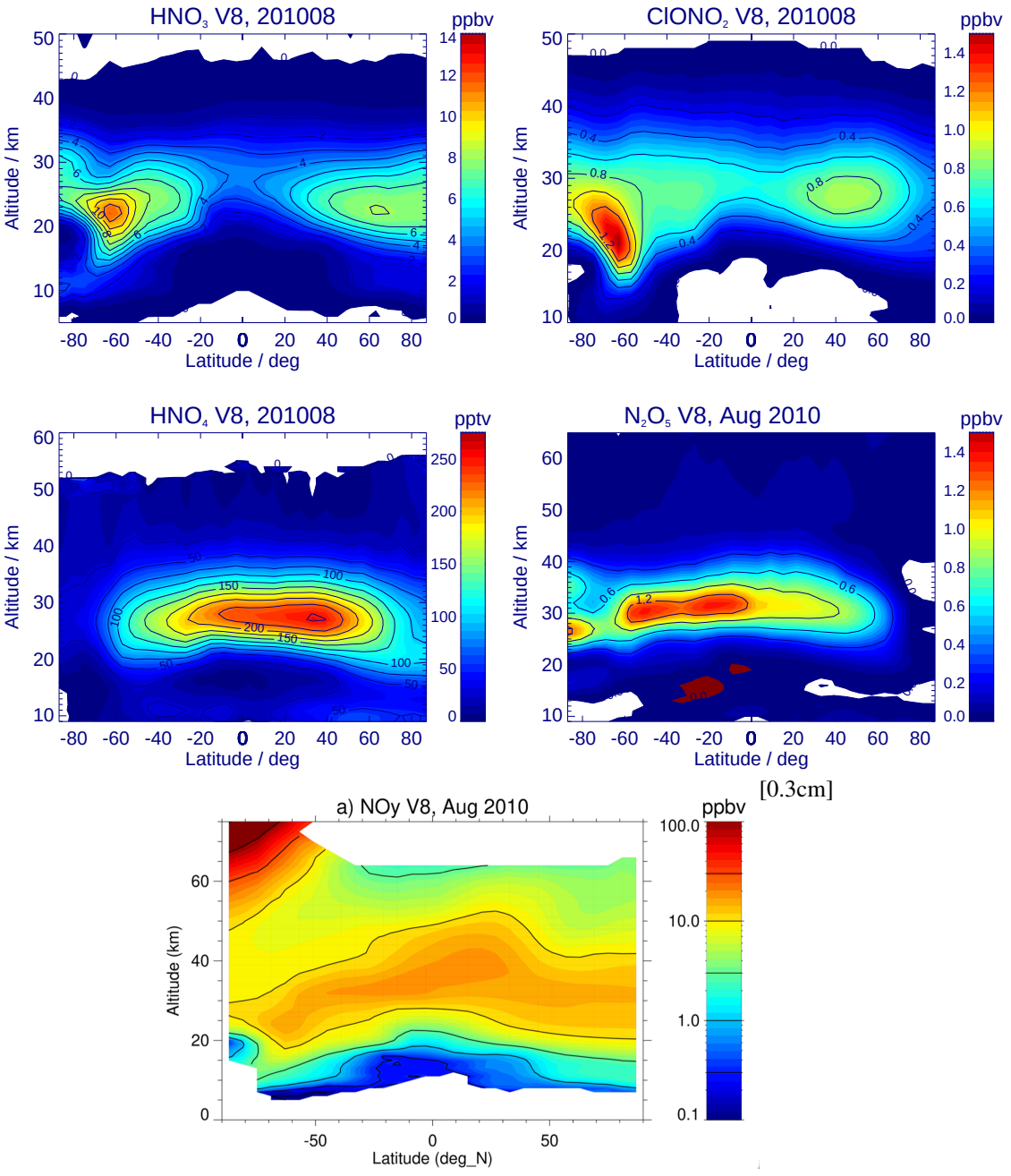


[0.3cm]

**Figure 22.** Monthly zonal mean distributions for August 2010 of $HNO_3$ (top left), $ClONO_2$ (top right), $HNO_4$ (middle left), $N_2O_5$ (middle right), and $NO_y$ (bottom). White areas are missing data due to clouds and polar stratospheric clouds (PSCs), or due to filter criteria.

transported downwards from the lower thermosphere in polar winter (Stiller et al., 2005; Verronen et al., 2008). Near the North Pole, the stratospheric $HNO_3$ maximum reaches its lowest values over the year during summer under permanent illumination

https://doi.org/10.5194/egusphere-2026-4116
Preprint. Discussion started: 29 July 2026


conditions. The overall lowest stratospheric $HNO_3$ abundances are found in the tropics. In the upper troposphere and lower stratosphere, we find enhanced values of $HNO_3$ from about 40° to the poles in both hemispheres with maxima in hemispheric spring (not shown), however not in the tropics.

Chlorine nitrate plays also a relevant role in polar winter ozone depletion as it forms from $NO_2$ and ClO in a three-body reaction (Brasseur and Solomon, 2005; Rowland et al., 1976; von Clarmann and Johansson, 2018) and thus, deactivates two of the major players in the catalytic ozone depletion cycle (see, e.g. Solomon, 1999). This deactivation, however, is not possible if $NO_x$ is removed from the gas phase by the formation of polar stratospheric clouds, as it happens in the Antarctic winter. Similar to $HNO_3$, the denitrified area in the Antarctic winter polar vortex that hinders the (re-)formation of $ClONO_2$ is obvious Fig. 22, top right panel. The $ClONO_2$-poor area is surrounded by a lid at the top and a latitudinal collar of high $ClONO_2$ were $NO_x$ is more abundant.

Within polar winter stratospheric ozone depletion, $HNO_4$ couples the $HO_x$ and $NO_x$ catalytic cycles (Brasseur and Solomon, 2005; Salawitch et al., 2002). Further, $HNO_4$ is destroyed by photolysis, leading to daytime reduction, and by reaction with OH, which represents a significant sink of odd- hydrogen radicals in the stratosphere. Similar to results from earlier MIPAS data versions (Stiller et al., 2007), we find a stratospheric maximum in the midlatitudes of the summer hemisphere, and a minimum near the Antarctic winter pole (see Fig. 22, middle left panel).

$N_2O_5$ is a nighttime reservoir for $NO_x$, and as such, also involved in polar ozone depletion. During illumination it is destroyed by photolysis, leading to daytime and polar summer reduction. In consequence we observe stratospheric maxima of $N_2O_5$ at the hemispheric winter pole above the altitude range of PSC formation, and deep minima at the spring-to-autumn pole under permanent sunlit conditions (Fig. 22, middle right panel).

The zonal mean distribution of $NO_y$ for August 2010 shows the characteristics of a largely inert tracer, representing the stratospheric global circulation with uplift over the tropics and subsidence at high latitudes. The increase with altitude up to the middle stratosphere reflects the formation of $NO_y$ from the photolysis of $N_2O$. Denitrification of the atmosphere due to PSC formation can be identified at the South Pole at around 20 km altitude. Large enhancements of $NO_y$ due to descent of odd nitrogen produced by energetic particles from $N_2$ is visible in the polar winter mesosphere and upper stratosphere.

Latitude-time cross sections of all four gases and $NO_y$ at an altitude of 24 km are displayed in Fig. 23. The $HNO_3$ time series at 24 km (Fig. 23, top left panel) confirms the regular denitrification in Southern polar winter after the preceding yearly maximum of $HNO_3$ in fall. In the Northern hemisphere, the stratospheric $HNO_3$ maximum reaches its lowest values over the year during summer. Denitrification cannot be observed regularly in the Northern polar winter, or at least not in an equally remarkable amount, since PSC formation is less frequent there due to higher temperatures. The late Arctic winters in 2011 and, to a smaller amount, 2007, were disturbed, however (Manney et al., 2011; Sinnhuber et al., 2011), and some sign of denitrification is visible, followed by unusually high $HNO_3$ abundances during the next spring and summer. The lowest $HNO_3$ abundances at 24 km are observed in the tropics, with regular minima during boreal winter.

$ClONO_2$ time series at 24 km (Fig. 23, top right panel) reveal minima during polar summer and fall and in the tropics. The formation of the $ClONO_2$ enhancements at the edge and outside of the Antarctic polar vortex is also visible in the time series at 24 km. Following the breakdown of the Antarctic polar vortex in November, high amounts of $ClONO_2$ reach the South Pole. In

https://doi.org/10.5194/egusphere-2026-4116
Preprint. Discussion started: 29 July 2026


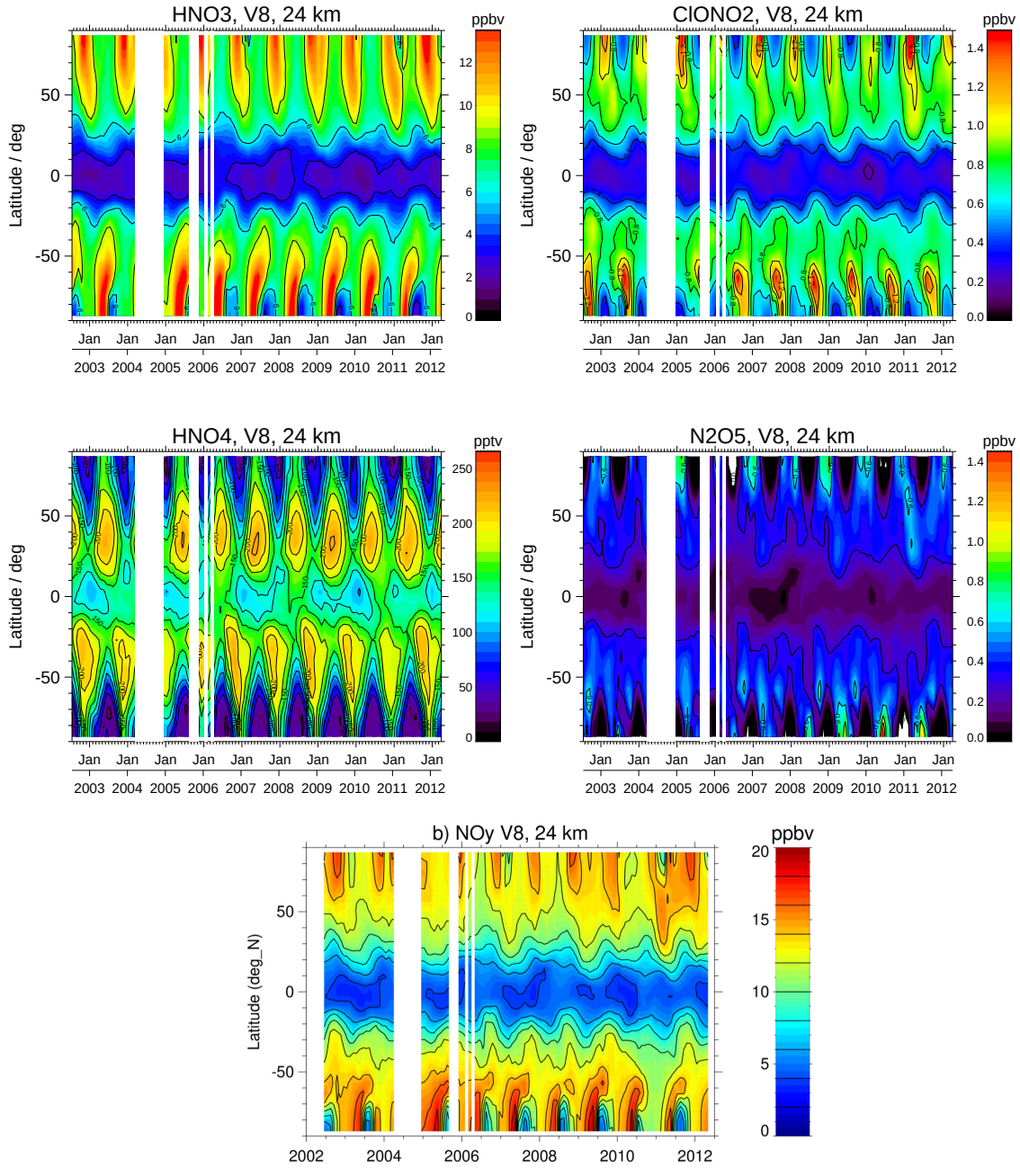


**Figure 23.** Time series at 24 km altitude over all latitudes of $HNO_3$ (top left), $ClONO_2$ (top right), $HNO_4$ (middle left), $N_2O_5$ (middle right), and $NO_y$ (bottom). White areas are missing data due to filter criteria. White stripes are missing data due to inactivity of MIPAS.

https://doi.org/10.5194/egusphere-2026-4116
Preprint. Discussion started: 29 July 2026


contrast, in the Arctic, high $ClONO_2$ amounts are observed up to the North Pole during longer periods during the winter, since denitrification occurs far less frequently than in Antarctic winters. Enhanced abundances are also observed during mid-latitude spring in both hemispheres, with unusually high values recorded in the northern hemisphere in spring 2003 and 2011, and in the southern hemisphere in spring 2002 and 2006.

The 24-km time series of $HNO_4$ (Fig. 23, middle left panel) shows regular maxima in the mid-latitudes in hemispheric summer, and minima during polar night. The respective minimum is less pronounced in the Arctic winter due to higher abundances of $NO_x$ available there. Inter-annual variations of the hemispheric mid-latitude maxima seem to be related to the global stratospheric dynamical situation. For example, the unusually low South hemispheric maximum around and after January 2011 occurs at the same time as the exceptionally persistent late Arctic winter vortex of 2011 (Ardra et al., 2022), which seems to demonstrate an event of inter-hemispheric dynamical coupling.

The $N_2O_5$ time series at 24 km (Fig. 23, middle right panel) is difficult to interpret since it represents the conditions at the lower edge of the stratospheric maximum (compare Fig. 22, middle right panel), and it is shown for completeness only. The variations observed are mainly due to inter-annual variations in the stratospheric circulation. We observe a polar fall to early winter maximum at this altitude in both hemispheres, and a minimum in spring and summer, the latter due to photolysis in permanent sunlight. In mid-latitudes, maxima at this altitude occur around spring equinox. While at higher altitudes, a stratospheric maximum is present in the tropics during all seasons (compare Fig. 22, middle right panel), the tropical abundances of $N_2O_5$ at 24 km are always low.

$NO_y$ time series at 24 km (Fig. 23, bottom panel) are characterized by the meridional transport and simultaneous subsidence of the stratospheric tropical $NO_y$ maximum around 40 km (see Fig. 22, bottom panel) by the Brewer-Dobson circulation. The enhancements are more pronounced and more regular in the Antarctic winter because of the more stable vortex there, providing more effective subsidence than in the Arctic. After the subsidence phase, denitrification is clearly visible in all Antarctic winters, while it is less pronounced in the Arctic where it is obvious in the winters 2003, 2007, 2010, and 2011 only. The end of the year 2010 and all the year 2011 are exceptional both in the Northern and the Southern hemisphere with relatively low $NO_y$ amounts in the Southern mid to high latitudes during end of 2010, and very high amounts in the Northern mid to high latitudes from spring 2011 on. This seems to be related to the unusual dynamical situation in spring 2011, leading to the unprecedented Arctic ozone loss in 2011 (Manney et al., 2011). At 24 km, the stratospheric $NO_y$ abundances are lowest in the tropics.

Altitude-time cross sections for 70°S to 90°S of $HNO_3$, $ClONO_2$, $HNO_4$, $N_2O_5$, and $NO_y$ are displayed in Fig. 24. The $NO_y$ time series (bottom panel) is characterized by strong intrusions from the mesosphere lasting from late fall to midwinter, resulting from the subsidence of high mesospheric $NO_x$ abundances that are regularly produced by high energetic particles precipitating into the upper atmosphere (Funke et al., 2014a, b). The intrusions shown here are in good agreement with those from an earlier MIPAS data version shown in Funke et al. (2014b) (their Fig.1). The denitrification due to PSC formation that takes place during mid and late winter leads to the strong reduction of $NO_y$ abundances that can be seen below about 25 km. The middle atmosphere summer maximum is consistent with the zonal mean distribution shown in Fig. 22. The $NO_x$ intrusions from the mesosphere can also be seen in the time series of $HNO_3$, $ClONO_2$, and $N_2O_5$. As discussed in Stiller et al. (2005),

https://doi.org/10.5194/egusphere-2026-4116
Preprint. Discussion started: 29 July 2026


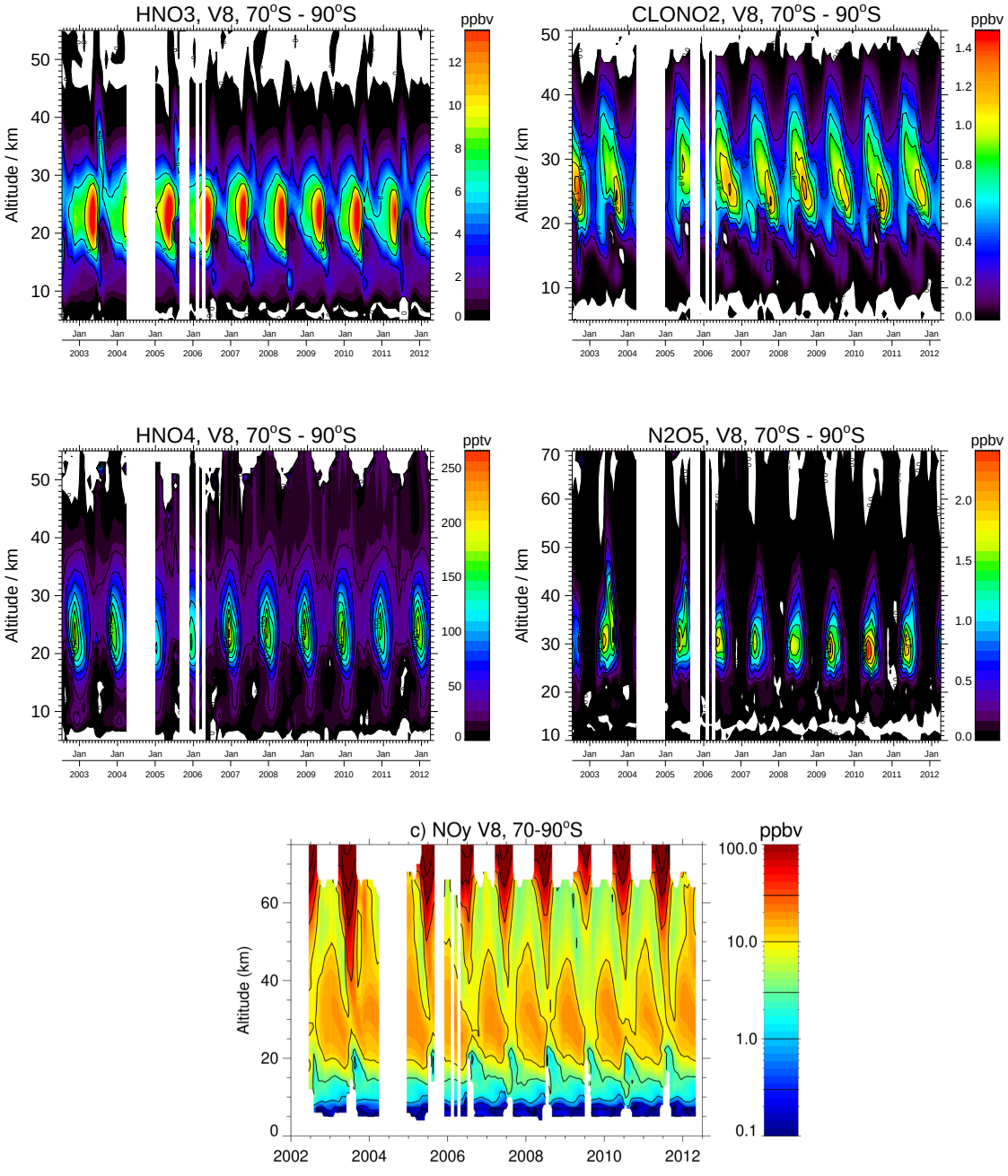


**Figure 24.** Altitude-time cross sections for 70°S - 90°S of $HNO_3$ (top left), $ClONO_2$ (top right), $HNO_4$ (middle left), $N_2O_5$ (middle right), and $NO_y$ (bottom). White areas are missing data due to filter criteria. White stripes are missing data due to inactivity of MIPAS.

https://doi.org/10.5194/egusphere-2026-4116
Preprint. Discussion started: 29 July 2026


$N_2O_5$ is formed earliest in winter at 40 km and above from the $NO_x$ intrusions, beginning approximately in May. $N_2O_5$ is then converted into $HNO_3$ via reactions on water ion clusters, and, at lower altitudes, at sulfate aerosols. $ClONO_2$ forms at the altitude of the upper maximum of ClO around 40 km (Glatthor et al., 2025). The $NO_y$ reservoir gases are converted into each other, by photolysis and further chemical reactions, during their further downward transport, and reach finally the main $NO_y$ layer in the middle stratosphere.

Denitrification is visible both in the $HNO_3$ and $ClONO_2$ time series below about 25 km. Sedimentation of PSC particles and re-evaporation causes $HNO_3$ enhancements between 10 and 15 km from midwinter on. The summertime tropospheric enhancement of $HNO_4$ (compare also Fig. 22, middle left panel) is remarkable but has not been analyzed so far.

## 8 Coarse grid representation

The regularization used in our retrieval implies that for quantitative analysis of the data averaging kernels have to be used. Not all data users are familiar with the averaging kernel concept, provision of averaging kernels causes heavy data traffic, and there are applications, such as time series of data of varying vertical resolution, where even averaging kernels do not offer an obvious straightforward solution. To overcome these problems, we offer an alternative representation of the data on a fixed vertical grid that is coarser than the original retrieval grid, and where all information on the vertical resolution is provided by the grid itself. That means that with this representation, oversampling is avoided, and, thus, no averaging kernels are needed (von Clarmann et al., 2015). However, there is a price to pay: the vertical grid has to comply with the coarsest resolution of the entire set of measurements and is, thus, too coarse to represent the independent pieces of information of a profile recorded under more favourable conditions.

The method, applied to FR and RR NOM data only, analyses the averaging kernels of the original retrieval to identify a vertical grid on which the retrieval is stable even without regularization. This new grid is then used for a maximum likelihood retrieval without regularization. For a given species, this grid is the same for all latitudes and times, while the grids may differ from one species to another. As one advantage of the coarse grid representation on a fixed pressure grid, time series at certain pressure levels do not suffer from a varying vertical resolution over time, that might, in case of the original retrievals, lead to some misrepresentation of temporal variability.

To further ease the comparison to model simulations, the volume mixing ratios are provided as layer means, with grid levels selected from the pressure gridpoints CCMVal/CCMI model data are represented on (see, e.g. https://www.pa.op.dlr.de/CCMVal/DataRequests/CCMVal-2_Datarequest_FINAL.pdf; Eyring et al. (2013)). The layer boundaries lie half way (in pressure) in between adjacent levels of the original CCMVal/CCMI grid. With this representation we come as close as possible to the representation of trace gas distributions in Eulerian atmospheric models. The coarse grid data version is available in addition to the regular one and is not meant to supersede it.

https://doi.org/10.5194/egusphere-2026-4116
Preprint. Discussion started: 29 July 2026


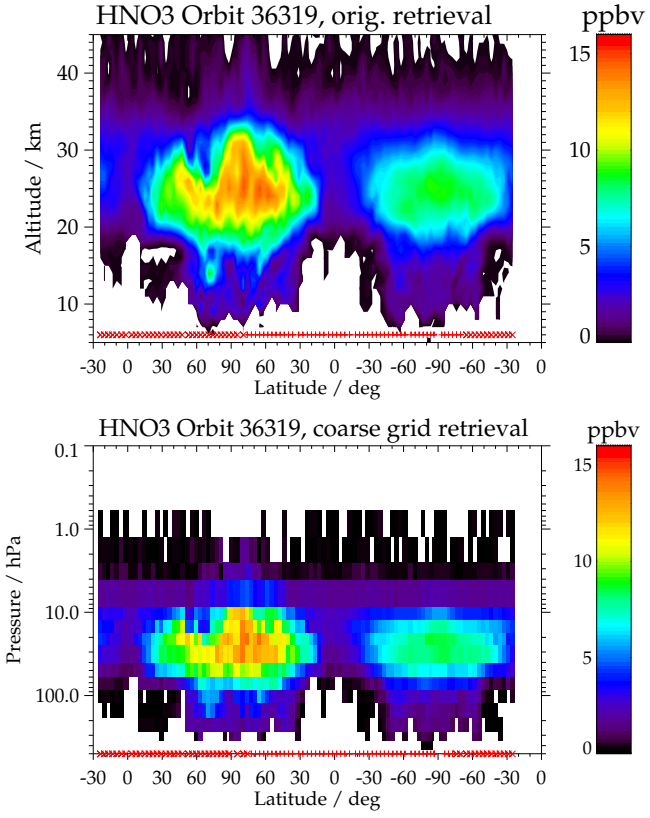


**Figure 25.** Coarse grid representation of MIPAS RR NOM $HNO_3$ data for orbit 36319, recorded on 9 February 2009. The top panel shows the regular retrieval, and the lower panel the result of the coarse grid retrieval after transformation to layers. The crosses and plus signs at the bottom of the two panels mark the ascending (10 pm) and descending (10 am) orbit legs, respectively. White areas are missing data, due to cloud interference or filter criteria, or negative values.

### 8.1 The coarse grid representation of $HNO_3$

An example of a coarse grid representation of $HNO_3$ along orbit 36319 measured on 9 February 2009 is shown in Figure 25. The respective data are provided as layer means around the following nominal pressures: 400, 300, 200, 150, 100, 70, 50, 30, 20, 15, 10, 5, 3, 1.5, and 0.7 hPa.

Since no regularization smooths the profiles, the vertical resolution in this representation is entirely defined by the grid width, and the averaging kernels are, by definition, unity. While the regular retrieval (Fig. 25, top panel) is richer in details, the coarse grid representation has the advantage that no averaging kernels are needed for quantitative data analysis, and that the vertical resolution is fully defined by the pressure grid and does not change with time.

https://doi.org/10.5194/egusphere-2026-4116
Preprint. Discussion started: 29 July 2026


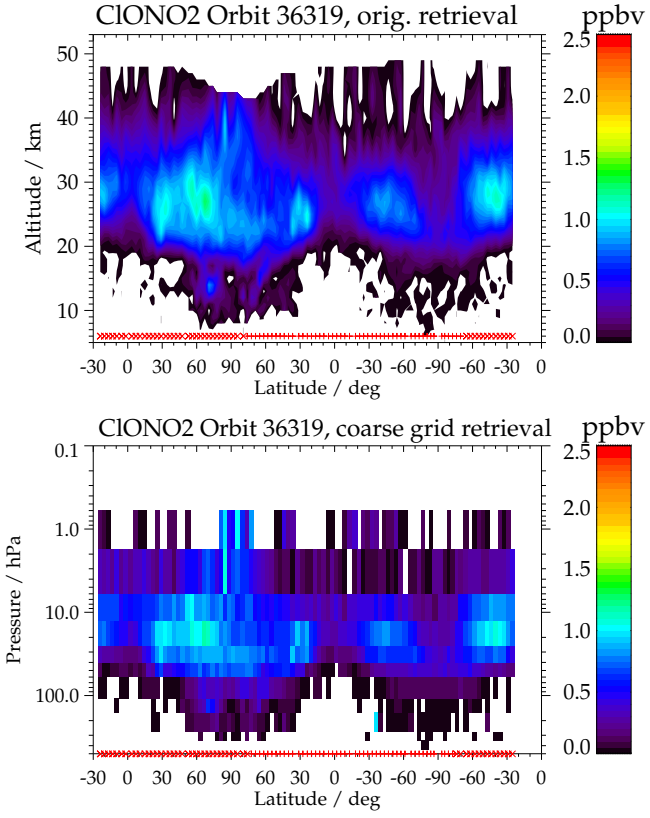


**Figure 26.** Coarse grid representation of MIPAS RR NOM $ClONO_2$ data for orbit 36319, recorded on 9 February 2009. The top panel shows the regular retrieval, and the lower panel the result of the coarse grid retrieval after transformation to layers. For more details, see Fig. 25.

### 8.2 The coarse grid representation of $ClONO_2$

The coarse grid representation of $ClONO_2$ is illustrated at the example of orbit 36319 measured on 9 February 2009 (Fig. 26).
705 The pressure grid for $ClONO_2$ layer means is 400, 300, 200, 130, 80, 50, 30, 15, 7, 3, and 1 hPa.

While the vertical resolution appears to be higher in the original regularized retrieval for most of the profiles, the main features of the $ClONO_2$ distribution along the orbit is reproduced in the coarse grid retrieval as well.

### 8.3 The coarse grid representation of $HNO_4$

Figure 27 shows the coarse grid representation of $HNO_4$ in comparison to the original retrieval for the same orbit as for $HNO_3$
710 and $ClONO_2$. The pressure grid had to be selected rather coarse in order to allow for a non-regularized retrieval on a fixed grid for all seasons and latitudes during the full mission period. The $HNO_4$ data in the coarse grid are provided as layer means

https://doi.org/10.5194/egusphere-2026-4116
Preprint. Discussion started: 29 July 2026


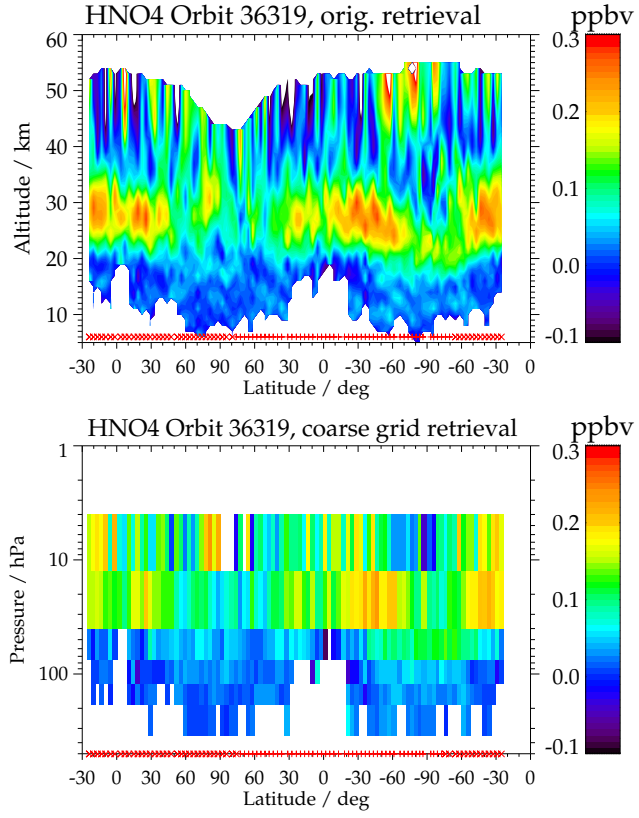


**Figure 27.** Coarse grid representation of MIPAS RR NOM $HNO_4$ data for orbit 36319, recorded on 9 February 2009. The top panel shows the regular retrieval, and the lower panel the result of the coarse grid retrieval after transformation to layers. For more details, see Fig. 25.

around the following nominal pressures: 250, 150, 90, 50, 20, 7, and 2 hPa. Because of the rather coarse vertical grid, some of the fine structure of the original retrievals is lost.

### 8.4 The coarse grid representation of $N_2O_5$

The coarse grid representation of $N_2O_5$ is provided in Fig. 28, together with the original retrieval, for the same example orbit as for the other gases. The pressure grid (layer centers) for $N_2O_5$ is 400, 200, 100, 50, 30, 20, 10, 5, 3, and 1.5 hPa. Again, the grid had to be selected quite coarse in order to allow for a non-regularized retrieval even under the most unfavourable conditions, where the original retrieval suffered from a coarse vertical resolution. Nevertheless, the main structures along the orbit are conserved.

https://doi.org/10.5194/egusphere-2026-4116
Preprint. Discussion started: 29 July 2026


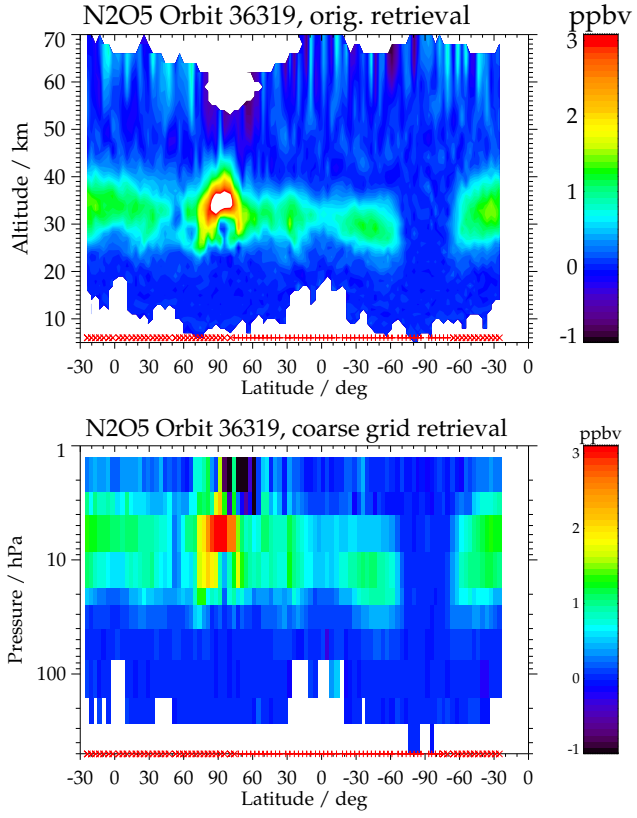


**Figure 28.** Coarse grid representation of MIPAS RR NOM $N_2O_5$ data for orbit 36319, recorded on 9 February 2009. The top panel shows the regular retrieval, and the lower panel the result of the coarse grid retrieval after transformation to layers. For more details, see Fig. 25.

## 9 Conclusions

We have presented the final IMK/IAA data version, V8, of MIPAS-Envisat global distributions of $HNO_3$, $ClONO_2$, $HNO_4$, $N_2O_5$, and the derived product $NO_y$ (generated from $[HNO_3] + [ClONO_2] + [HNO_4] + 2\times[N_2O_5] + [NO] + [NO_2]$). The data sets cover 10 years (although with some short gaps), have a global latitude coverage, from pole to pole during day and night, and an altitude coverage from about 6 to 80 km. We have described in detail the assumptions incorporated into the retrieval set-ups, the data characterization in terms of averaging kernels and spatial (vertical and horizontal) resolution, and the full TUNER-compliant error budget. We have compared the data version 8 data with the previous fully processed data version (V5), and have discussed changes in biases that were derived in validation efforts involving earlier data versions of both MIPAS and the reference data sets. As discussed along time series, the new data version provides improved consistency between the full- and reduced-resolution mission period of MIPAS, as well as between the observation modes covering different altitude

https://doi.org/10.5194/egusphere-2026-4116
Preprint. Discussion started: 29 July 2026


ranges. Finally, we have discussed the global distributions at the examples of zonal mean distributions and time series, and identified the most relevant signatures of processes that are expected to be observed, for example in polar winter.

The retrieval has been done on basis of all knowledge and experience gained during about 20 years of data processing and results, as we believe, in the best possible data product from MIPAS satellite observations we can produce. The data sets are publicly available and will hopefully be useful to the community in further scientific studies.

The supplement related to this article is available on-line at: https://doi.org/10.5194/amt-0-1-2026-supplement

*Data availability.* $HNO_3$, $ClONO_2$, $HNO_4$, $N_2O_5$, and $NO_y$ data can be downloaded after registration from https://www.imk-asf.kit.edu/english/308.php (last access: 22 April 2026).

*Author contributions.* GS identified necessary improvements of the retrieval, organized the interfacing between IMK and IAA, took care of quality control and largely contributed to the final decisions w.r.t. the retrieval setup, and wrote parts of the manuscript. She has the final editorial responsibility for this paper. NG developed the retrieval setup, performed related test calculations, was responsible for spectroscopy issues, and coded parts of the error estimation software. UG provided and maintained the retrieval software and coded parts of the error estimation software. MK performed the error estimation and the calculation of the horizontal averaging kernels. TvC drafted large parts of the text, organized related discussions and cared about TUNER compliance of error estimates. BF, SB, MGC and MLP took care that the retrieval setup was developed in a way that inter-consistence with the retrieval setups of middle and upper atmospheric measurement modes was maintained. BF and SB generated the $NO_y$ data product and provided its characterization. SK and A. Linden ran the retrievals, provided data visualisation, and helped with data analysis. A. Laeng contributed to quality control. All authors contributed to the development of the retrieval setup, discussed the results, and contributed to the final text.

*Competing interests.* Some authors are members of the editorial board of AMT. The authors have no other competing interests to declare.

*Acknowledgements.* Spectra used for this work were provided by the European Space Agency. We would like to thank the MIPAS Quality Working Group for enlightening discussions, Claus Zehner for invaluable support, and Guido Levrini for motivating us to develop an independent MIPAS data processor. The computations were done in the frame of a Bundesprojekt (grant MIPAS_V7) on the Cray XC40 “Hazel Hen” and on the HPE Apollo “Hawk” of the High-Performance Computing Center Stuttgart (HLRS) of the University of Stuttgart. The project on which this manuscript is based was funded by the Federal Ministry for Economic Affairs under the grant number 50EE1547 (SEREMISA). The IAA team acknowledges financial support from the Agencia Estatal de Investigación, MCIN/AEI/10.13039/501100011033, through grants PID2022-141216NB-I00 and CEX2021-001131-S. The responsibility for the content of this publication is the responsibility of the authors. Error estimation was carried out in the framework of the WRCP-APARC Activity TUNER.

https://doi.org/10.5194/egusphere-2026-4116
Preprint. Discussion started: 29 July 2026


## References

Adams, C., Bourassa, A. E., McLinden, C. A., Sioris, C. E., von Clarmann, T., Funke, B., Rieger, L. A., and Degenstein, D. D.: Effect of volcanic aerosol on stratospheric $NO_2$ and $N_2O_5$ from 2002-2014 as measured by Odin-OSIRIS and Envisat-MIPAS, Atmos. Chem. Phys., 17, 8063–8080, https://doi.org/10.5194/acp-17-8063-2017, 2017.

Ardra, D., Kuttippurath, J., Roy, R., Kumar, P., Raj, S., Müller, R., and Feng, W.: The Unprecedented Ozone Loss in the Arctic Winter and Spring of 2010/2011 and 2019/2020, ACS Earth and Space Chemistry, 6, 683–693, https://doi.org/10.1021/acsearthspacechem.1c00333, 2022.

Baumgaertner, A. J. G., Jöckel, P., Riede, H., Stiller, G., and Funke, B.: Energetic particle precipitation in ECHAM5/MESSy – Part 2: Solar Proton Events, Atmospheric Chemistry and Physics, 10, 7285–7302, https://doi.org/10.5194/acp-10-7285-2010, 2010.

Brasseur, G. and Solomon, S.: Aeronomy of the Middle Atmosphere–Chemistry and Physics of the Stratosphere and Mesosphere, Atmospheric and Oceanographic Sciences Library 32, Springer, P. O. Box 17, 3300 AA Dordrecht, The Netherlands, ISBN 978-1-4020-3284-4, doi:10.1007/1-4020-3824-0, third edn., https://doi.org/10.1007/1-4020-3824-0, 2005.

Brühl, C., Steil, B., Stiller, G., Funke, B., and Jöckel, P.: Nitrogen compounds and ozone in the stratosphere: comparison of MIPAS satellite data with the chemistry climate model ECHAM5/MESSy1, Atmospheric Chemistry and Physics, 7, 5585–5598, https://doi.org/10.5194/acp-7-5585-2007, 2007.

Chauhan, S., Höpfner, M., Stiller, G. P., von Clarmann, T., Funke, B., Glatthor, N., Grabowski, U., Linden, A., Kellmann, S., Milz, M., Steck, T., Fischer, H., Froidevaux, L., Lambert, A., Santee, M. L., Schwartz, M., Read, W. G., and Livesey, N. J.: MIPAS reduced spectral resolution UTLS-1 mode measurements of temperature, $O_3$, $HNO_3$, $N_2O$, $H_2O$ and relative humidity over ice: retrievals and comparison to MLS, Atmospheric Measurement Techniques, 2, 337–353, https://doi.org/10.5194/amt-2-337-2009, 2009.

Chipperfield, M. P., Lutman, E. R., Kettleborough, J. A., Pyle, J. A., and Roche, A. E.: Model studies of chlorine deactivation and formation of $ClONO_2$ collar in the Arctic polar vortex, J. Geophys. Res., 102, 1467–1478, 1997.

Chirkov, M., Stiller, G. P., Laeng, A., Kellmann, S., von Clarmann, T., Boone, C., Elkins, J. W., Engel, A., Glatthor, N., Grabowski, U., Harth, C. M., Kiefer, M., Kolonjari, F., Krummel, P. B., Linden, A., Lunder, C. R., Miller, B. R., Montzka, S. A., Mühle, J., O'Doherty, S., Orphal, J., Prinn, R. G., Toon, G., Vollmer, M. K., Walker, K. A., Weiss, R. F., Wiegele, A., and Young, D.: Global HCFC-22 measurements with MIPAS: retrieval, validation, global distribution and its evolution over 2005-2012, Atmos. Chem. Phys., 16, 3345–3368, https://doi.org/10.5194/acp-16-3345-2016, 2016.

Crutzen, P. J.: Ozone Production Rates in an Oxygen–Hydrogen–Nitrogen Oxide Atmosphere, J. Geophys. Res., 76, 7311–7327, 1971.

Damiani, A., Funke, B., Marsh, D. R., López-Puertas, M., Santee, M. L., Froidevaux, L., Wang, S., Jackman, C. H., von Clarmann, T., Gardini, A., Cordero, R. R., and Storini, M.: Impact of January 2005 solar proton events on chlorine species, Atmos. Chem. Phys., 12, 4159–4179, https://doi.org/10.5194/acp-12-4159-2012, 2012.

Damiani, A., Funke, B., López-Puertas, M., Gardini, A., von Clarmann, T., Santee, M. L., Froidevaux, L., and Cordero, R. R.: Changes in the composition of the northern polar upper stratosphere in February 2009 after a sudden stratospheric warming, J. Geophys. Res. Atmos., 119, 11,429–11,444, https://doi.org/10.1002/2014JD021698, 2014.

Eckert, E., von Clarmann, T., Laeng, A., Stiller, G. P., Funke, B., Glatthor, N., Grabowski, U., Kellmann, S., Kiefer, M., Linden, A., Babenhauserheide, A., Wetzel, G., Boone, C., Engel, A., Harrison, J. J., Sheese, P. E., Walker, K. A., and Bernath, P. F.: MIPAS IMK/IAA carbon tetrachloride ($CCl_4$) retrieval and first comparison with other instruments, Atmos. Meas. Tech., 10, 2727–2743, https://doi.org/10.5194/amt-10-2727-2017, 2017.

https://doi.org/10.5194/egusphere-2026-4116
Preprint. Discussion started: 29 July 2026


Emmert, J. T., Drob, D. P., Picone, J. M., Siskind, D. E., Jones Jr., M., Mlynczak, M. G., Bernath, P. F., Chu, X., Doornbos, E., Funke, B., Goncharenko, L. P., Hervig, M. E., Schwartz, M. J., Sheese, P. E., Vargas, F., Williams, B. P., and Yuan, T.: NRLMSIS 2.0: A whole-atmosphere empirical model of temperature and neutral species densities, Earth and Space Science, 7, e2020EA001 321, https://doi.org/10.1029/2020EA001321, 2020.

Ennis, C. A.: Scientific Assessment of Ozone Depletion: 2002, World Meteorological Organization, Geneva, 2003.

Eyring, V., Lamarque, J.-F., Hess, P., Arfeuille, F., Bowman, K., Chipperfield, M. P., Duncan, B., Fiore, A., Gettelman, A., Giorgetta, M. A., Granier, C., Hegglin, M., Kinnison, D., Kunze, M., Langematz, U., Luo, B., Martin, R., Matthes, K., Newman, P. A., Peter, T., Robock, A., Ryerson, T., Saiz-Lopez, A., Salawitch, R., Schultz, M., Shepherd, T. G., Shindell, D., Staehelin, J., Tegtmeier, S., Thomason, L., Tilmes, S., Vernier, J.-P., Waugh, D. W., and Young, P. J.: Overview of IGAC/SPARC Chemistry-Climate Model Initiative (CCMI) Community Simulations in Support of Upcoming Ozone and Climate Assessments, in: SPARC Newsletter No. 40, January 2013, available at http://www.aparc-climate.org/publications/newsletter, 2013.

Fahey, D. W., Kawa, S. R., and Chan, K. R.: Nitric oxide measurements in the Arctic winter stratosphere, Geophys. Res. Lett., 17, 489–492, 1990.

Fischer, H., Birk, M., Blom, C., Carli, B., Carlotti, M., von Clarmann, T., Delbouille, L., Dudhia, A., Ehhalt, D., Endemann, M., Flaud, J. M., Gessner, R., Kleinert, A., Koopmann, R., Langen, J., López-Puertas, M., Mosner, P., Nett, H., Oelhaf, H., Perron, G., Remedios, J., Ridolfi, M., Stiller, G., and Zander, R.: MIPAS: an instrument for atmospheric and climate research, Atmos. Chem. Phys., 8, 2151–2188, https://doi.org/10.5194/acp-8-2151-2008, 2008.

Flaud, J.-M., Perrin, A., and Ridolfi, M.: New release of MIPAS spectroscopic database v.4.45: hitran_mipas_pf_v4.45, presentation at MIPAS QWG 38 ESA-ESRIN, 18-19 February 2015., 2015.

Forster, P., Ramaswamy, V., Artaxo, P., Berntsen, T., Betts, R., Fahey, D. W., Haywood, J., Lean, J., Lowe, D. C., Myhre, G., Nganga, J., Prinn, R., Raga, G., Schulz, M., and Van Dorland, R.: Changes in Atmospheric Constituents and in Radiative Forcing, in: Climate Change 2007: The Physical Science Basis. Contribution of Working Group I to the Fourth Assessment Report of the Intergovernmental Panel on Climate Change, Cambridge University Press, Cambridge, United Kingdom and New York, NY, USA, 2007.

Friederich, F., von Clarmann, T., Funke, B., Nieder, H., Orphal, J., Sinnhuber, M., Stiller, G. P., and Wissing, J. M.: Lifetime and production rate of $NO_x$ in the upper stratosphere and lower mesosphere in the polar spring/summer after the solar proton event in October-November 2003, Atmos. Chem. Phys., 13, 2531–2539, https://doi.org/10.5194/acp-13-2531-2013, 2013.

Friederich, F., Sinnhuber, M., Funke, B., von Clarmann, T., and Orphal, J.: Local impact of solar variation on $NO_2$ in the lower mesosphere and upper stratosphere from 2007-2012, Atmos. Chem. Phys., 14, 4055–4064, https://doi.org/10.5194/acp-14-4055-2014, 2014.

Friedl, R. R., May, R. D., and Duxbury, G.: The $\nu_6$, $\nu_7$, $\nu_8$, and $\nu_{10}$ Bands of $HO_2NO_2$, Journal of Molecular Spectroscopy, 165, 481–493, https://doi.org/https://doi.org/10.1006/jmsp.1994.1151, 1994.

Funke, B., López-Puertas, M., Gil-López, S., von Clarmann, T., Stiller, G. P., Fischer, H., and Kellmann, S.: Downward transport of upper atmospheric $NO_x$ into the polar stratosphere and lower mesosphere during the Antarctic 2003 and Arctic 2002/2003 winters, J. Geophys. Res., 110, D24308, https://doi.org/10.1029/2005JD006463, 2005a.

Funke, B., López-Puertas, M., von Clarmann, T., Stiller, G. P., Fischer, H., Glatthor, N., Grabowski, U., Höpfner, M., Kellmann, S., Kiefer, M., Linden, A., Mengistu Tsidu, G., Milz, M., Steck, T., and Wang, D. Y.: Retrieval of stratospheric $NO_x$ from 5.3 and 6.2 $\mu$m nonlocal thermodynamic equilibrium emissions measured by Michelson Interferometer for Passive Atmospheric Sounding (MIPAS) on Envisat, J. Geophys. Res., 110, D09302, https://doi.org/10.1029/2004JD005225, 2005b.

https://doi.org/10.5194/egusphere-2026-4116
Preprint. Discussion started: 29 July 2026


Funke, B., Baumgaertner, A., Calisto, M., Egorova, T., Jackman, C. H., Kieser, J., Krivolutsky, A., López-Puertas, M., Marsh, D. R., Reddmann, T., Rozanov, E., Salmi, S.-M., Sinnhuber, M., Stiller, G. P., Verronen, P. T., Versick, S., von Clarmann, T., Vyushkova, T. Y., Wieters, N., and Wissing, J. M.: Composition changes after the "Halloween" solar proton event: the High Energy Particle Precipitation in the Atmosphere (HEPPA) model versus MIPAS data intercomparison study, Atmos. Chem. Phys., 11, 9089–9139, 2011.

Funke, B., López-Puertas, M., Holt, L., Randall, C. E., Stiller, G. P., and von Clarmann, T.: Hemispheric distributions and interannual variability of NOy produced by energetic particle precipitation in 2002-2012, J. Geophys. Res. Atmos., 119, 13,565–13,582, https://doi.org/10.1002/2014JD022423, 2014a.

Funke, B., López-Puertas, M., Stiller, G. P., and von Clarmann, T.: Mesospheric and stratospheric NOy produced by energetic particle precipitation during 2002-2012, J. Geophys. Res. Atmos., 119, 4429–4446, https://doi.org/10.1002/2013JD021404, 2014b.

Funke, B., López-Puertas, M., Stiller, G. P., Versick, S., and von Clarmann, T.: A semi-empirical model for mesospheric and stratospheric $NO_y$ produced by energetic particle precipitation, Atmos. Chem. Phys., 16, 8667–8693, https://doi.org/10.5194/acp-16-8667-2016, 2016.

Funke, B., Ball, W., Bender, S., Gardini, A., Harvey, V. L., Lambert, A., López-Puertas, M., Marsh, D. R., Meraner, K., Nieder, H., Päivärinta, S.-M., Pérot, K., Randall, C. E., Reddmann, T., Rozanov, E., Schmidt, H., Seppälä, A., Sinnhuber, M., Sukhodolov, T., Stiller, G. P., Tsvetkova, N. D., Verronen, P. T., Versick, S., von Clarmann, T., Walker, K. A., and Yushkov, V.: HEPPA-II model-measurement intercomparison project: EPP indirect effects during the dynamically perturbed NH winter 2008-2009, Atmos. Chem. Phys., 17, 3573–3604, https://doi.org/10.5194/acp-17-3573-2017, 2017.

Funke, B., Arsénovic, P., López-Puertas, M., Marsh, D., Rosanov, E., Sinnhuber, M., Stiller, G., von Clarmann, T., and Versick, S.: The Stratospheric Reactive Nitrogen Budget, Oral presentation at the 27th IUGG General Assembly, Montreal, Canada, 8 - 18 July 2019, 2019.

Funke, B., García-Comas, M., Glatthor, N., Grabowski, U., Kellmann, S., Kiefer, M., Linden, A., López-Puertas, M., Stiller, G. P., and von Clarmann, T.: Michelson Interferometer for Passive Atmospheric Sounding Institute of Meteorology and Climate Research/Instituto de Astrofísica de Andalucía version 8 retrieval of nitric oxide and lower-thermospheric temperature, Atmospheric Measurement Techniques, 16, 2167–2196, https://doi.org/10.5194/amt-16-2167-2023, 2023.

Funke, B., von Clarmann, T., García-Comas, M., Glatthor, N., Grabowski, U., Kellmann, S., Kiefer, M., Linden, A., López-Puertas, M., and Stiller, G. P.: MIPAS IMK/IAA version 8 retrieval of $NO_2$, Atmos. Meas. Tech. Disc., in preparation, 2026.

Fytterer, T., Mlynczak, M. G., Nieder, H., Pérot, K., Sinnhuber, M., Stiller, G., and Urban, J.: Energetic particle induced intra-seasonal variability of ozone inside the Antarctic polar vortex observed in satellite data, Atmos. Chem. Phys., 15, 3327–3338, https://doi.org/10.5194/acp-15-3327-2015, 2015.

García, R. R., Smith, A. K., Kinnison, D. E., de la Cámara, Á., and Murphy, D.: Modification of the Gravity Wave Parameterization in the Whole Atmosphere Community Climate Model: Motivation and Results, J. Atmos. Sci., 74, 275–291, https://doi.org/10.1175/JAS-D-16-0104.1, 2017.

Glatthor, N., von Clarmann, T., Fischer, H., Funke, B., Grabowski, U., Höpfner, M., Kellmann, S., Linden, A., Milz, M., Steck, T., and Stiller, G. P.: Global peroxyacetyl nitrate (PAN) retrieval in the upper troposphere from limb emission spectra of the Michelson Interferometer for Passive Atmospheric Sounding (MIPAS), Atmospheric Chemistry and Physics, 7, 2775–2787, https://doi.org/10.5194/acp-7-2775-2007, 2007.

Glatthor, N., von Clarmann, T., Stiller, G. P., Funke, B., Koukouli, M. E., Fischer, H., Grabowski, U., Höpfner, M., Kellmann, S., and Linden, A.: Large-scale upper tropospheric pollution observed by MIPAS HCN and $C_2H_6$ global distributions, Atmos. Chem. Phys., 9, 9619–9634, https://doi.org/10.5194/acp-9-9619-2009, 2009.

https://doi.org/10.5194/egusphere-2026-4116
Preprint. Discussion started: 29 July 2026


Glatthor, N., Höpfner, M., Leyser, A., Stiller, G. P., von Clarmann, T., Grabowski, U., Kellmann, S., Linden, A., Sinnhuber, B.-M., Krysztofiak, G., and Walker, K. A.: Global carbonyl sulfide (OCS) measured by MIPAS/Envisat during 2002-2012, Atmos. Chem. Phys., 17, 2631–2652, https://doi.org/10.5194/acp-17-2631-2017, 2017.

Glatthor, N., von Clarmann, T., Funke, B., García-Comas, M., Grabowski, U., Höpfner, M., Kellmann, S., Kiefer, M., Laeng, A., Linden, A., López-Puertas, M., and Stiller, G. P.: IMK–IAA MIPAS retrieval version 8: $CH_4$ and $N_2O$, Atmospheric Measurement Techniques, 17, 2849–2871, https://doi.org/10.5194/amt-17-2849-2024, 2024a.

Glatthor, N., von Clarmann, T., Funke, B., Grabowski, U., Kellmann, S., Kiefer, M., Linden, A., and Stiller, G. P.: MIPAS IMK/IAA version 8 retrieval of ClO and HOCl, Atm. Meas. Tech. Disc., in preparation, 2024b.

Glatthor, N., von Clarmann, T., Grabowski, U., Kellmann, S., Kiefer, M., Laeng, A., Linden, A., Stiller, G. P., Funke, B., Garcia-Comas, M., Lopez-Puertas, M., Kirner, O., and Santee, M. L.: Version 8 IMK/IAA MIPAS measurements of ClO, EGUsphere, 2025, 1–44, https://doi.org/10.5194/egusphere-2025-3352, 2025.

Gordon, I. E., Rothman, L. S., Hill, C., Kochanov, R. V., Tan, Y., Bernath, P. F., Birk, M., Boudon, V., Campargue, A., Chance, K. V., Drouin, B. J., Flaud, J.-M., Gamache, R. R., Hodges, J. T., Jacquemart, D., Perevalov, V. I., Perrin, A., Shine, K. P., Smith, M.-A. H., Tennyson, J., Toon, G. C., Tran, H., Tyuterev, V. G., Barbe, A., Császár, A. G., Devi, V. M., Furtenbacher, T., Harrison, J. J., Hartmann, J.-M., Jolly, A., Johnson, T. J., Karman, T., Kleiner, I., Kyuberis, A. A., Loos, J., Lyulin, O. M., Massie, S. T., Mikhailenko, S. N., Moazzen-Ahmadi, N., Müller, H. S. P., Naumenko, O. V., Nikitin, A. V., Polyansky, O. L., Rey, M., Rotger, M., Sharpe, S. W., Sung, K., Starikova, E., Tashkun, S. A., Vander Auwera, J., Wagner, G., Wilzewski, J., Wcisło, P., Yu, S., and Zak, E. J.: The HITRAN2016 molecular spectroscopic database, J. Quant. Spectrosc. Radiat. Transfer, 203, 3–69, https://doi.org/10.1016/j.jqsrt.2017.06.038, 2017.

Granier, C. and Brasseur, G.: Impact of Heterogeneous Chemistry on Model Predictions of Ozone Changes, J. Geophys. Res., 97, 18,015–18,033, 1992.

Grooß, J.-U., Engel, I., Borrmann, S., Frey, W., Günther, G., Hoyle, C. R., Kivi, R., Luo, B. P., Molleker, S., Peter, T., Pitts, M. C., Schlager, H., Stiller, G., Vömel, H., Walker, K. A., and Müller, R.: Nitric acid trihydrate nucleation and denitrification in the Arctic stratosphere, Atmos. Chem. Phys., 14, 1055–1073, https://doi.org/10.5194/acp-14-1055-2014, 2014.

Günther, A., Höpfner, M., Sinnhuber, B.-M., Griessbach, S., Deshler, T., von Clarmann, T., and Stiller, G.: MIPAS observations of volcanic sulphate aerosol and sulphur dioxide in the stratosphere, Atmos. Chem. Phys, 18, 1217–1239, https://doi.org/10.5194/acp-18-1217-2018, 2018.

Hase, F.: Transformation of irradiated to measured spectral distribution due to finite spectral resolution and field of view extent of a Fourier transform spectrometer, in: The Karlsruhe Optimized and Precise Radiative transfer Algorithm (KOPRA), edited by Stiller, G. P., Wissenschaftliche Berichte FZKA 6487, pp. 119–132, Forschungszentrum Karlsruhe, 2000.

Hase, F.: The instrument line shape of MIPAS, Oral presentation at the 2nd MIPAS Quality Working Group Meeting, Florence, 3 Dec. 2003, 2003.

Hegglin, M., Tegtmeier, S., Anderson, J., Bourassa, A. E., Brohede, S., Degenstein, D., Froidevaux, L., Funke, B., Gille, J., Kasai, Y., Kyrölä, E., Lumpe, J., Murtagh, D., Neu, J. L., Pérot, K., Remsberg, E., Rozanov, A., Toohey, M., Urban, J., von Clarmann, T., Walker, K. A., Wang, H.-J., Arosio, C., Damadeo, R., Fuller, R., Lingenfelser, G., McLinden, C., Pendlebury, D., Roth, C., Ryan, N. J., Sioris, C., Smith, L., and Weigel, K.: Overview and update of the SPARC Data Initiative: comparison of stratospheric composition measurements from satellite limb sounders, Earth Syst. Sci. Data, 13, 1855–1903, https://doi.org/10.5194/essd-13-1855-2021, 2021.

Hegglin, M. I. and Tegtmeier, S., eds.: The SPARC Data Initiative: Assessment of stratospheric trace gas and aerosol climatologies from satellite limb sounders, SPARC Report No. 8, WCRP-5/2017, SPARC, https://doi.org/10.3929/ethz-a-010863911, 2017.

https://doi.org/10.5194/egusphere-2026-4116
Preprint. Discussion started: 29 July 2026


Höpfner, M., von Clarmann, T., Fischer, H., Glatthor, N., Grabowski, U., Kellmann, S., Kiefer, M., Linden, A., Mengistu Tsidu, G., Milz, M., Steck, T., Stiller, G. P., Wang, D.-Y., and Funke, B.: First spaceborne observations of Antarctic stratospheric $ClONO_2$ recovery: Austral spring 2002, J. Geophys. Res., 109, D11308, https://doi.org/10.1029/2004JD004609, 2004.

Höpfner, M., Larsen, N., Spang, R., Luo, B., Ma, J., Svendsen, S., Eckerman, S. D., Knudsen, B., Massoli, P., Cairo, F., Stiller, G. P., von Clarmann, T., and Fischer, H.: MIPAS detects Antarctic stratospheric belt of NAT PSC's caused by mountain waves, Atmospheric Chemistry and Physics, 6, 1221–1230, https://doi.org/10.5194/acp-6-1221-2006, 2006a.

Höpfner, M., Luo, B. P., Massoli, P., Cairo, F., Spang, R., Snels, M., Di Donfrancesco, G., Stiller, G. P., von Clarmann, T., Fischer, H., and Biermann, U.: Spectroscopic evidence for $\beta$–NAT, STS, and ice in MIPAS infrared limb emission measurements of polar stratospheric clouds, Atmos. Chem. Phys., 6, 1201–1219, https://doi.org/10.5194/acp-6-1201-2006, 2006b.

Höpfner, M., von Clarmann, T., Fischer, H., Funke, B., Glatthor, N., Grabowski, U., Kellmann, S., Kiefer, M., Linden, A., Milz, M., Steck, T., Stiller, G. P., Bernath, P., Blom, C. E., Blumenstock, T., Boone, C., Chance, K., Coffey, M. T., Friedl-Vallon, F., Griffith, D., Hannigan, J. W., Hase, F., Jones, N., Jucks, K. W., Keim, C., Kleinert, A., Kouker, W., Liu, G. Y., Mahieu, E., Mellqvist, J., Mikuteit, S., Notholt, J., Oelhaf, H., Piesch, C., Reddmann, T., Ruhnke, R., Schneider, M., Strandberg, A., Toon, G., Walker, K. A., Warneke, T., Wetzel, G., Wood, S., and Zander, R.: Validation of MIPAS $ClONO_2$ measurements, Atmos. Chem. Phys., 7, 257–281, https://doi.org/10.5194/acp-7-257-2007, 2007.

Höpfner, M., Orphal, J., von Clarmann, T., Stiller, G., and Fischer, H.: Stratospheric $BrONO_2$ observed by MIPAS, Atmos. Chem. Phys., 9, 1735–1746, 2009.

Höpfner, M., Boone, C. D., Funke, B., Glatthor, N., Grabowski, U., Günther, A., Kellmann, S., Kiefer, M., Linden, A., Lossow, S., Pumphrey, H. C., Read, W. G., Roiger, A., Stiller, G., Schlager, H., von Clarmann, T., and Wissmüller, K.: Sulfur dioxide ($SO_2$) from MIPAS in the upper troposphere and lower stratosphere 2002-2012, Atmos. Chem. Phys., 15, 7017–7037, https://doi.org/10.5194/acp-15-7017-2015, 2015.

Höpfner, M., Deshler, T., Pitts, M., Poole, L., Spang, R., Stiller, G., and von Clarmann, T.: The MIPAS/Envisat climatology (2002–2012) of polar stratospheric cloud volume density profiles, Atmos. Meas. Tech., 11, 5901–5923, https://doi.org/10.5194/amt-11-5901-2018, 2018.

Höpfner, M., Kirner, O., Wetzel, G., Sinnhuber, B.-M., Haenel, F., Johansson, S., Orphal, J., Ruhnke, R., Stiller, G., and von Clarmann, T.: The Michelson Interferometer for Passive Atmospheric Sounding global climatology of $BrONO_2$ 2002–2012: a test for stratospheric bromine chemistry, Atmos. Chem. Phys., 21, 18 433–18 464, https://doi.org/10.5194/acp-21-18433-2021, 2021.

Jackman, C. H., Marsh, D. R., Vitt, F. M., Garcia, R. R., Fleming, E. L., Labow, G. J., Randall, C. E., López-Puertas, M., Funke, B., von Clarmann, T., and Stiller, G. P.: Short- and medium-term atmospheric constituent effects of very large solar proton events, Atmospheric Chemistry and Physics, 8, 765–785, https://doi.org/10.5194/acp-8-765-2008, 2008.

Jackman, C. H., Marsh, D. R., Vitt, F. M., Roble, R. G., Randall, C. E., Bernath, P. F., Funke, B., López-Puertas, M., Versick, S., Stiller, G. P., Tylka, A. J., and Fleming, E. L.: Northern Hemisphere atmospheric influence of the solar proton events and ground level enhancement in January 2005, Atmos. Chem. Phys., 11, 6153–6166, 2011.

Junge, C. E. and Manson, J. E.: Stratospheric aerosol studies, J. Geophys. Res., 66, 2163–2182, https://doi.org/10.1029/JZ066i007p02163, 1961.

Kellmann, S., von Clarmann, T., Stiller, G. P., Eckert, E., Glatthor, N., Höpfner, M., Kiefer, M., Orphal, J., Funke, B., Grabowski, U., Linden, A., Dutton, G. S., and Elkins, J. W.: Global CFC-11 ($CCl_3F$) and CFC-12 ($CCl_2F_2$) Measurements with the Michelson Interferometer for Passive Atmospheric Sounding (MIPAS): retrieval, climatologies and trends, Atmos. Chem. Phys., 12, 11 857–11 875, https://doi.org/10.5194/acp-12-11857-2012, 2012.

https://doi.org/10.5194/egusphere-2026-4116
Preprint. Discussion started: 29 July 2026


Khosrawi, F., Kirner, O., Stiller, G., Höpfner, M., Santee, M. L., Kellmann, S., and Braesicke, P.: Comparison of ECHAM5/MESSy Atmospheric Chemistry (EMAC) simulations of the Arctic winter 2009/2010 and 2010/2011 with Envisat/MIPAS and Aura/MLS Observations, Atmos. Chem. Phys., 18, 8873–8892, https://doi.org/10.5194/acp-18-8873-2018, 2018.

Kiefer, M., von Clarmann, T., and Grabowski, U.: State parameter Data Base for MIPAS Data Analysis, Adv. Space Res., 30, 2387–2392, https://doi.org/https://doi.org/10.1016/S0273-1177(02)80284-8, 2002.

Kiefer, M., von Clarmann, T., Funke, B., García-Comas, M., Glatthor, N., Grabowski, U., Kellmann, S., Kleinert, A., Laeng, A., Linden, A., López-Puertas, M., Marsh, D., and Stiller, G. P.: IMK/IAA MIPAS temperature retrieval version 8: nominal measurements, Atmos. Meas. Tech., 14, 4111–4138, https://doi.org/10.5194/amt-14-4111-2021, 2021.

Kiefer, M., von Clarmann, T., Funke, B., García-Comas, M., Glatthor, N., Grabowski, U., Höpfner, M., Kellmann, S., Laeng, A., Linden, A., López-Puertas, M., and Stiller, G. P.: Version 8 IMK/IAA MIPAS ozone profiles: nominal observation mode, Atmos. Meas. Tech., 16, 1443–1460, https://doi.org/10.5194/amt-16-1443-2023, 2023.

Kiefer, M., García-Comas, M., Glatthor, N., Funke, B., Grabowski, U., Kellmann, S., Laeng, A., Linden, A., López-Puertas, M., Stiller, G. P., and von Clarmann, T.: Version 8 IMK/IAA MIPAS water vapour profiles, in preparation, 2024.

Kleinert, A., Birk, M., Perron, G., and Wagner, G.: Level 1b error budget for MIPAS on ENVISAT, Atmos. Meas. Tech., 11, 5657–5672, https://doi.org/10.5194/amt-11-5657-2018, 2018.

Konopka, P., Engel, A., Funke, B., Müller, R., Grooß, J.-U., Günther, G., Wetter, T., Stiller, G. P., von Clarmann, T., Glatthor, N., Oelhaf, H., Wetzel, G., López-Puertas, M., Pirre, M., Huret, N., and Riese, M.: Ozone loss driven by nitrogen oxides and triggered by stratospheric warmings can outweigh the effect of halogens, J. Geophys. Res., 112, D05105, https://doi.org/10.1029/2006JD007064, 2007.

López-Puertas, M., Funke, B., Gil-López, S., von Clarmann, T., Stiller, G. P., Höpfner, M., Kellmann, S., Fischer, H., and Jackman, C. H.: Observation of $NO_x$ Enhancement and Ozone Depletion in the Northern and Southern Hemispheres after the October–November 2003 Solar Proton Events, J. Geophys. Res., 110, A09S43, https://doi.org/10.1029/2005JA011050, 2005a.

López-Puertas, M., Funke, B., Gil-López, S., von Clarmann, T., Stiller, G. P., Höpfner, M., Kellmann, S., Mengistu Tsidu, G., Fischer, H., and Jackman, C. H.: $HNO_3$, $N_2O_5$ and $ClONO_2$ Enhancements after the October–November 2003 Solar Proton Events, J. Geophys. Res., 110, A09S44, https://doi.org/10.1029/2005JA011051, 2005b.

Manney, G. L., Santee, M. L., Rex, M., Livesey, N. J., Pitts, M. C., Veefkind, P., Nash, E. R., Wohltmann, I., Lehmann, R., Froidevaux, L., Poole, L. R., Schoeberl, M. R., Haffner, D. P., Davies, J., Dorokhov, V., Johnson, H. G. B., Kivi, R., Kyrö, E., Larsen, N., Levelt, P. F., Makshtas, A., McElroy, C. T., Nakajima, H., Parrondo, M. C., Tarasick, D. W., von der Gathen, P., Walker, K. A., and Zinoviev, N. S.: Unprecedented Arctic ozone loss in 2011, Nature, 478, 469–475, https://doi.org/10.1038/nature10556, 2011.

Marsh, D. R.: Chemical-dynamical coupling in the mesosphere and lower thermosphere, in: Aeronomy of the Earth's atmosphere and ionosphere, edited by Abdu, M. A. and Pancheva, D., vol. 2 of *IAGA Special Sopron Book*, pp. 3–17, doi:10.1007/978-94-007-0326-1, ISBN: 978-94-007-0326-1, Springer, Dordrecht, 1st edn., 2011.

Marsh, D. R., Mills, M. J., Kinnison, D. E., Lamarque, J.-F., Calvo, N., and Polvani, L. M.: Climate change from 1850 to 2005 simulated in CESM1(WACCM), J. Clim., 26, 7372–7391, https://doi.org/10.1175/JCLI-D-12-00558.1, 2013.

May, R. D. and Friedl, R. F.: Integrated band intensities of $HO_2NO_2$ at 220 K, J. Quant. Spectrosc. Radiat. Transfer, 50, 257–266, 1993.

McElroy, M. B. and McConnell, J.: Nitrous Oxide: A Natural Source of Stratospheric NO, J. Atmos. Sci., 28, 1095–1098, 1971.

McLinden, C. A., Prather, M. J., and Johnson, M. S.: Global modeling of the isotopic analogues of $N_2O$: Stratospheric distributions, budgets, and the $^{17}O$–$^{18}O$ mass-independent anomaly, Journal of Geophysical Research Atmospheres, 108, https://doi.org/10.1029/2002/JD002560, 2003.

https://doi.org/10.5194/egusphere-2026-4116
Preprint. Discussion started: 29 July 2026


Mengistu Tsidu, G., von Clarmann, T., Stiller, G. P., Höpfner, M., Fischer, H., Glatthor, N., Grabowski, U., Kellmann, S., Kiefer, M., Linden, A., Milz, M., Steck, T., Wang, D.-Y., and Funke, B.: Stratospheric $N_2O_5$ in the austral spring 2002 as retrieved from limb emission spectra recorded by the Michelson Interferometer for Passive Atmospheric Sounding (MIPAS), J. Geophys. Res., 109, D18301, https://doi.org/10.1029/2004JD004856, 2004.

Mengistu Tsidu, G., Stiller, G. P., von Clarmann, T., Funke, B., Höpfner, M., Fischer, H., Glatthor, N., Grabowski, U., Kellmann, S., Kiefer, M., Linden, A., López-Puertas, M., Milz, M., Steck, T., and Wang, D. Y.: $NO_y$ from Michelson Interferometer for Passive Atmospheric Sounding on Environmental Satellite during the Southern Hemisphere polar vortex split in September/October 2002, J. Geophys. Res., 110, D11301, https://doi.org/10.1029/2004JD005322, 2005.

Minschwaner, K. and Siskind, D. E.: A new calculation of nitric oxide photolysis in the stratosphere, mesosphere, and lower thermosphere, J. Geophys. Res., 98, 20,401–20,412, 1993.

Montzka, S. A. and Fraser, P. J.: Controlled substances and other source gases, p. 1.1–1.83, World Meteorological Organization, Geneva, 2003.

Morgan, C. G., Allen, M., Liang, M. C., Shia, R. L., Blake, G. A., and Yung, Y. L.: Isotopic fractionation of nitrous oxide in the stratosphere: Comparison between model and observations, J. Geophys. Res., 109, D04305, https://doi.org/10.1029/2003JD003402, 2004.

Murcray, D. G., Kyle, T. G., Murcray, F. H., and Williams, W. J.: Nitric Acid and Nitric Oxide in the Lower Stratosphere, Nature, 218, 78–79, 1968.

Murcray, D. G., Goldman, A., Csoeke-Poeckh, A., Murcray, F. H., Williams, W. J., and Stocker, R. N.: Nitric Acid Distribution in the Stratosphere, J. Geophys. Res., 78, 7033–7038, 1973.

Murcray, D. G., Goldman, A., Murcray, F. H., Murcray, F. J., and Williams, W. J.: Stratospheric Distribution of $ClONO_2$, Geophys. Res. Lett., 6, 857–859, 1979.

Neely III, R. R., English, J. M., Toon, O. B., Solomon, S., Mills, M., and Thayer, J. P.: Implications of extinction due to meteoritic smoke in the upper stratosphere, Geophys. Res. Lett., 38, L24808, https://doi.org/10.1029/2011GL049865, 2011.

Niedziela, R. F., Norman, M. L., DeForest, C. L., Miller, R. E., and Worsnop, D. R.: A Temperature- and Composition-Dependent Study of $H_2SO_4$ Aerosol Optical Constants Using Fourier Transform and Tunable Diode Laser Infrared Spectroscopy, J. Phys. Chem. (A), 103, 8030–8040, https://doi.org/10.1021/jp991323o, 1999.

Noxon, J. F.: Stratospheric $NO_2$ 2. Global Behavior, J. Geophys. Res., 84, 5067–5076, 1979.

Phillips, D.: A Technique for the numerical solution of certain integral equations of first kind, J. Ass. Comput. Mat., 9, 84–97, https://doi.org/10.1145/321105.321114, 1962.

Plieninger, J., von Clarmann, T., Stiller, G. P., Grabowski, U., Glatthor, N., Kellmann, S., Linden, A., Haenel, F., Kiefer, M., Höpfner, M., Laeng, A., and Lossow, S.: Methane and nitrous oxide retrievals from MIPAS-ENVISAT, Atmos. Meas. Tech., 8, 4657–4670, https://doi.org/10.5194/amt-8-4657-2015, 2015.

Prather, M. J., Hsu, J., DeLuca, N. M., Jackman, C. H., Oman, L. D., Douglass, A. R., Fleming, E. L., Strahan, S. E., Steenrod, S. D., Søvde, O. A., Isaksen, I. S. A., Froidevaux, L., and Funke, B.: Measuring and modeling the lifetime of nitrous oxide including its variability, Journal of Geophysical Research: Atmospheres, 120, 5693–5705, https://doi.org/10.1002/2015JD023267, 2015.

Ravishankara, A. R., Daniel, J. S., and Portmann, R. W.: Nitrous Oxide ($N_2O$): The Dominant Ozone–Depleting Substance Emitted in the 21st Century, Science, 326, 123–125, https://doi.org/10.1126/science.1176985, 2009.

Ridley, B. A. and Hastie, D. R.: Stratospheric Odd Nitrogen: NO Measurements at 51$^o$ N in Summer', J. Geophys. Res., 86, 3162–3166, 1981.

https://doi.org/10.5194/egusphere-2026-4116
Preprint. Discussion started: 29 July 2026


Rinsland, C. P., Zander, R., Farmer, C. B., Norton, R. H., and Russell III, J. M.: Concentrations of ethane ($C_2H_6$) in the lower stratosphere and upper troposphere and acetylene ($C_2H_2$) in the upper troposphere deduced from Atmospheric Trace Molecule Spectroscopy/Spacelab 3 spectra, J. Geophys. Res., 92, 11,951–11,964, 1987.

Rinsland, C. P., Toon, G. C., Farmer, C. B., Norton, R. H., and Namkung, J. S.: Stratospheric $N_2O_5$ Profiles at Sunrise and Sunset From Further Analysis of the ATMOS/Spacelab 3 Solar Spectra, J. Geophys. Res., 94, 18,341–18,349, 1989.

Roche, A. E., Kumer, J. B., Mergenthaler, J. L., Ely, G. A., Uplinger, W. G., Potter, J. F., James, T. C., and Sterritt, L. W.: The Cryogenic Limb Array Etalon Spectrometer CLAES on UARS: Experiment Description and Performance, J. Geophys. Res., 98, 10,763–10,775, 1993.

Rodgers, C. D.: Inverse Methods for Atmospheric Sounding: Theory and Practice, vol. 2 of *Series on Atmospheric, Oceanic and Planetary Physics, F. W. Taylor, ed.*, World Scientific, doi:10.1142/3171, Singapore, New Jersey, London, Hong Kong, https://doi.org/10.1142/3171, 2000.

Rothman, L. S., Gordon, I. E., Barbe, A., Benner, D. C., Bernath, P. F., Birk, M., Boudon, V., Browng, L. R., Campargueh, A., Champion, J.-P., Chance, K., Coudert, L. H., Dana, V., Devi, V. M., Fally, S., Flaud, J.-M., Gamache, R. R., Goldman, A., , Jacquemart, D., Kleiner, I., Lacome, N., Lafferty, W. J., Mandin, J.-Y., Massie, S., Mikhailenko, S. N., Miller, C. E., Moazzen-Ahmadi, N., Naumenko, O. V., Nikitin, A. V., Orphal, J., Perevalov, V. I., Perrin, A., Predoi-Cross, A., Rinsland, C. P., Rotger, M., Šimečková, M., Smith, M. A. H., Sung, K., Tashkun, S. A., Tennyson, J., Toth, R. A., Vandaele, A. C., and Vander Auwera, J.: The HITRAN 2008 molecular spectroscopic database, J. Quant. Spectrosc. and Radiat. Transfer, 110, 533–572, https://doi.org/https://doi.org/10.1016/j.jqsrt.2009.02.013, hITRAN, 2009.

Rowland, F. S., Spencer, J. E., and Molina, M. J.: Stratospheric formation and photolysis of chlorine nitrate, J. Phys. Chem., 80, 2711–2713, https://doi.org/10.1021/j100565a019, 1976.

Salawitch, R. J., Gobbi, G. P., Wofsy, S. C., and McElroy, M. B.: Denitrification in the Antarctic stratosphere, Nature, 339, 525–527, https://doi.org/10.1038/339525a0, 1989.

Salawitch, R. J., Wennberg, P. O., Toon, G. C., Sen, B., and Blavier, J.-F.: Near IR photolysis of $HO_2NO_2$: Implications for $HO_x$, Geophys. Res. Lett., 29, https://doi.org/10.1029/2002GL015006, 2002.

Sheese, P. E., Walker, K. A., Boone, C. D., McLinden, C. A., Bernath, P. F., Bourassa, A. E., Burrows, J. P., Degenstein, D. A., Funke, B., Fussen, D., Manney, G. L., McElroy, C. T., Murtagh, D., Randall, C. E., Raspollini, P., Rozanov, A., Russell III, J. M., Suzuki, M., Shiotani, M., Urban, J., von Clarmann, T., and Zawodny, J. M.: Validation of ACE-FTS version 3.5 $NO_y$ species profiles using correlative satellite measurements, Atmospheric Measurement Techniques, 9, 5781–5810, https://doi.org/10.5194/amt-9-5781-2016, 2016.

Sheese, P. E., Walker, K. A., Boone, C. D., Bernath, P. F., Froidevaux, L., Funke, B., Raspollini, P., and von Clarmann, T.: ACE-FTS ozone, water vapour, nitrous oxide, nitric acid, and carbon monoxide profile comparisons with MIPAS and MLS, J. Quant. Spectrosc. Radiat. Transfer, 186, 63–80, https://doi.org/10.1016/j.jqsrt.2016.06.026, 2017.

Sinnhuber, B.-M., Stiller, G., Ruhnke, R., von Clarmann, T., Kellmann, S., and Aschmann, J.: Arctic winter 2010/2011 at the brink of an ozone hole, Geophys. Res. Lett., 38, L24814, https://doi.org/10.1029/2011GL049784, 2011.

Sinnhuber, M., Funke, B., von Clarmann, T., López-Puertas, M., Stiller, G. P., and Seppälä, A.: Variability of $NO_x$ in the polar middle atmosphere from October 2003 to March 2004: vertical transport vs. local production by energetic particles, Atmos. Chem. Phys., 14, 7681–7692, https://doi.org/10.5194/acp-14-7681-2014, 2014.

Sinnhuber, M., Berger, U., Funke, B., Nieder, H., Reddmann, T., Stiller, G., Versick, S., von Clarmann, T., and Wissing, J. M.: $NO_y$ production, ozone loss and changes in net radiative heating due to energetic particle precipitation in 2002–2010, Atmos. Chem. Phys., 18, 1115–1147, https://doi.org/10.5194/acp-18-1115-2018, 2018.

Solomon, S.: Stratospheric Ozone Depletion: A Review of Concepts and History, Rev. Geophys., 37, 275–315, 1999.

https://doi.org/10.5194/egusphere-2026-4116
Preprint. Discussion started: 29 July 2026


Steck, T. and von Clarmann, T.: Constrained profile retrieval applied to the obervation mode of the Michelson Interferometer for Passive Atmospheric Sounding, Appl. Opt., 40, 3559–3571, https://doi.org/10.1364/AO.40.003559, 2001.

Stiller, G. P., ed.: The Karlsruhe Optimized and Precise Radiative Transfer Algorithm (KOPRA), Forschungszentrum Karlsruhe, Karlsruhe, https://doi.org/10.5445/IR/270048971, doi:10.5445/IR/270048971, 22.02.11; LK 01; Wissenschaftliche Berichte, FZKA-6487 (Dezember 2000), 2000.

Stiller, G. P., von Clarmann, T., Funke, B., Glatthor, N., Hase, F., Höpfner, M., and Linden, A.: Sensitivity of trace gas abundances retrievals from infrared limb emission spectra to simplifying approximations in radiative transfer modelling, J. Quant. Spectrosc. Radiat. Transfer, 72, 249–280, https://doi.org/10.1016/s0022-4073(01)00123-6, 2002.

Stiller, G. P., Mengistu Tsidu, G., von Clarmann, T., Glatthor, N., Höpfner, M., Kellmann, S., Linden, A., Ruhnke, R., Fischer, H., López-Puertas, M., Funke, B., and Gil-López, S.: An enhanced $HNO_3$ second maximum in the Antarctic mid–winter upper stratosphere 2003, J. Geophys. Res., 110, D20303, https://doi.org/10.1029/2005JD006011, 2005.

Stiller, G. P., von Clarmann, T., Brühl, C., Fischer, H., Funke, B., Glatthor, N., Grabowski, U., Höpfner, M., Jöckel, P., Kellmann, S., Kiefer, M., Linden, A., López-Puertas, M., Mengistu Tsidu, G., Milz, M., Steck, T., and Steil, B.: Global distributions of $HO_2NO_2$ as observed by the Michelson Interferometer for Passive Atmospheric Sounding (MIPAS), J. Geophys. Res., 112, D09314, https://doi.org/10.1029/2006JD007212, 2007.

Stolarski, R., Douglass, A., Oman, L., and Waugh, D.: Impact of future nitrous oxide and carbon dioxide emissions on the stratospheric ozone layer, Environ. Res. Lett., 10, 034011, 2015.

Tikhonov, A.: On the solution of incorrectly stated problems and method of regularization, Dokl. Akad. Nauk. SSSR, 151, 501–504, 1963.

Tilmes, S., Müller, R., Grooß, J.-U., Höpfner, M., Toon, G. C., and Russell III, J. M.: Very early chlorine activation and ozone loss in the Arctic winter 2002–2003, Geophys. Res. Lett., 30, 2201, https://doi.org/10.1029/2003GL018079, 2003.

Toon, G. C., Farmer, C. B., and Norton, R. H.: Detection of stratospheric $N_2O_5$ by infrared remote sounding, Nature, 319, 570–571, 1986.

Twomey, S.: On the Numerical Solution of Fredholm Integral Equations of the First Kind by the Inversion of the Linear System Produced by Quadrature, Journal of the ACM, 10, 97–101, https://doi.org/10.1145/321150.321157, 1963.

Verronen, P. T., Funke, B., López-Puertas, M., Stiller, G. P., von Clarmann, T., Glatthor, N., Enell, C.-F., Turunen, E., and Tamminen, J.: About the increase of $HNO_3$ in the stratopause region during the Halloween 2003 solar proton event, Geophys. Res. Lett., 35, L20809, https://doi.org/10.1029/2008GL035312, 2008.

Virolainen, Y. A., Timofeev, Y. M., Poberovskii, A. V., Kirner, O., and Höpfner, M.: Chlorine Nitrate in the Atmosphere over St. Petersburg, Izvestiya, Atmospheric and Oceanic Physics, 51, 49–56, https://doi.org/10.1134/S0001433815010119, 2015.

Volk, C. M., Elkins, J. W., Fahey, D. W., Dutton, G. S., Gilligan, J. M., Loewenstein, M., Podolske, J. R., Chan, K. R., and Gunson, M. R.: Evaluation of source gas lifetimes from stratospheric observations, J. Geophys. Res., 102, 25,543–25,564, https://doi.org/10.1029/97JD02215, 1997.

von Clarmann, T. and Johansson, S.: Chlorine nitrate in the atmosphere, Atmos. Chem. Phys., 18, 15 363–15 386, https://doi.org/10.5194/acp-18-15363-2018, 2018.

von Clarmann, T., Fischer, H., Friedl-Vallon, F., Linden, A., Oelhaf, H., Piesch, C., Seefeldner, M., and Völker, W.: Retrieval of Stratospheric $O_3$, $HNO_3$ and $ClONO_2$ Profiles From 1992 MIPAS–B Limb Emission Spectra: Method, Results and Error Analysis, J. Geophys. Res., 98, 20,495–20,506, 1993.

von Clarmann, T., Glatthor, N., Grabowski, U., Höpfner, M., Kellmann, S., Kiefer, M., Linden, A., Mengistu Tsidu, G., Milz, M., Steck, T., Stiller, G. P., Wang, D. Y., Fischer, H., Funke, B., Gil-López, S., and López-Puertas, M.: Retrieval of temperature and tangent altitude

https://doi.org/10.5194/egusphere-2026-4116
Preprint. Discussion started: 29 July 2026


pointing from limb emission spectra recorded from space by the Michelson Interferometer for Passive Atmospheric Sounding (MIPAS), J. Geophys. Res., 108, 4736, https://doi.org/10.1029/2003JD003602, 2003.

von Clarmann, T., De Clercq, C., Ridolfi, M., Höpfner, M., and Lambert, J.-C.: The horizontal resolution of MIPAS, Atmos. Meas. Techn., 2, 47–54, https://doi.org/10.5194/amt-2-47-2009, 2009a.

von Clarmann, T., Höpfner, M., Kellmann, S., Linden, A., Chauhan, S., Funke, B., Grabowski, U., Glatthor, N., Kiefer, M., Schieferdecker, T., Stiller, G. P., and Versick, S.: Retrieval of temperature, $H_2O$, $O_3$, $HNO_3$, $CH_4$, $N_2O$, $ClONO_2$ and ClO from MIPAS reduced resolution nominal mode limb emission measurements, Atmos. Meas. Tech., 2, 159–175, https://doi.org/10.5194/amt-2-159-2009, 2009b.

von Clarmann, T., Funke, B., López-Puertas, M., Kellmann, S., Linden, A., Stiller, G. P., Jackman, C. H., and Harvey, V. L.: The solar proton events in 2012 as observed by MIPAS, Geophys. Res. Lett., 40, 1–5, https://doi.org/10.1002/grl.50119, 2013.

von Clarmann, T., Glatthor, N., and Plieninger, J.: Maximum likelihood representation of MIPAS profiles, Atmos. Meas. Tech., 8, 2749–2757, https://doi.org/10.5194/amt-8-2749-2015, 2015.

von Clarmann, T., Degenstein, D. A., Livesey, N. J., Bender, S., Braverman, A., Butz, A., Compernolle, S., Damadeo, R., Dueck, S., Eriksson, P., Funke, B., Johnson, M. C., Kasai, Y., Keppens, A., Kleinert, A., Kramarova, N. A., Laeng, A., Langerock, B., Payne, V. H., Rozanov, A., Sato, T. O., Schneider, M., Sheese, P., Sofieva, V., Stiller, G. P., von Savigny, C., and Zawada, D.: Overview: Estimating and Reporting Uncertainties in Remotely Sensed Atmospheric Composition and Temperature, Atmos. Meas. Tech., 13, 4393–4436, https://doi.org/10.5194/amt-13-4393-2020, 2020.

von Clarmann, T., Glatthor, N., Grabowski, U., Funke, B., Kiefer, M., Kleinert, A., Stiller, G. P., Linden, A., and Kellmann, S.: TUNER–compliant error estimation for MIPAS: methodology, Atmos. Meas. Tech., 15, 6991–7018, https://doi.org/10.5194/amt-15-6991-2022, 2022.

Wagner, G. and Birk, M.: New infrared spectroscopic database for chlorine nitrate, J. Quant. Spectrosc. Radiat. Transfer, 82, 443–460, https://doi.org/10.1016/S0022-4073(03)00169-9, 2003.

Wang, D. Y., Höpfner, M., Mengistu Tsidu, G., Stiller, G. P., von Clarmann, T., Fischer, H., Blumenstock, T., Glatthor, N., Grabowski, U., Hase, F., Kellmann, S., Linden, A., Milz, M., Oelhaf, H., Schneider, M., Steck, T., Wetzel, G., López-Puertas, M., Funke, B., Koukouli, M. E., Nakajima, H., Sugita, T., Irie, H., Urban, J., Murtagh, D., Santee, M. L., Toon, G., Gunson, M. R., Irion, F. W., Boone, C. D., Walker, K., and Bernath, P. F.: Validation of nitric acid retrieved by the IMK-IAA processor from MIPAS/ENVISAT measurements, Atmospheric Chemistry and Physics, 7, 721–738, https://doi.org/10.5194/acp-7-721-2007, 2007.

Wetzel, G., Oelhaf, H., Höpfner, M., Friedl-Vallon, F., Ebersoldt, A., Gulde, T., Kazarski, S., Kirner, O., Kleinert, A., Maucher, G., Nordmeyer, H., Orphal, J., Ruhnke, R., and Sinnhuber, B.-M.: Diurnal variations of $BrONO_2$ observed by MIPAS-B at midlatitudes and in the Arctic, Atmospheric Chemistry and Physics, 17, 14 631–14 643, https://doi.org/10.5194/acp-17-14631-2017, 2017.

Wiegele, A., Glatthor, N., Höpfner, M., Grabowski, U., Kellmann, S., Linden, A., Stiller, G., and von Clarmann, T.: Global distributions of $C_2H_6$, $C_2H_2$, HCN, and PAN retrieved from MIPAS reduced spectral resolution measurements, Atmospheric Measurement Techniques, 5, 723–734, https://doi.org/10.5194/amt-5-723-2012, 2012.

Wolff, M. A., Kerzenmacher, T., Strong, K., Walker, K. A., Toohey, M., Dupuy, E., Bernath, P. F., Boone, C. D., , Brohede, S., Catoire, V., von Clarmann, T., Coffey, M., Daffer, W. H., De Mazière, M., Duchatelet, P., Glatthor, N., Griffith, D. W. T., Hannigan, J., Hase, F., Höpfner, M., Huret, N., Jones, N., Jucks, K., Kagawa, A., Kasai, Y., Kramer, I., Küllmann, H., Kuttippurath, J., Mahieu, E., Manney, G., McElroy, C. T., McLinden, C., Mébarki, Y., Mikuteit, S., Murtagh, D., Piccolo, C., Raspollini, P., Ridolfi, M., Ruhnke, R., Santee, M., Senten, C., Smale, D., Tétard, C., Urban, J., and Wood, S.: Validation of $HNO_3$, $ClONO_2$ and $N_2O_5$ from the Atmospheric Chemistry Experiment

https://doi.org/10.5194/egusphere-2026-4116
Preprint. Discussion started: 29 July 2026


Fourier Transform Spectrometer (ACE-FTS), Atmospheric Chemistry and Physics, 8, 3529–3562, https://doi.org/10.5194/acp-8-3529-2008, 2008.

Zander, R., Rinsland, C. P., Farmer, C. B., Brown, L. R., and Norton, R. H.: Observation of several chlorine nitrate ($ClONO_2$) bands in stratospheric infrared spectra, Geophys. Res. Lett., 13, 757–760, https://doi.org/10.1029/GL013i008p00757, 1986.